General Disclaimer

One or more of the Following Statements may affect this Document

- This document has been reproduced from the best copy furnished by the organizational source. It is being released in the interest of making available as much information as possible.

- This document may contain data, which exceeds the sheet parameters. It was furnished in this condition by the organizational source and is the best copy available.

- This document may contain tone-on-tone or color graphs, charts and/or pictures, which have been reproduced in black and white.

- This document is paginated as submitted by the original source.

- Portions of this document are not fully legible due to the historical nature of some of the material. However, it is the best reproduction available from the original submission.

GCA-TR-68-6-N

STUDY OF THEORY AND APPLICABILITY OF LASER TECHNIQUE FOR MEASURING ATMOSPHERIC PARAMETERS

J. Pressman
C. Schuler
T. Wentink

Bedford, Massachusetts

INTERIM SCIENTIFIC REPORT
CONTRACT NO. NAS12-540

PREPARED FOR
NATIONAL AERONAUTICS AND SPACE ADMINISTRATION
ELECTRONICS RESEARCH CENTER
CAMBRIDGE, MASSACHUSETTS

OCTOBER 1968

GCA-TR-68-6-N

STUDY OF THEORY AND APPLICABILITY OF LASER TECHNIQUE FOR MEASURING ATMOSPHERIC PARAMETERS

J. Pressman
C. Schuler
T. Wentink

INTERIM SCIENTIFIC REPORT

Contract No. NAS12-540

GCA CORPORATION
GCA TECHNOLOGY DIVISION
Bedford, Massachusetts

Prepared for

NATIONAL AERONAUTICS AND SPACE ADMINISTRATION
Electronics Research Center
Cambridge, Massachusetts

TABLE OF CONTENTS

I. INTRODUCTION

The present document represents the Interim Scientific Report on Contract NAS12-540, Theory of Laser Atmospheric Interactions. The major purpose of the program involved development of a comprehensive understanding of the nature of laser energy interactions in the atmosphere. The derived results are to be applied to the design and operation of modulated, coherent ground-based laser communications links in planetary atmospheres. In this regard, the various scatter modes which are possible when such transmission occurs includes potentially important resonant interactions which can effectively degrade the transmissivity of the atmospheric medium. In order to evaluate the magnitude of this problem, atmospheric constituents have been categorized as potential resonant scattering species to assist in the selection of optimal communications system operational wavelengths. As a consequence of the above requirements, the basic objective of the present investigation was the performance of a critical and systematic analysis of the absorption characteristics of real atmospheric constituents.

A specific task which has been performed under the contract involves the compilation from the literature of molecular species and pertinent transitions of interest in the laser energy-atmospheric constituent interaction problem described above. The results of this facet of the program are presented and discussed in Section II and Appendix A of the present report.

The second major task performed under the contract has involved a bibliographic survey augmented theoretically where required, to establish

suitable techniques of obtaining pertinent data on major and trace constituents of planetary atmospheres appropriate to the laser interaction problem. In this regard, it was decided to concentrate the effort on a limited number of the most pertinent applications in order to avoid dilution of the contemplated investigation. Furthermore, the final phase of the program has involved establishment of the planetary atmospheric parameters which are most amenable to investigation employing the previously derived survey data. The results of this phase of the program are presented in the several additional sections of the report. Specifically, a mathematical analytical treatment of the general laser probe problem is presented in Section III while the area of Raman scattering in atmospheric gases is discussed in Section IV. The laser analysis of isotopic abundances is considered in Section V. The possibilities are explored in Section VI of probing for both MgO, a highly suspect meteoritically deposited specie, and for AlO, which is known to be deposited artificially in chemical release programs. Finally, in Section VII an analysis is presented of the feasibility of measuring the ambient wind field using laser density observations from a ground-based site.

It should be noted that although a major portion of the results presented in this document has appeared in the Quarterly Progress Reports submitted under the contract, it was felt that the review and edit of the material served a valuable purpose in that a unified compilation of the survey data under a single cover would be available for distribution to the interested scientific community.

II. SPECTROSCOPIC SURVEY OF ATMOSPHERIC MOLECULES

The current requirement for information pertaining to the molecular absorption and scattering of laser radiation has been discussed in the previous section. Under the present effort, the recent results of Wentink, et al.,[1-3] and Nicholls and his co-workers[4] have been reviewed in detail. The recent (1964) encyclopedic tabulation of Dalby[5] is already obsolete on the basis of coverage alonge. A similar situation exists with respect to the work of Soshnikov.[6] Furthermore, much of the available data for air has been superseded by significantly different values derived by changes in interpretation of the original experimental observations.

A. General Status of Known Absolute Intensities for Excited Electronic States

Although detailed effort has been placed on molecules expected in the planetary atmospheres of Earth, Mars, and Venus, additional consideration has been accorded to other molecules which may possibly be present due to natural or intentional contamination. For example, MgO is probably introduced principally as a meteor debris species while the major injection mechanism for BaO would be artificial seeding in upper atmosphere chemical release programs.

An interesting observation which emerges from correlation of extensive absolute intensity data compiled as a result of the present and other survey investigations, is that the known absolute intensity constants, such as transition probabilities, for excited electronic states

of diatomic molecules are confined largely to combinations of the lighter atoms (i.e., H through A). Even accounting for the fragmentary data on K_2 and Cs_2 and the results for I_2 and Hg_2, it should be noted that the measured <u>absolute</u> intensity constants involve combinations of only about fifteen of the elements of the periodic system. The molecules measured so far are listed in Table 1A while some molecular electronic transitions involving ground states are presented in Table 1B. In the case of the measured species, several band systems are reported frequently for a given parent molecule. Examples of some absolute intensity constants for N_2, N_2^+, and CO are presented in Tables 2, 3, and 4 respectively.

The most obvious reason for the present state of affairs involves the greater interest in the major atmospheric gases, as well as the volatility and relative simplicity of handling and purifying the lighter molecules. However, the oxides of heavier elements are of atmospheric interest as well as being of considerable astrophysical importance. Examples of these heavier molecules are considered in greater detail subsequently in this section of the report. Experimental investigations are currently being pursued on some of these oxides, so that some experimental data should be forthcoming in the near future.

Only the bandheads or, alternatively, the origins of the band systems which seem to be attractive candidates for laser probing are considered in the present report. Detailed calculations of exact line locations are reserved for individual circumstances where such action is warranted.

TABLE 1A

DIATOMIC MOLECULES FOR WHICH MEASURED TRANSITION PROBABILITIES BETWEEN ELECTRONIC STATES ARE KNOWN[a,b] (As of December 1967)

Atom	H	He	Li	Be	B	C	N	O	F	Ne	Na	Mg	Aℓ	Si	P	S	Cℓ	A
H	H_2	.	.	.	.	CH	NH	OH	.	.	.	.	.	.	PH	.	HCℓ	.
He		He_2	.	.	.	.	.	.	.	.	.	.	.	.	.	.	.	.
Li			Li_2	.	.	.	.	.	.	.	.	.	.	.	.	.	.	.
Be				.	.	.	.	BeO	.	.	.	.	.	.	.	.	.	.
B					.	.	.	.	BF	.	.	.	.	.	.	.	BCℓ	.
C						C_2	CN	CO	CF	.	.	.	.	.	.	.	.	.
N							N_2	NO	.	.	.	.	.	.	.	.	.	.
O								O_2	.	.	.	MgO	AℓO	SiO	.	.	.	.
F									F_2	.	.	.	.	SiF	.	.	.	.
Ne										.	.	.	.	.	.	.	.	.
Na											.	.	.	.	.	.	.	.
Mg												.	.	.	.	.	.	.
Aℓ													.	.	.	.	.	.
Si														.	.	.	.	.
P															.	.	.	.
S																.	.	.
Cℓ																	$Cℓ_2$	.
A																		.

(a) Matrix representation is inherently symmetric.
(b) Some intensity data for K_2, Cs_2, I_2 and Hg_2 also reported.

TABLE 1B

SOME MOLECULAR ELECTRONIC TRANSITIONS INVOLVING GROUND STATES

Molecule	Upper State	Ground State	System Name	λ_{00}, Å	Band f_{mn00}	Upper State τ
N_2	$A\ ^3\Sigma_g^+$	$X\ ^1\Sigma_g^+$	Vegard-Kaplan	2010	$\sim 10^{-8}$	13 sec
	$a\ ^1\Pi_g$	$X\ ^1\Sigma_g^+$	Lyman-Birge-Hopfield	1450	10^{-6}	$\sim 20\ \mu s$
O_2	$a\ ^1\Delta$	$X\ ^3\Sigma_g^-$	Red	6340	$< 10^{-10}$	1 hr**
NO	$A\ ^2\Sigma^+$	$X\ ^2\Pi$	Gamma	2262	4.2×10^{-4}	197 ns
CO	$A\ ^1\Pi$	$X\ ^1\Sigma^+$	Fourth Positive	1544	1.3×10^{-2}	11 ns
CH	$A\ ^2\Delta$	$X\ ^2\Pi$	4315	4315	5.0×10^{-3}	550 ns
NH	$A\ ^3\Sigma$	$X\ ^3\Sigma$	----	3360	7.3×10^{-3}	460 ns
OH	$A\ ^2\Sigma$	$X\ ^2\Sigma$	Violet	3125	7.3×10^{-4}	1.0 μs
CS*	$A\ ^1\Pi$	$X\ ^1\Sigma^+$	----	2576	1.4×10^{-2}	112 ns
MgO*	$B\ ^1\Sigma$	$X\ ^1\Sigma^+$	Green	5007	9.3×10^{-3}	400 ns

*Intensity constants calculated on basis legislated transition moment of 1 Debye.

**However, see text for 25 ms value for complex $(O_2\ (a'\Delta))_2$.

TABLE 2

SOME ABSOLUTE INTENSITY CONSTANTS OF N_2

Transition (upper-lower)	System Name	λ_{00} (a)	τ (b)	Band f_{mn00}	System f_{mn}	Remarks
$D\ ^3\Sigma - B\ ^3\Pi$	Fourth Positive	2258	184 ns	2.8×10^{-4}	2.8×10^{-3}	
$C\ ^3\Pi - B\ ^3\Pi$	Second Positive	3371	47 ns	1.6×10^{-2}	3.6×10^{-2}	
$C\ ^3\Pi - X\ ^1\Sigma$	Tanaka	1123	47 ns			Forbidden
$B'\ ^3\Sigma - B\ ^3\Pi$	IR Afterglow	1.53μ	~50μs(c)			
$B'\ ^3\Sigma - X\ ^1\Sigma$	Ogawa-Tanaka-Wilkinson	1518	~50μs			Forbidden
$B\ ^3\Pi - A\ ^3\Sigma$	First Positive	1.05μ	8-19μs	2×10^{-3}	5×10^{-3}	Strong Cascading
$A\ ^3\Sigma - X\ ^1\Sigma$	Vegard-Kaplan	2010	13 sec			Forbidden
$p'\ ^1\Sigma - X\ ^1\Sigma$	Unnamed	959	0.9 ns		1.6×10^{-1}	
$p'\ ^1\Sigma - a\ ^1\Pi$	Gaydon-Herman-Janin	---	0.9 ns			
$b'\ ^1\Sigma - X\ ^1\Sigma$	Birge-Hopfield #1	965	~2 ns		$\sim 4 \times 10^{-1}$	
$b\ ^1\Pi - X\ ^1\Sigma$	Birge-Hopfield #2	986	~20 ns		$\sim 4 \times 10^{-2}$	
$b\ ^1\Pi - a\ ^1\Pi$	Janin	3075	~20 ns			
$a\ ^1\Pi - X\ ^1\Sigma$	Lyman-Birge-Hopfield	1450	10-150μs	$\sim 10^{-6}$	$\sim 3 \times 10^{-5}$	Strong Cascading

TABLE 2 (continued)

Transition (upper-lower)	System Name	λ_{00}	τ	Band f_{mn00}	System f_{mn}	Remarks
$a\ ^1\Pi - X\ ^1\Sigma$	Unnamed	8.21 μ	10-150 μs			
$w\ ^1\Delta - a\ ^1\Pi$	Unnamed	3.64 μ	·460 μs(c)			
$w\ ^1\Delta - X\ ^1\Sigma$	Unnamed	1390	·460 μs(c)	$\sim 10^{-8}$		
$a'\ ^1\Sigma - X\ ^1\Sigma$	Wilkinson-Mulliken Ogawa-Tanaka	1479	0.7 sec(c)			τ depends on τ of LBH System

(a) In Angstroms unless noted otherwise.

(b) Measured, unless calculated and so designated by (c)

TABLE 3

SOME ABSOLUTE INTENSITY CONSTANTS OF N_2^+ (ION)

Transition (Upper-Lower)	System Name	λ_{00} (Angstroms)	τ	Band f_{mn00}	System f_{mn}	Remarks
$C\ ^2\Sigma - X\ ^2\Sigma$	Second Negative	1549	33 ns(c)	1.7×10^{-4}	1.5×10^{-2}	Note (a)
$D\ ^2\Pi - A\ ^2\Pi$	Janin-d'Incan	Ultraviolet	?	---	---	No Intensity data
$B\ ^2\Sigma - X\ ^2\Sigma$	First Negative	3914	67 ns(m)	2.3×10^{-2}	3.6×10^{-2}	Intense
$A\ ^2\Pi - X\ ^2\Sigma$	Meinel-Auroral	11091	~ 3μs	---	---	Estimate
			26μs(c)	1.0×10^{-3}	2.1×10^{-3}	Note (a)

(a) Calculated on basis R_e = 1 Debye.

(m) Measured

(c) Calculated

TABLE 4

SOME ABSOLUTE INTENSITY CONSTANTS OF CO

Transition (Upper-Lower)	System Name	λ_{00} (Angstroms)	τ	Band f_{mn00}	System f_{mn}	Remarks
A $^1\Pi$ - X $^1\Sigma$	Fourth Positive	1544	11.5 ns(m)	1.25×10^{-2}	1.09×10^{-1}	Very strong system
B $^1\Sigma$ - X $^1\Sigma$	Hopfield-Birge #1	1151	25 ns(m)	8.0×10^{-3}	7.9×10^{-3}	
B $^1\Sigma$ - A $^1\Pi$	Angstrom	4509	25 ns(m)	---	---	B State Branching; NID
C $^1\Sigma$ - X $^1\Sigma$	Hopfield-Birge #2	1088	1.4 ns(m)	1.27×10^{-1}	1.27×10^{-1}	
C $^1\Sigma$ - A $^1\Pi$	Herzberg	3681	1.4 ns(m)	---	---	C State branching; NID
a' $^3\Sigma$ - a $^3\Pi$	Asundi	14535	12-34μs(c)	---	---	Spread-out system
d $^3\Delta$ - a $^3\Pi$	Triplet	8215	3.1μs(c)	1.4×10^{-4}	6.4×10^{-3}	Spread-out system
e $^3\Sigma$ - a $^3\Pi$	Herman	Near IR	---	---	---	NID
b $^3\Sigma$ - a $^3\Pi$	Third Positive and 5B	2827	180 ns(m)	3.2×10^{-4}	5.5×10^{-3}	
c $^3\Sigma$ - a $^3\Pi$	3A	2296	---	---	---	NID

NID - No Intensity Data

The question of suitable laser transitions is a broad topic which constituted an important aspect of the present program. Unfortunately, the lower transition states with the desired large transition probabilities frequently either reside in the ultraviolet spectral region or are several eV above the ground state. In the present work, particular consideration has been accorded molecular transitions which involve ground state and occur at longer wavelengths. From this point of view, CS, CH, and MgO appear to offer promising results.

It is expected that the tabular results presented previously for specific molecules will undergo future revision. The presently reported measurements involve either relative intensities or absolute intensity constants (i.e., radiative lifetimes, absorption coefficients, etc.).

1. Nitrogen systems. — An extensive and excellent compilation of spectroscopic information on N_2 and N_2^+ has been compiled by Lofthus.[7] More recent works by Tilford, et al.[8] have extended and refined these earlier data, especially by many high-resolution measurements. These are particularly pertinent to line-position (wavelength) calculations. In addition, the results of Tanaka, et al.[9] are considered to be basic references on the subject of the excited states of N_2 and N_2^+.

The λ_{00} and absolute intensity constants are presented in Table 2 for the N_2 band systems of major importance. The $N_2(2+)$ and (1+) bands are of major interest because of λ_{00} and the relatively large (for bands) transition probabilities. The pertinence of these data to the laser-probing problem will be demonstrated subsequently in the present section of the report.

2. Potential application of molecular transitions of N_2. – An outline is presented below of the type of analysis which must be performed in considering the application of a particular laser to a given molecular specie and band system (or line). Also this represent an example of how cascading between levels may influence the choice of probing wavelengths. The feasibility will depend on the atmosphere under consideration and the state of technology.

It has been pointed out that if a fluorescence transition is more efficient than the direct resonance then the receiver should be tuned to the fluorescence line rather than the excitation (resonance) line. This would reduce interference in the receiver from the transmitted pulse, as well as eliminating the Rayleight scattering background source at the receiver wavelength. In exploring such possible situations, the case of the B, B′, and C states of N_2 is considered as shown in Figure 1. Direct excitation of these states from the ground $X\ ^1\Sigma$ state of N_2 would represent a relatively inefficient process, since the transitions like Vegard-Kaplan, Ogawa-Tanaka-Wilkinson, and Tanaka bands are highly forbidden. However, the high ground state population would be a mitigating factor. A more serious problem is that vacuum ultraviolet transitions are involved which establishes limitations on the laser location (i.e., above the atmosphere). Clearly, in the present state of the laser art, this requires currently unavailable euv lasers, or at least the use of harmonics of available lasers with the implicit power penalty.

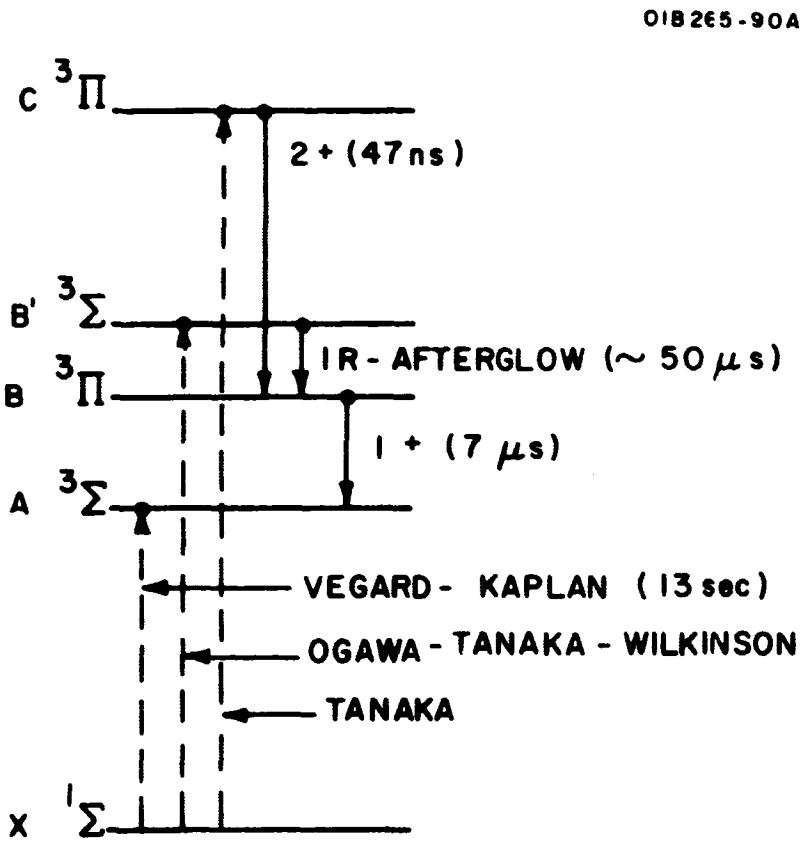

SOME TRANSITIONS IN N_2 (NOT TO SCALE)

Solid vertical lines = allowed

Dashed vertical lines = forbidden

( ) indicates radiative lifetime of upper state in absence of collisional quenching

Figure 1.

An attractive alternative, if sufficient populations are available, involves the application of realistically available lasers* to excite the C state through a resonance with the B → C (N_2 Second Positive, 2+) transition. Then, in the case of fluorescence at excitation pulse termination the C state decays (in 47 ns or less, depending on the pressure) to the B state which then decays (in about 7 μs) to the A state, yielding the fully allowed N_2 (1+) system in emission.

Another possible alternative involves the use of an infrared laser to similarly excite the B′ state via B → B′. Then, after the B′ decay (in about 50 μs) to B the N_2 (1+) system would be produced.

Among the many facets of this problem which require detailed analysis in any real atmosphere are included:

(1) What is the ambient population of the B state and the resulting population of C or B′ by allowed transitions and reasonably available lasers, compared to the population of C or B′ resulting from excitation from the vastly greater reservoir of X state molecules through forbidden and ultraviolet transitions?

(2) What is the trade-off in observing the direct resonances (1+, 2+, or IR afterglow systems) in the presence of a Rayleigh scattering background versus monitoring (1+) with no such background and with receiver-transmitter wavelength isolation?

(3) Given initial excitation of a single vibrational-rotational

---

*e.g., Avco's N_2 laser, using the 2+ transition; present peak power 200 kW, pulse length about 15 ns. Avco states 500 kW is feasible.

level of C or B′, what is the population distribution of the several B state levels after pulse cessation and decay of C or B′?

3. N_2^+ Systems. – It is clear that the First Negative (1-) bands of N_2^+ are the most attractive transitions in probing for N_2^+. The bands of this fully allowed transition, $B\ ^2\Sigma - X\ ^2\Sigma$, are strong in N_2 bombarded by electrons, protons, and photons of suitable wavelength. Appreciable concentrations of N_2^+ result from photoionization, and N_2^+ (1-) emission is a prominent spectral feature in aurora and dayglow. Additionally, the wavelength (λ_{00} = 3914Å) is convenient for monitoring in an air atmosphere. The absolute intensity constants for N_2^+ (1-) are now well established as shown in Table 3. The mean radiative lifetime for the $v' = 0$ level, from several independent investigations, is 64 ns ± 10 percent.

Although other N_2^+ band systems are not as well characterized, the Second Negative (2-) system, due to the $C\ ^2\Sigma - X\ ^2\Sigma$ transition, should also be strong. Absolute intensity estimates derived under the present program are presented in Table 3. The transition occurs in the vacuum ultraviolet and often only weakly. Frequently it is not observed in ordinary discharges in pure N_2, but this seems to be due to excitation conditions rather than transition probabilities for emission. Electron velocities above 40 eV appear to be required for appreciable excitation of the C state.

The Meinel bands from the N_2^+ transition $A\ ^2\Pi - X\ ^2\Sigma$ are observable in the near infrared, although usually masked or dominated by N_2 (1+) bands. Only an estimate of the Meinel upperstate lifetime (3 μs) is

available so that further study is required. A related problem is the lifetime of the D state, which produces the Janin-d' Incan bands, $D\ ^2\Pi - A\ ^2\Pi$. The lower electronic state of the Janin-d' Incan possibly can influence the Meinel intensity due to cascading. The direct utilization of the Janin-d' Incan bands for monitoring appears somewhat questionable since it is expected to be rather weak and subject to severe interference from portions of the N_2 (1-) and N_2 (LBH) bands. The actual interference, of course, depends on the nature of the atmosphere and the excitation mechanism.

4. CO systems. – Intensity data for most of the CO band systems are listed in Table 4. CO has been surveyed extensively by Krupenie[10] and recently by Wentink, et al.[3] The most intense system is the CO Fourth Positive (4+) which represents one of the strongest absorbing band systems known. However, unfortunately from the laser standpoint, it occurs in the vacuum and near ultraviolet spectral regions. It might be excited to some extent by cascading from the $B\ ^1\Sigma$ and $C\ ^1\Sigma$ states; i.e., laser resonance with some of the Angstrom or Herzberg band transitions.

The Asundi and Triplet band systems are relatively broad systems covering the visible and near infrared spectral regions, so that some bands would be more accessible to available tunable lasers. Unfortunately, none of these bands are very strong absorbers or emitters. However, the $a\ ^3\Pi$ state is known to be both highly stable chemically (long specie lifetime) and highly metastable in terms of radiative lifetime. Thus, one

may encounter in some atmospheres sufficient ambient populations of the a $^3\Pi$ state of CO to permit appreciable excitation of some lines of the Asundi, Triplet, Herman, Third Positive-5B and 3A band systems.

5. CS radical. – The CS molecule rates attention since it is known qualitatively as a strong absorber and emitter (A $^1\Pi$ - X $^1\Sigma$ transition) and may exist in some planetary atmospheres. In addition, it may be of future interest in the terrestrial upper atmosphere when the supersonic transport program becomes active. The principal SST fuel constituent, kerosene, usually contains from 0.05 to 0.11 percent sulfur (maximum limit about 0.3 percent). This should be considered in view of the anticipated deposition of about 5 x 10^5 tons of exhaust products per day from some 10^3 SST's by the end of 1979!

Absolute intensity data for CS (A $^1\Pi$ - X $^1\Sigma$) are not available. Using the Morse $q_{v'v''}$ of Felenbok (Reference F-7 of Appendix A) and a reasonable assigned constant transition moment of 1 Debye, the band absorption f-number for the 0,0 band, f_{mn00} have been estimated. (See first Quarterly Report, pp. 14-17 for definitions and method of computation.) The resulting $f_{mn00} = 0.013$. The short wavelength of CS, $\lambda_{00} = 2576\text{Å}$, although undesirable is not out of the question for resonance with future lasers. The radiative lifetime of the A $^1\Pi$ state of CS is similarly predicted to be 112 nanoseconds.

These predictions indicate that CS (A- X) should be examined further on a line-by-line basis as a promising candidate for probing for CS. Of

course, the more probable molecule SO_2 must be considered in oxidizing atmospheres.

6. Status of metallic oxide intensity constants. – A recent excellent assessment of metallic-oxide f-values obtained from an IDA meeting are presented in Table 5 which also contains some GCA calculations useful for estimation and scaling. Much of the following material has been abstracted from the survey of Main[12] and notes of the meeting.[11]

MgO. – Specifically the MgO transition $B\ ^1\Sigma - X\ ^1\Sigma$ is considered since it is a relatively strong emitter and is expected to be present in the atmosphere due to meteoric debris deposition. The 0,0 band of the so-called "green bands" at $\lambda_{00} = 5007\text{Å}$ has a large q_{00} (= 0.98) and is favorably narrow (10Å total bandwidth). Proceeding as for the CS molecule discussed previously, the estimated f_{mn00} is 0.0093 and the corresponding radiative lifetime of the $B\ ^1\Sigma$ state is 400 nanoseconds. The $q_{v'v''}$ of Nicholls (Reference N-1 of Appendix A) were employed in the calculations.

It should be noted that the $^1\Sigma$ assignment for the ground state of MgO has been accepted. Whether the ground state is a triplet or singlet state has been a subject of much controversy since about 1950, but the consensus now is that the singlet ground state is most probable.

An absolute f-number for the MgO "green system" B - X is now available, due to the results of Main, et al.[13] (Table 5) It is believed that the corresponding transition moment of 0.37 Debye is unusually and unexpectedly low. Although Main, et al. have accepted the fact that the

ground state is a singlet, they also noted that if the expected but so far not-observed triplet states were included in the thermodynamics yielding the concentration, the f-number deduced from the same experimental data might be increased by a factor of about 4.

Another input to this still unresolved question is the result of Brewer[14] who observed several different new states tentatively assigned as singlet states. Brewer[14] remarks that, "However, some of the singlet states are closely grouped in energy and have almost identical molecular constants which suggests that possibly the so-called singlet states are actually components of a $^3\Pi$ state."

This condition suggests that another situation where laser blowoff and associated lifetimes might resolve this important (especially theoretically) question. The spectroscopy of MgO and the expected lifetime (0.4 to 2.9 μs) should make this a reasonable straightforward experiment.

AℓO ($A\,^2\Sigma - X\,^2\Pi$ transition). – At the IDA meeting, Wurster[11] reported a large and probably unrealistic system (electronic) f-value (f_e) based on a careful experimental program. Vanpee, et al.[15] reported many measured band f-values for AℓO, and $f_e = 0.0037$. Johnson, et al.[16] deduced an f_e-value of about 0.005 from a complex analysis of absolute measurements of a twilight cloud of AℓO from a grenade exploded at 155-km altitude. The Vanpee, et al. results appear to be the best available values. From Table 5 it can be seen that the radiative lifetime of AℓO should be about 0.8 μs, and, in view of the following discussion on SiO, the AℓO lifetime should be measurable by the laser

TABLE 5

ABSOLUTE INTENSITY CONSTANTS OF SOME OXIDE BANDS

Molecule	System	Method	v'v"	Band[a] $f_{mnv'v''}$	$q_{v'v''}$	System[a] f_{mn} at 0,0	$r_{v'v''}$	R_e, Debye[b]
SiO	A $^1\Pi$ - X $^1\Sigma$	ST-e	0,0	7.0 - 4	0.142	5.0 - 3	0.388	0.50
		Laser	0,0	2.05 - 3	0.142	1.4 - 2	~0.135	0.85
		ST-a	0,0	4.3 - 3	0.142	3.0 - 2	0.065	1.22
		Calc.	0,0	2.85 - 3	0.142	2.0 - 2	0.097	1.00(L)
BeO	B $^1\Sigma$ - X $^1\Sigma$	Calc.	0,0	2.23 - 3	0.894	2.49 - 3	1.37	0.50(L)
		ST-e	0,0	1.89 - 3	0.894	2.11 - 3	-	0.46
MgO	B $^1\Sigma$ - X $^1\Sigma$	Calc.	0,0	9.26 - 3	0.983	9.42 - 3	0.400	1.00(L)
		Rocket	0,0	1.3 - 3	0.983	1.32 - 3	2.92	0.37
BaO	A $^1\Sigma$ - X $^1\Sigma$	Calc.	0,0	7.72 - 5	0.0098	7.88 - 3	1.15	1.00(L)
			4,0	1.41 - 3	0.160	8.81 - 3	1.15	1.00(L)
SrO	A $^1\Sigma$ - X $^1\Sigma$	Calc.	0,0	1.45 - 3	0.284	5.11 - 3	3.0	1.00(L)
			0,1	1.98 - 3	0.412	4.81 - 3	3.0	1.00(L)
			2,0	1.21 - 3	0.212	5.71 - 3	2.9	1.00(L)
BO(α)	A $^2\Pi$ - X $^2\Sigma$	Calc.	0,0	2.08 - 4	0.038	5.47 - 3	2.03	1.00(L)
			0,2	1.06 - 3	0.228	4.65 - 3	1.96	1.00(L)
BO(β)	B $^2\Pi$ - X $^2\Sigma$	Calc.	0,0	1.82 - 3	0.180	1.01 - 2	0.10	1.00(L)
AlO	A $^2\Sigma$ - X $^2\Sigma$	Calc.	0,0	3.55 - 3	0.730	4.86 - 3	0.76	1.00(L)
		ST-a	0,0	Analysis pending		--	-	--
		Emission	0,0	2.70 - 3		3.70 - 3	1.00	0.87
		Cloud	0,0	--		~5.0 - 3	-	--

(a) 7.0 - 4 means 7.0×10^{-4}, etc.

(b) Constant R_e assumption; (L) means legislated value assigned for estimation and scaling.

blowoff technique. Thus a check on the AlO f-number independent of knowledge of the AlO concentration is feasible and worthwhile.

SiO ($A^1\Pi - X\ ^1\Sigma$). – New experimental results by Main, et al.[12,17] yield $F_e = 0.030 \pm 0.013$, from absorption in shock-tube-excited SiO. This compares reasonably well with $f_e = 0.020$ obtained by the laser blowoff experiments by Wentink, et al.[18] Both of the foregoing values are considerably larger than $f_e = 0.005$ given by Kivel and Camm,[19] which probably is a lower limit due to chemical reaction complications.[18] The reasonable agreement between the shock-tube and laser experiments suggests that the laser work should be pursued for other refractory molecules. This is because a major problem in shock-tube studies of the very low vapor pressure compounds is determination of the concentration, and in the laser studies no knowledge of the absolute concentration is needed.

BaO and SrO. – The moecules BaO and SrO were also examined in terms of the expected magnitude of the molecular absorption and emission transition probabilities and for comparison with the behavior of the natural and ionized atoms. These results are pertinent to both the laser probe and the study of artificial clouds excited by solar radiation (chemical releases). Results of the calculations are presented in Table 6, the comparisons being made in terms of the integrated scattering coefficient, α_λ, where

$$\alpha_\lambda = \frac{\pi e^2}{mc^2} \lambda^2 f_{mnv'v''} \qquad (1)$$

In the table, the atomic α_λ data were taken from the survey of Sauermann and Schultz,[20] which also gives the detailed development of the expression for α_λ. The comparison of α_λ (atom) to α_λ (molecular band) highlights the fact that, in situations where an atomic line, especially a resonance line, is spectrally accessible and where the molecule may be appreciably dissociated, the atomic line represents a better candidate for laser sampling. It should be borne in mind that, in the above molecular discussions, band f-values have been cited. These, in turn, are greater than (but not equal to the sums of) the f-numbers of the rotational lines comprising the band. Even in cases of very strong bands such as CO (4+) and CN (violet), the individual rotational lines have low transition strengths compared to the atomic transitions.

LaO ($B\ ^2\Sigma - X\ ^4\Sigma$). — LaO and the homologous molecules ScO and YO are of astrophysical interest, and are additional cases where the characterization of the ground electronic state has been doubtful. Walsh[21] has determined that the ground state is a $^4\Sigma$ state. This is the lower state of the so-called "yellow-green" system $B\ ^2\Sigma - X\ ^4\Sigma$, wherein the 0,0 band is at 5600Å. Walsh presented preliminary absolute intensity data of f_e (f of system) of the order of 0.1, and the lifetime of the B state of approximately 50 nanoseconds. It is suggested that laser blowoff from a La_2O_3 target and measurement of the radiative lifetime would permit refinement or checks on this preliminary estimate.

7. Methane and decomposition products (CH_n). — Methane (CH_4) is of considerable interest in several planetary atmospheres, but only the

TABLE 6

RESONANCE SCATTERING CROSS SECTIONS OF ALKALINE EARTH METALS AND OXIDES

Atom or Molecule	λ,Å	Transition (v',v")[b]	$10^{22}\sigma_\lambda$,cm^3	$\tau_{v'}$,μs	$\frac{\sigma_\lambda(\text{atom})}{\sigma_\lambda(\text{molecule})}$[a][b]
Mg I	2852	resonance line	12.0		----
Mg II	2796		3.7		----
Mg II	2803		2.0		----
MgO	5007	B $^1\Sigma$ - X $^1\Sigma$ (0,0)	0.21[c]	0.40[c]	59
MgO	28500	A $^1\Sigma$ - X $^1\Sigma$ (0,0)	----	----	----
Ba I	5536	resonance line	41.0		----
Ba I	3501		3.7		----
Ba II	4554		12.0		----
Ba II	4934		7.0		----
BaO	5350	A $^1\Sigma$ - X $^1\Sigma$ (4,0)	0.036[c]	1.2[c]	1140
Sr I	4607	resonance line	27.0		----
Sr II	4078		8.3		----
Sr II	4215		4.2		----
SrO	8259	A $^1\Sigma$ - X $^1\Sigma$ (2,0)	0.073[c]	2.9[c]	370

a: σ_λ (atom) is for the line with largest listed σ_λ for the neutral atom.

b: σ_λ (molecule) is for the entire band with v'v" given in column 3.

c: Estimated for constant transition moment of 1 Debye unit; resulting probable maximum uncertainty in σ_λ and radiative lifetime $\tau_{v'}$ is factor of 4.

ground state (infrared) spectrum is well-characterized. There are apparently several unclassified electronic transitions in the vacuum ultraviolet that together yield continuous absorption which peaks at 930Å.[22] No lifetime, intensity, or high resolution data on this continuous region are known.

Electron impact on, or photodecomposition of, CH_4 can lead to appreciable quantities of CH_3 CH_2, and CH in the higher altitudes of a planetary atmosphere. Herzberg's Bakerian Lecture[23] of 1960 was an excellent exposition of the spectroscopy of CH_3 and CH_2. Unlike CH_4, the various electronic states have been identified and characterized, but again no lifetime or intensity data for any of the excited states or accompanying transitions are known.

The ground state (chemical) lifetime of CH_2 is evidently very short (less than 100 times the collision time) so that, once formed, it survives for more than a few microseconds only at pressures below about 0.01 mm Hg. When all factors are considered, it is concluded that CH_3 and CH_2 do not appear to be promising candidates for detection by resonant scattering of laser radiation.

The CH radical is more interesting in that relatively few electronic states exist at low energies, and the known three-band systems all involve the ground state. As such, most of the total population of any available excited CH will be restricted to levels yielding band systems located in the near ultraviolet and visible regions.

The absolute intensity data on the A $^2\Delta$ - X $^2\Pi$, B $^2\Sigma$ - X $^2\Pi$, and C $^2\Sigma^+$ - X $^2\Pi$ systems of CH were reviewed recently by Wentink, et al.[24] A subsequent compilation by Fink and Welge[25] essentially confirmed the transition probabilities and the heats of formation and dissociation of CH deduced by Linevsky.[26] In addition the Fink and Welge results confirm the radiative lifetime of the A state and refine the less precise B state results reported earlier by Bennett and Dalby.[27] The Fink-Welge analysis is slightly remiss in that the available $q_{v'v''}$ of Childs (Reference C-1 of Appendix A) was not considered; these were included in the present investigation in extending the Fink-Welge calculations as shown in Table 7.

B. Franck-Condon Factors and r-centroids

The availability of the Franck-Condon factors $q_{v'v''}$ and r-centroids $r_{v'v''}$ are discussed below and in Appendix A.

The $q_{v'v''}$ or so-called square of the overlap integral, is defined by and evaluated through the expression

$$q_{v'v''} = \left| \int_0^\infty \psi_{v'} \, \psi_{v''} \, dr \right|^2 \qquad (2)$$

where the ψ's are the vibrational wavefunctions of levels v' and v'' and r is the internuclear distance of the diatomic molecule. These $q_{v'v''}$ exert the dominant effect on the intensity variation among bands of an electronic band system. The corresponding r-centroid is defined by and similarly evaluated through the expression

TABLE 7

ABSOLUTE INTENSITY CONSTANTS OF CH BAND SYSTEMS.

	System and Transition		
	4315Å System $A\ ^2\Delta \rightarrow X\ ^2\Pi$	3900Å System $B\ ^2\Sigma^- \rightarrow X\ ^2\Pi$	3143Å System $C\ ^2\Sigma^+ \rightarrow X\ ^2\Pi$
$\tau_{v'} = 0$, μs	0.56 ± 0.06^{a} 0.54 ± 0.04^{b}	1.0 ± 0.4^{a} 0.40 ± 0.06^{b}	0.12^{c-d}
f_{mn00}	4.9×10^{-3} c-a 5.2×10^{-3} b	9.5×10^{-4} c-a 2.4×10^{-3} c-b	6.0×10^{-3}d
f_{mn}(at 0,0)	4.9×10^{-3} c-a 5.2×10^{-3} b	1.2×10^{-3} a 1.6×10^{-3} c-a 1.6×10^{-3} b 2.8×10^{-3} c-b 4.0×10^{-3} d 3.0×10^{-3} d	6.0×10^{-3}d
$R_{v'v''} = R_e$, Debye	1.36^{c-a}	1.15^{c-b}	1.6^{c-d}
λ_{00}, Å	4314	3889	3143
q_{00} used	0.9996	0.5937	1.000

a: BD Results[27]

b: FW Results[25]

c: Our calculations from corresponding τ listed, on basis of constant transition moment.

d: Linevsky Results[26]

$$\bar{r}_{v'v''} = \frac{\int_0^\infty \psi_{v'}\, r\psi_{v''}\, dr}{\int_0^\infty \psi_{v'}\, \psi_{v''}\, dr} \qquad (3)$$

Thus, the $\bar{r}_{v'v''}$ is the "characteristic" internuclear distance associated with the transition $v' \rightleftarrows v''$. Since the denominator is $(q_{v'v''})^{1/2}$, for very small $q_{v'v''}$ (say 0.005 or less), there may be large computational errors involved in $\bar{r}_{v'v''}$. However, possible errors will not be treated further since the emphasis of the present survey involves compilation of references to serve as an initial source of data.

The results of several other such surveys require updating such as those of Spindler[28] and Nicholls[29] who tabulated known $q_{v'v''}$ values. In the latter compilation, 29 of the 87 arrays listed were published as of 1964 although many of these have since become available. The Nicholls work is particularly noteworthy and useful since it provides graphs which can be employed by interpolation to deduce Morse $q_{v'v''}$ for other band systems (where a transition parameter $t = \beta\Delta r_e$ can be calculated for the system desired). In turn, in Table 1 of Appendix A, additional unpublished data are presented which were obtained through reports or personal communications. Main and Bauer[30] presented a summary of many available source of $q_{v'v''}$ but only covered molecules related to hydrocarbon-air mixtures. A recent paper by Ortenberg and Antropov[31] represents an excellent survey of $q_{v'v''}$ through about 1965.

The present survey differs from the above available results in that it covers the literature through mid-1967 and known sources of $\bar{r}_{v'v''}$ are included.

The history from 1930 of the methods employed to evaluate $q_{v'v''}$ has been traced by Nicholls.[32] This chronology includes the early work on an array for RbH in 1939, when Gaydon and Pearse performed numerically exacting and tedious calculations. Since then and particularly with the advent of the modern digital computer, there has been a steady flow of publication of arrays for many diatomic molecules. Hence, there is no need for further justification of the calculations or discussion of the analytical basis for the various machine codes that have made these computations routine. Ortenberg and Antropov[31] have also reviewed the different approximations involved in the various methods for calculating $q_{v'v''}$ and $\bar{r}_{v'v''}$.

However, some problems exist especially associated with the earlier works. Frequently the computer capacity and number of significant figures available were small, so that the matrix size was limited, or for some v'' or v' the progression was incomplete (i.e., $\sum_{v''} q_{v'v''}$ or $\sum_{v'} q_{v'v''}$ less less than unity, the theoretical limit). This is a result, usually for high v values, of the failure (or limit of the machine memory) to provide for the needed small interval in r to define the many-node vibrational wavefunctions (for example, see Childs[32a] or the early work of Ortenberg[33]). However, as in the case of Spindler's programs used with the IBM system 360 machine in double precision, 16 significant figure calculations and

with sufficiently small potential intervals (Δr) was performed. When the larger computers were employed, the remaining practical limit seems to be on the validity of the tabular input potential functions, as used in RKR-type calculations.

The numerous works of several Indian groups (e.g., Pathak, et al.[34]) should be considered with care. Some of the work is excellent; however, due evidently to lack of access to large computers, they frequently employed the 1953 approximate analytical methods of Fraser and Jarmain and, apparently, small calculators. As such, the results are often of limited use, especially in matrix size.

A basic factor in assessing the validity of the $q_{v'v''}$ or $\bar{r}_{v'v''}$ results involves the reliability of the spectroscopic data, either in determining the vibrational constants (like ω_e, X_e, etc.) or energy levels and the rotational constants yielding the internuclear distances. Thus, for any $q_{v'v''}$ or $\bar{r}_{v'v''}$ matrix, these constants should be evaluated criticallyas a first step in the procedure.

Under the present program time was spent cross-checking computer codes of various sources of $q_{v'v''}$. The codes of Spindler produce results for RKR potentials in excellent agreement with those of Zare and Benesch when identical experimental data and potential functions are employed. It should also be noted that the practically identical results are derived by Nicholls and Spindler for Morse $q_{v'v''}$. In Table 8 results for the N_2 Lyman-Birge-Hopfield system are presented for one such comparison. Of interest is the change in $q_{v'v''}$ due to change in

TABLE 8

RKR AND MORSE FRANCK-CONDON FACTORS FOR N_2 (LBH)

v''	v' = 0	1	2	3	4	5	6
0	4.079-2	1.111-1	1.676-1	1.831-1	1.616-1	1.230-1	8.368-2
	4.308	1.155	1.707	1.832	1.600	1.217	8.296
	4.315	1.162	1.713	1.885	1.603	1.214	8.287
1	1.476-1	1.921-1	1.016-1	1.495-2	4.703-3	4.335-2	8.080-2
	1.526	1.931	9.710-2	1.232	6.199	4.655	8.456
	1.517	1.932	9.677	1.212	6.391	4.706	8.542
2	2.446-1	8.421-2	1.932-3	7.098-2	9.726-2	5.036-2	6.344-3
	2.495	7.983	3.407	7.583	9.643	4.658	4.521
	2.477	8.049	3.276	7.554	9.661	4.668	4.538
3	2.526-1	9.193-5	1.027-1	7.192-2	1.317-3	3.008-2	7.002-2
	2.502	5.680-4	1.084	6.864	4.799-4	3.444	7.273
	2.492	4.018	1.074	6.931	5.812	3.392	7.289
4	1.797-1	8.565-2	8.857-2	2.594-3	7.460-2	5.845-2	4.060-3
	1.728	9.050	8.488	4.177	7.834	5.591	7.171
	1.731	8.732	8.598	3.606	7.744	5.670	2.192
5	8.970-2	1.895-1	1.063-3	9.453-2	3.826-2	7.743-3	6.187-2
	8.679	1.882	4.928-4	9.685	3.555	9.399	6.401
	8.808	1.851	8.554	9.511	3.735	8.364	6.347
6	3.293-2	1.786-1	6.666-2	6.630-2	1.732-2	7.931-2	1.506-2
	3.306	1.755	6.907	6.357	1.909	7.899	1.323
	3.399	1.752	6.451	6.580	1.689	7.882	1.485
7	9.422-3	1.024-1	1.682-1	2.922-4	9.806-2	7.184-3	4.122-2
	9.684	1.014	1.682	5.541	9.785	6.290	4.320
	1.017-2	1.032	1.640	1.481	9.667	7.912	4.042
8	2.213-3	4.086-2	1.617-1	8.293-2	3.445-2	4.947-2	5.384-2
	2.210	4.104	1.612	8.533	3.279	5.127	5.269
	2.392	4.250	1.614	7.840	3.615	4.675	5.502
9	4.252-4	1.223-2	9.205-2	1.667-1	1.153-2	8.464-2	2.774-3
	3.933	1.201	9.090	1.668	1.244	8.354	3.557
	4.454	1.289	9.406	1.632	9.168-3	8.536	2.010

TABLE 8 (continued)

v″	v′=0	1	2	3	4	5	6
10	5.924-5	2.825-3	3.584-2	1.423-1	1.165-1	5.683-3	8.151-2
	5.505	2.674	3.469	1.405	1.161	5.291	8.222
	6.389	2.968	3.718	1.431	1.085	7.958	7.874
11		4.745-4	9.868-3	7.195-2	1.647-1	4.727-2	4.084-2
		4.502	9.607	7.124	1.644	4.687	4.631
		5.266	1.060-2	7.518	1.626	3.911	5.144
12		5.273-5	1.947-3	2.444-2	1.138-1	1.490-1	4.167-3
		5.839	1.958	2.434	1.136	1.472	3.962
		7.250	2.253	2.675	1.179	1.402	1.628
13			2.757-4	5.889-3	4.905-2	1.499-1	1.022-1
			2.931	5.952	4.912	1.481	9.858-2
			3.629	6.824	5.304	1.499	8.717
14			3.002-5	9.791-4	1.371-2	8.088-2	1.652-1
			3.332	1.056-3	1.433	8.134	1.602
			4.459	1.285	1.632	8.715	1.569
15				1.053-4	2.479-3	2.668-2	1.168-1
				1.367	2.991	2.880	1.165
				1.811	3.597	3.262	1.221
16				6.484-6	2.966-4	5.772-3	4.739-2
				1.435-5	4.451	7.055	5.072
				1.919	5.812	8.443	5.632
17					3.113-5	9.404-4	1.272-2
					4.841	1.210-3	1.454
					6.957	1.566	1.721
18					6.356-6	1.604-4	2.827-3
					3.776	1.451	2.881
					6.169	2.116	3.672
19						3.066-5	5.238-4
						1.402	3.933
						2.092	4.605

In each block (given v′,v″) first entry RKR (Spindler) - unpublished
second entry RKR (Benesch, et al. - Ref. 37)
third entry Morse (Nicholls - Ref. 32)

The minus sign and integer following each first entry is the negative exponent of 10 applying to each value in the block, unless indicated otherwise.

potential functions. The first entry in each block (i.e., given v'v") of Table 8 is from Avco,[35] using an earlier RKR potential;[36] the second entry is from the University of Maryland,[37] using a revised RKR potential.[38] Since the Avco results for this potential are essentially identical, they are not tabulated. The third entry is for the Morse potential, identical from Avco[35] and NBS.[32] This comparison was made possible by the full cooperation of W. Benesch and R. Spindler.

C. Radiative Lifetimes and Collisional Quenching

In the following discussions. values of the spontaneous radiative lifetime (τ) are presented which are directly related to the transition probability. These allow the prediction of the emission intensity from a known population provided the excited state population is not depleted by the competition of the collisional deactivation. Thus, the cross sections for collision quenching also require tabulation.

The quenching can be stipulated by the Stern-Volmer[38] expression, which, as given in a readily available reference[39] is

$$\frac{1}{\tau_m} = \frac{1}{\tau} + \Gamma \tag{4}$$

where τ_m is the effective or measured lifetime at some pressure p and Γ is the number of effective quenching collisions/unit time, given by

$$\Gamma = 2n_B Q \left(\frac{kT}{\pi} \frac{M_A + M_B}{M_A M_B}\right)^{1/2} \tag{5}$$

where n_B, M_B, and Q are the number of molecules/cc, the mass of the quenching particle B, and the quenching cross section respectively. The quantity M_A is the mass of the excited particle A. While Q is usually of the order of 1 [illegible] it can vary considerably.

Although the survey of molecular quenching cross sections is still incomplete, some pertinent results are presented in Table 9.

Often, the Stern-Volmer equation does not fit the experimental data well; the low pressure (below ~ 50μ) results in the C $^3\Pi$ and D $^3\Sigma$ states of N_2 are examples. In these cases, the dependence of $1/\tau$ on pressure is non-linear and also leads to unreasonably large Q values. At present, the question remains open. The problem of chemical reaction of an excited state also complicates the quenching problem.

The effectiveness of collision varies significantly from one molecular state to another, even for the same molecule. For example, the A $^3\Sigma$ state of N_2 (yielding the Vegard-Kaplan bands) has a τ value of about 13 seconds[40] but apparently is extremely reactive and is deactivated (by reaction or radiationless decay) by almost every collision with N or NO. Another interesting case is the a $^1\Delta_g$ state of O_2 leading to the red band at 6340Å. It has a radiative lifetime[41] of about one hour and is remarkably stable, chemically. However, when two such atoms collide, the resulting complex $[O_2\ (^1\Delta_g)]_2$ has a τ value of 25 ms, a 10^5 increase in the radiative transition probability (leading to the X $^3\Sigma_g^-$ state).

TABLE 9

SOME MOLECULAR SPONTANEOUS RADIATIVE LIFETIMES AND QUENCHING CROSS SECTIONS

Molecular Radiating State		Band System Observed	τ	$10^{16}Q$, cm^2	Pressure Range Used	Major Quencher	Remarks	Ref.
OH	$A\ ^2\Sigma$	Violet	1.1μs	70 ± 15	0.2 - 22μ	H_2O		1
				110 ± 45	0.2 - 22μ	CH_3OH		1
N_2	$C\ ^3\Pi_u$	Second Positive	37±3 ns	2.2	15-250 mm	N_2	No data below about 15 mm.	2
			49±5 ns	10.2*	70-600μ	N_2	Unexplained deviations below 70μ.	3
N_2	?	Gaydon-Green	29 ns	1.0		N_2	Source state not known.	2
CO_2^+	$^2\Pi_u$	Fox-Duffenback-Barker	100 ns	13.5		CO_2		2
CO	$a'\ ^3\Sigma$	Asundi	~ 7μs	6.0 ± 2.5	10-70μ	CO	Averaged data from seven different bands.	4
CO	$d\ ^3\Delta$	Triplet	~4.5μs	7.0 ± 1.5	10-70μ	CO	Averaged data from five different bands.	4

References

1. Bennett, R.G. and Dalby, F.W., J. Chem. Phys. 40, 1414 (1964).
2. Anton, H., Ann. Physik 18, 178 (1966).
3. Jeunehomme, M., J. Chem. Phys. 44, 2672 (1966).
4. Data of Reference 24 (main text) converted; to be published in J. Chem. Phys.

*Calculated from quenching diameter given in Reference 3.

The effectiveness of quenching also depends on the quenching particle. For example, while for $O_2\ ^1\Delta_g$ the state is very stable in the presence of most all neutral molecules, the quenching is very much more rapid when due to ions or electrons.[41] Thus, in a final detailed analysis of the problem when the pressure is appreciable, the nature of the deactivating particle must be examined closely.

The τ values of many molecular states are shown in Figure 2 along with a scale indicating the time between collisions equivalent to one mean radiative lifetime. In addition, a curve is plotted from which the collision frequency for the terrestrial atmosphere can be deduced as a function of altitude. Similar curves should be prepared for each state and for other planetary atmospheres so that, when the collision quenching cross sections are known, one can determine the altitude at which a given molecular state has a reasonable opportunity for survival (significant population) for remote sensing, as in the laser probe method.

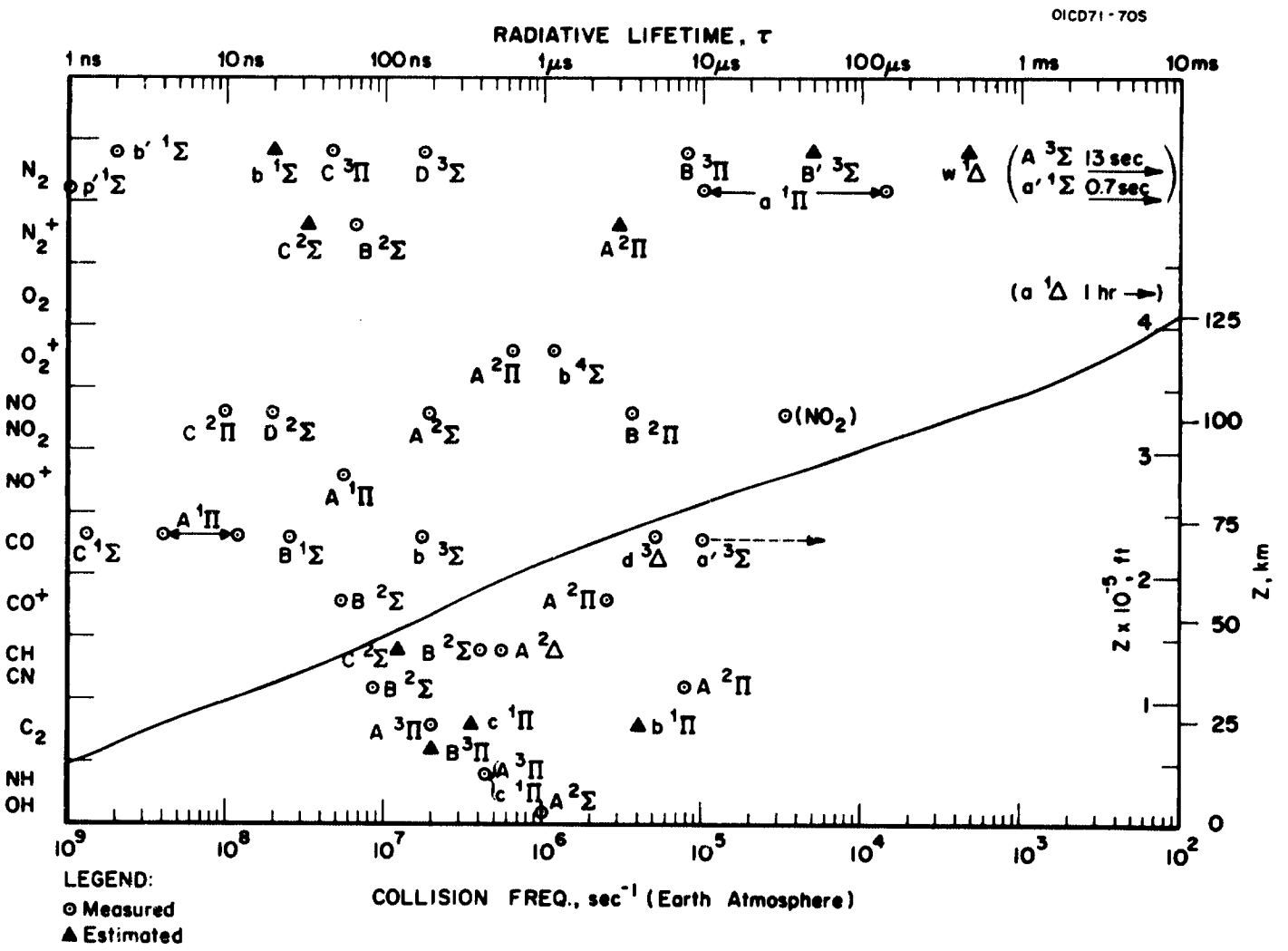

Figure 2. Molecular radiative lifetimes and collision frequencies.

III. MATHEMATICAL ANALYSIS OF LASER PULSE SOUNDING OF PLANETARY ATMOSPHERE

A. Introduction

In the following section a general analysis is presented of laser pulse probing of the atmosphere. In the discussions, independent values are assumed of the pulsewidth τ_p, the receiver time constant τ_r, the fluorescent time constant τ_F, as well as parametrically, the vertical distribution of the scattering species designated by τ_T. The results of the analysis are applicable to the variety of future laser communications and experimental situations. The optical pulsewidth, τ_p, is assumed to range between CW to 10^{-13} seconds. The receiver time constant τ_r is also assumed to be relatively variable between nanoseconds and present research attempt at lowering it to 10^{-11} to 10^{-13} seconds. The "fluorescent" lifetime can vary from extremely short times ($\sim 10^{-18}$ seconds) for Rayleigh and Mie scattering to seconds for metastable molecules.

At present, laser atmospheric probes are being developed to measure a variety of planetary atmospheric parameters and molecules. An increasing concern has been evidenced on absolute scale measurements and relating the signal returns more exactly to the appropriate region of the atmosphere.

The signal received during the time interval t_i to $t_i + \tau_r$ is obtained by integrating the signals obtained from each altitude R (or ct/2) with respect to R. The signal obtained from each altitude R is obtained by integrating the received signal over the time interval, τ_r.

The signal generation geometry dictates setting up the signal return from various zones and integrating as a function of range as shown in Figures 3 and 4.

The signal return for an effective time period τ_e which is less than τ_p or τ_r is given by

$$dS(R) = \frac{k(R)\ n(R)\ N_o\ E(R)\ dR}{4\pi\ R^2} \tag{6}$$

where

$$k(r) = \sigma\ \eta(R)\ T^2(R)\ Q(R) \tag{7}$$

$n(R)$ = absorbing centers at altitude R,

R = altitude (range),

σ = scattering cross section or resonant absorption cross section,

$\eta(R)$ = fluorescence efficiency,

$T(R)$ = one-way atmospheric transmission,

$Q(R)$ = quenching reduction factor,

$E(R)$ = efficienty factor of the fraction of light emitted at an altitude that goes into the recording interval t_i to $t_i + \tau_r$,

N_o = total number of photons in pulse.

B. Analysis of Various Fluorescence Situations

As a preliminary to the complete analysis for the laser situation which involves time-delays because of the space-time relation, the following discussion involves the fluorescence due to a system in which the fluorescent atoms are created uniformly over a period of time τ_p and

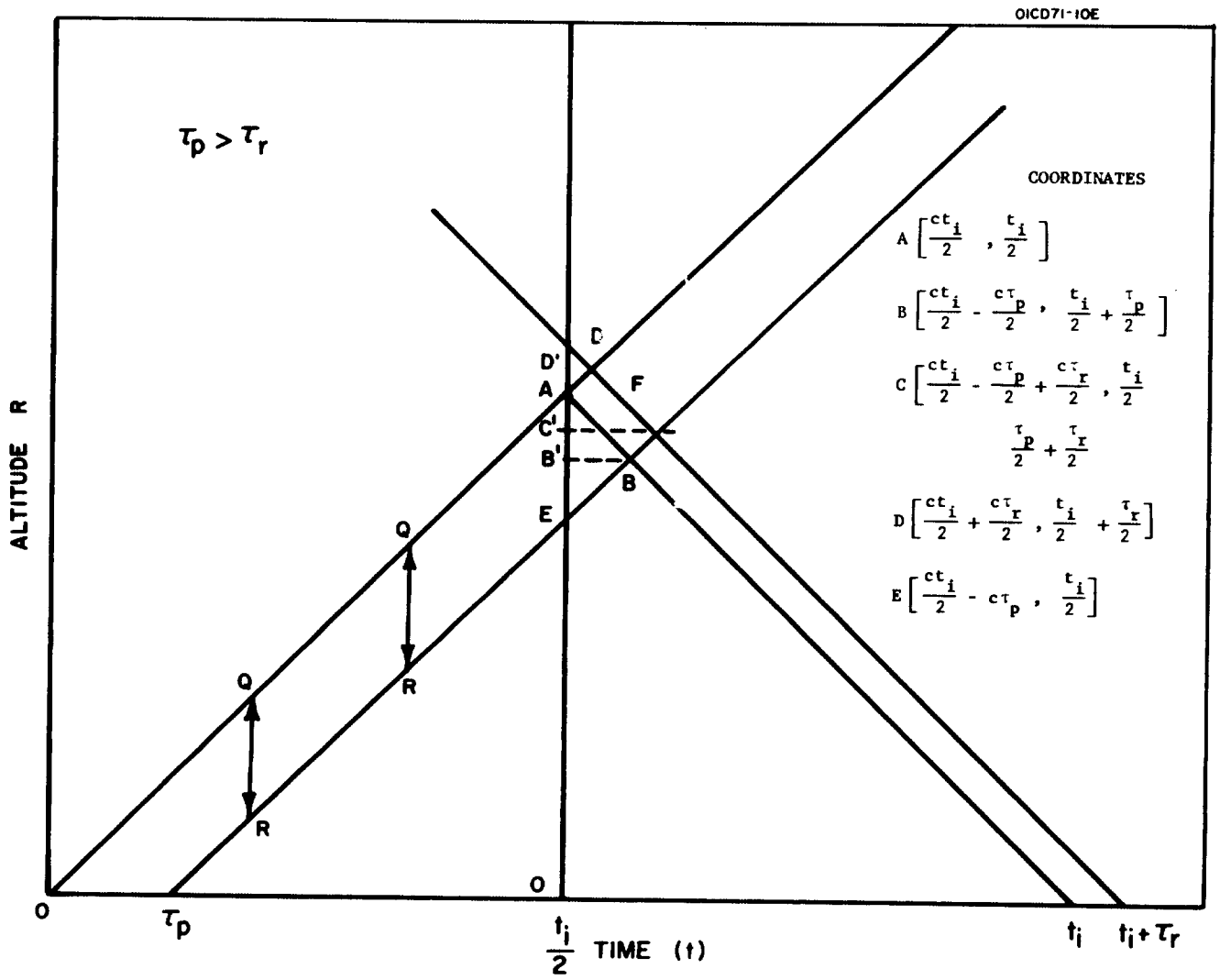

Figure 3. Schematic of laser scattering for $\tau_p > \tau_r$.

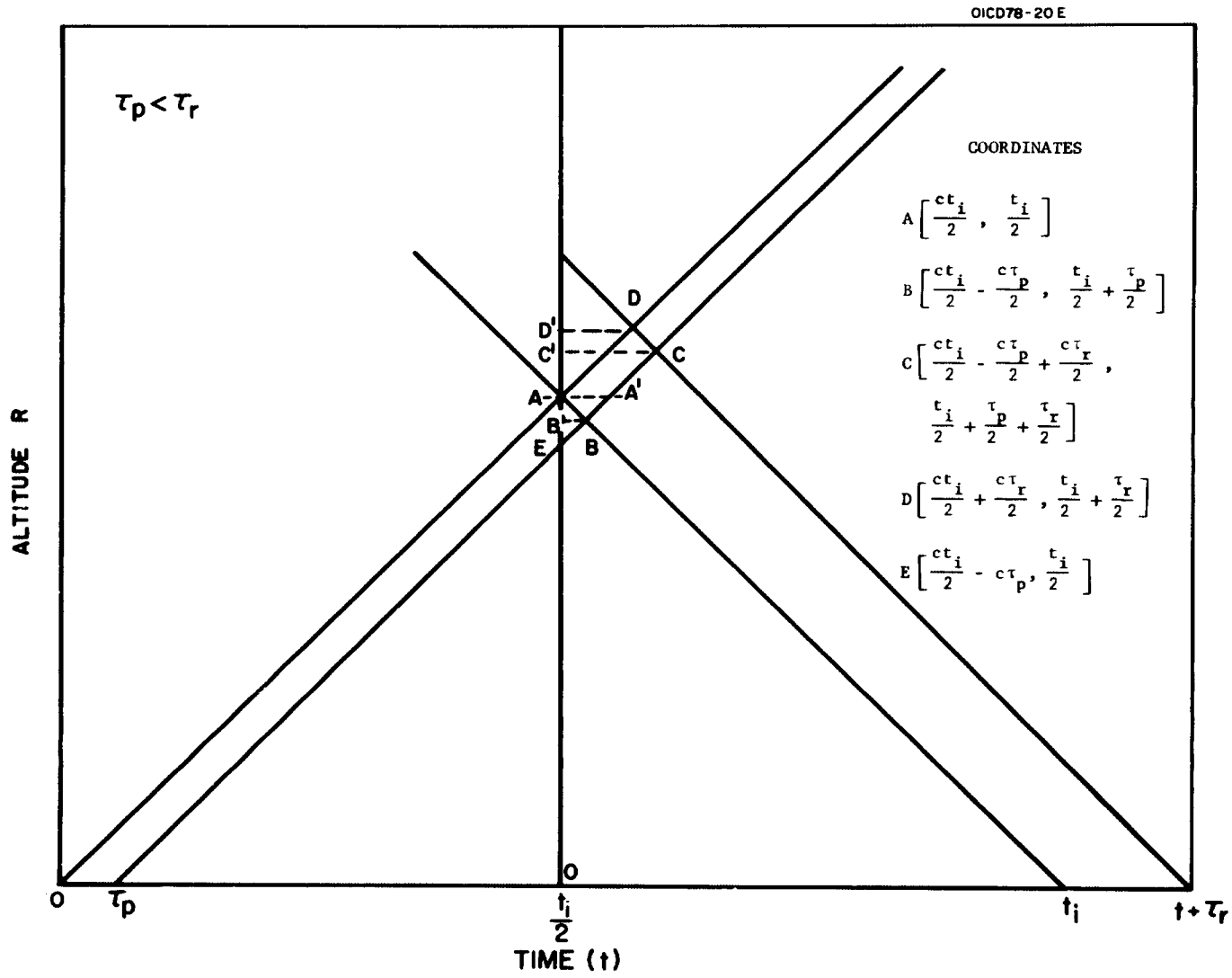

Figure 4. Schematic of laser scattering for $\tau_p < \tau_r$.

decaying over a time interval between t_i to $t_i + \tau_r$. The formulae will be employed subsequently in the report.

1. Simple decay of U_o fluorescent molecules in interval t_i to $t_i+\tau_r$.- The number of fluorescent atoms U at time, t_i, is given by the well known expression

$$U(t_i) = U_o \exp - (t_i/\tau_F) . \tag{8}$$

The fluorescence in the interval t_i to $t_i + \tau_r$ is given by

$$F = U(t_i) - U(t_i + \tau_r) = U_o \exp-(t_i/\tau_F) [1 - \exp(- t_r/\tau_F)] \tag{9}$$

as shown in Figure 5A.

If

$$t_i = 0, \quad F = U_o[1 - \exp(-t_r/\tau_F)] \tag{10}$$

as shown in Figure 5B.

If τ_r is small,

$$F = U_o \frac{\tau_r}{\tau_F} \exp (-t_i/\tau_F) . \tag{11}$$

2. Generation of fluorescent molecules at rate U_o/τ_p over time interval τ_p and decay into time interval t_i to $t_i + \tau_r$ (see Figure 5C) where $t_i \geq \tau_p$. - The fluorescence for this situation is given by replacing t_i by $t_i - T$ [Equation (9)] and integrating Equation (12)

$$F = \frac{U_o}{\tau_p} \int_o^{\tau_p} \exp- [(t_i - T)/\tau_F][1 - \exp (- \tau_r/\tau_F)] \, dT \tag{12}$$

or

$$F = U_o \frac{\tau_F}{\tau_p} [1 - \exp(-\tau_r/\tau_F)] [\exp(\tau_p/\tau_F) - 1] \exp(-t_i/\tau_F) \quad (13)$$

as shown in Figure 5C.

If $t_i = \tau_p$, then

$$F = U_o \frac{\tau_F}{\tau_p} [1 - \exp(-\tau_r/\tau_F)] [1 - \exp(-\tau_p/\tau_F)] \quad (14)$$

as shown in Figure 5D.

If $t_i = \tau_p$ and $\tau_r = \infty$, then

$$F = U_o \frac{\tau_F}{\tau_p} [1 - \exp(-\tau_p/\tau_F)] \quad (15)$$

as shown in Figure 5E.

3. Generation of fluorescent molecules at rate U_o/τ_p in time interval 0 to τ_p and decay in that interval 0 to τ_o. — The solution lies in recognizing that [Equation (10)] is applicable if U_o is replaced by U_o/τ_p and τ_r by $(\tau_p - T)$ where T is the variable of integration from 0 to τ_p

$$F = \frac{U_o}{\tau_p} \int_o^{\tau_p} [1 - \exp-(\tau_p - T)/\tau_F] \, dt \quad (16)$$

$$F = U_o \left\{ 1 - \frac{\tau_F}{\tau_p} [1 - \exp(-\tau_p/\tau_F)] \right\} \quad (17)$$

as shown in Figure 5F. The sum of Equations (15) and (17) equals U_o as it should.

4. Generation of fluorescent molecules at rate U_o/τ_p in time interval 0 to τ_p and decay in time interval t_i to $t_i + \tau_r$ where t_i and $t_i + \tau_r < \tau_p$. - The key here is the recognition that generation and decay in the time interval 0 to $t_i + \tau_r$ minus the decay in the interval 0 to t_i, caused by the generation in the interval 0 to t_i, yields the desired result. This is due to the fact that generation of fluorescent molecules after the recording interval is inconsequential. Making use of Equation (17):

$$F(0 \rightarrow t_i + \tau_r) = U_o\left\{1 - \frac{1}{t_i + \tau_r}\left[1 - \exp\left(-\frac{t_i + \tau_r}{\tau_F}\right)\right]\right\} \tag{18}$$

$$F(0 \rightarrow t_i) = U_o\left\{1 - \frac{\tau_F}{t_i}\left[1 - \exp(-t_i/\tau_F)\right]\right\} . \tag{19}$$

Subtracting yields

$$F(t_i \rightarrow t_i + \tau_r) = U_o\left[\frac{\tau_F}{t_i} - \frac{\tau_F}{t_i + \tau_r} + \frac{\tau_F}{t_i + \tau_r}\exp\left(\frac{t_i + \tau_r}{\tau_F}\right) - \frac{\tau_F}{t_i}\exp\left(-t_i/\tau_F\right)\right] \tag{20}$$

as shown in Figure 5G.

If $t_i = 0$ then

$$F(0 \rightarrow \tau_r) = U_o\left\{1 - \frac{\tau_F}{\tau_r}\left[1 - \exp\left(-\tau_r/\tau_F\right)\right]\right\} \tag{21}$$

as shown in Figure 5H.

If t_i τ_p and $t_i + \tau_r = \tau_p$, then

$$F(t_i \rightarrow \tau_p) = U_o\left[\frac{\tau_F}{t_i} - \frac{\tau_F}{\tau_p} + \frac{\tau_F}{\tau_p}\exp\left(-t_p/\tau_F\right) - \frac{\tau_F}{t_i}\exp(-t_i/\tau_F)\right] \tag{22}$$

as shown in Figure 5I.

5. Generation of fluorescent molecules at rate U_o/τ_p in time interval τ_p and decay in time interval t_i to $t_i + \tau_r$ where $t_i < \tau_p$ and $t_i + \tau_r > \tau_p$.- The fluorescence during this interval t_i to $t_i + \tau_r$ where $t_i < \tau_p$ and $\tau_p < t_i + \tau_r$ may be broken up into that during two subintervals: that from t_i to τ_p and that from τ_p to $t_i + \tau_r$. Both cases have been solved previously and are presented with proper change of time interval by Equations (22) and (14), respectively

$$F(t_i \rightarrow t_i + \tau_r) = U_o\left[\frac{\tau_F}{t_i} - \frac{\tau_F}{\tau_p} + \frac{\tau_F}{\tau_p}\exp\left(-t_p/\tau_F\right) - \frac{\tau_F}{t_i}\exp\left(-t_i/\tau_F\right)\right]$$

$$+ U_o\frac{\tau_F}{\tau_p}\left[1 - \exp - \left(t_i+\tau_r-\tau_p/\tau_F\right)\right]\left[1 - \exp\left(-\tau_p/\tau_F\right)\right] \quad (23)$$

as shown in Figure 5J.

As $t_i \rightarrow 0$ and $\tau_r \rightarrow \infty$; $F \rightarrow U_o$ as it should. When $t_i = 0$ and $\tau_r > \tau_p$

$$F(0 \rightarrow \tau_r) = U_o\left\{1 - \frac{\tau_F}{\tau_p}\left[1 - \exp\left(-\tau_p/\tau_F\right)\right]\right\}$$

$$+ U_o\frac{\tau_F}{\tau_p}\left[1 - \exp - \left(\tau_r-\tau_p\right)/\tau_F\right]\left[1 - \exp\left(-\tau_p/\tau_F\right)\right] \quad (24)$$

as shown in Figure 5K.

This completes the category of cases which are necessary for including fluorescence in the laser probing problem.

C. Analysis of Laser Atmospheric Probing Including Effect of Fluorescence

1. Analysis of complete scattering for situation $\tau_p \geq \tau_r$ and $\tau_F \geq 0$.- The complete analysis breaks down into the integration over four altitude regions as described below:

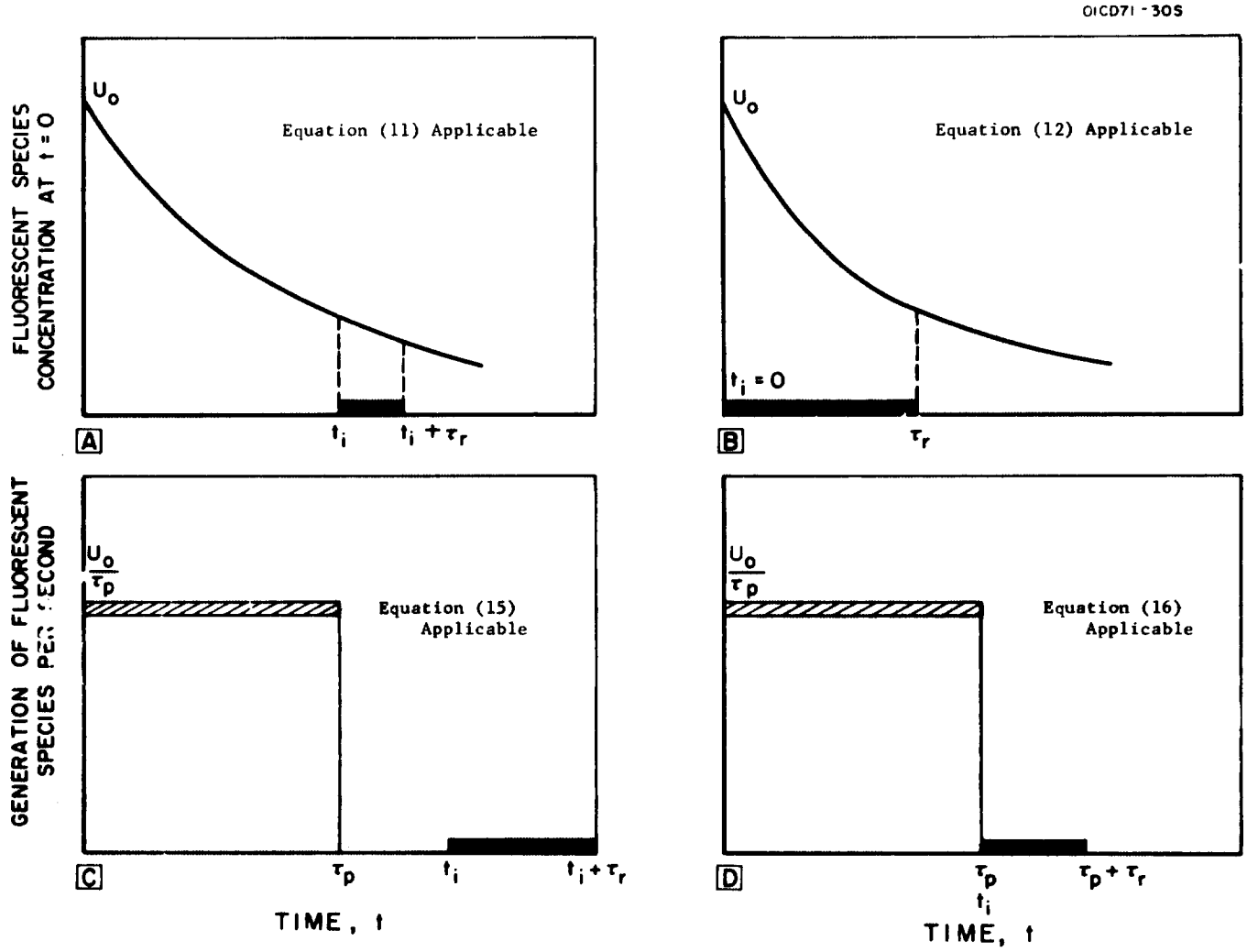

Figure 5. Diagram of fluorescence situations.

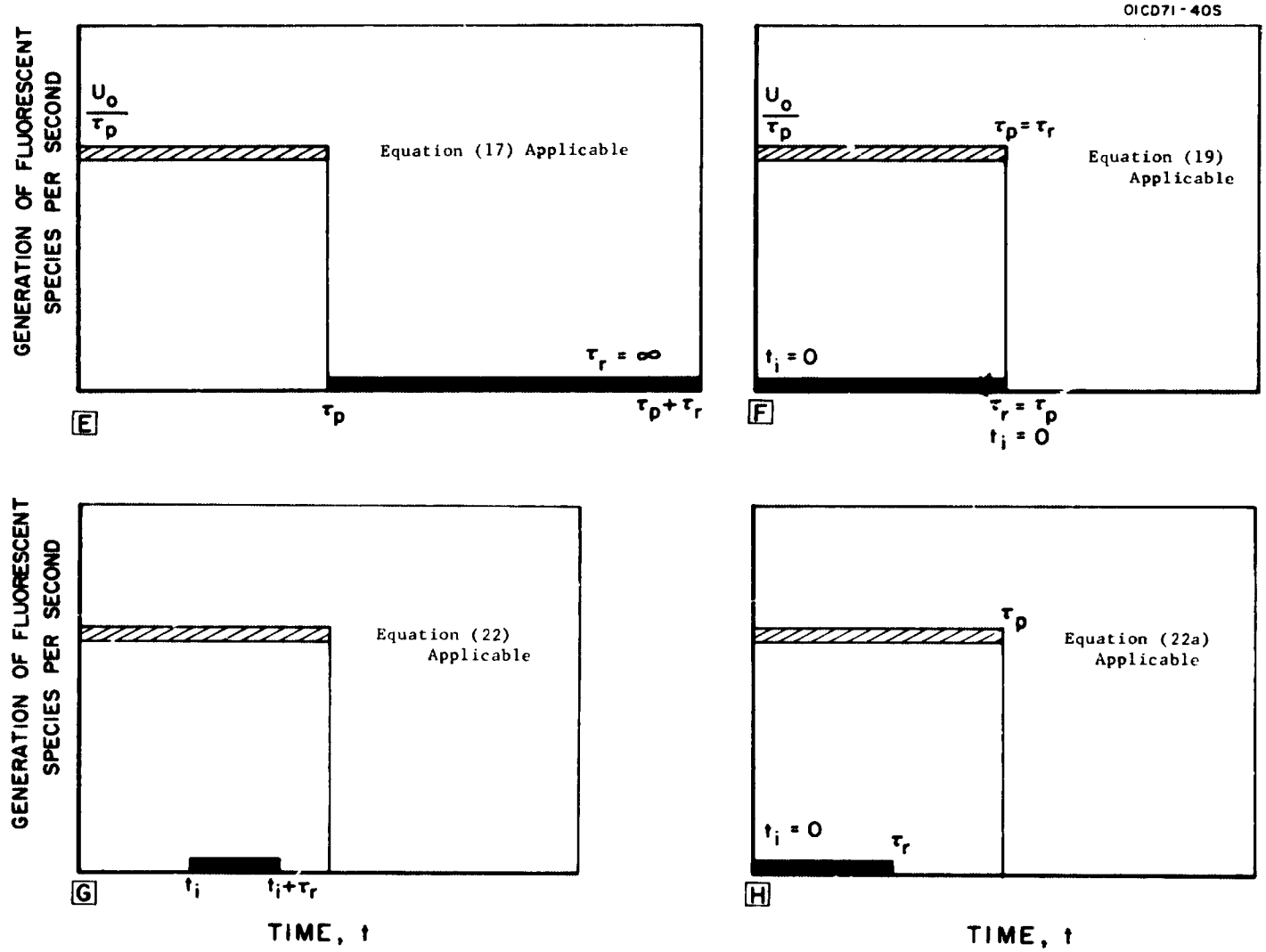

Figure 5. (continued)

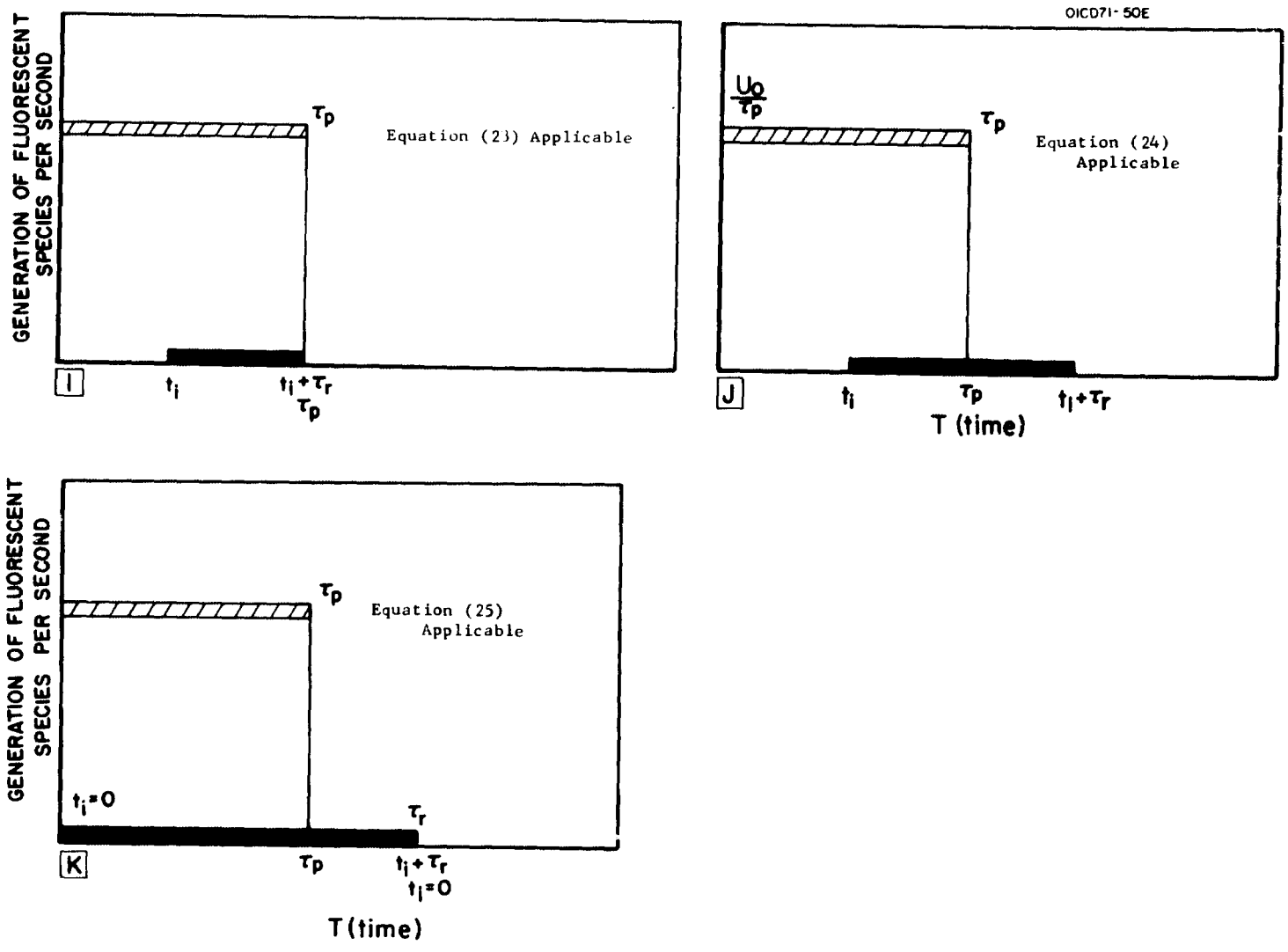

Figure 5. (continued)

Region	Altitude Designation in Figure 3	Limits
I	OB'	0 to $\frac{ct_i}{2} - \frac{c\tau_p}{2}$
II	$B'C'$	$\frac{ct_i}{2} - \frac{c\tau_p}{2}$ to $\frac{ct_i}{2} - \frac{c\tau_p}{2} + \frac{c\tau_r}{2}$
III	$C'A'$	$\frac{ct_i}{2} - \frac{c\tau_p}{2} + \frac{c\tau_r}{2}$ to $\frac{ct_i}{2}$
IV	AD'	$\frac{ct_i}{2}$ to $\frac{ct_i}{2} + \frac{c\tau_r}{2}$

The nature of the signal from each of these regions into t_i to $t_i + \tau_r$ is analyzed below.

Effective signal from Region I. — The governing equation is Equation (13) and the appropriate schematic is Figure 5C. The only transformation necessary is to replace t_i by $t_i - 2R/c$. The efficiency factor E(R) then becomes

$$E(R) = U_o \frac{\tau_F}{\tau_p} [1 - \exp(-\tau_r/\tau_F)][\exp(\tau_p/\tau_F) - 1] \exp\left(-\frac{t_i - \frac{2R}{c}}{\tau_F}\right) \quad (25)$$

with the integration limits given above.

Effective signal from Region II. — The governing equation is Equation (23) and the appropriate schematic is Figure 5I. In the atmospheric situation under consideration, t_i is originally outside the generating interval and then moves inside a distance τ_r. The transformation necessary in this regime is simple to replace t_i by $(t_i - 2R/c)$ in Equation (23).

The effectiveness factor then becomes

$$E(R) = U_o\left\{\frac{\tau_F}{t_i - \frac{2R}{c}} - \frac{\tau_F}{\tau_p} + \frac{\tau_F}{\tau_p}\exp\left(-\tau_p/\tau_F\right) - \frac{\tau_F}{\left(t_i - \frac{2R}{c}\right)}\exp\left(\frac{t_i - \frac{2R}{c}}{\tau_F}\right)\right\}$$

$$+ U_o\frac{\tau_F}{\tau_p}\left\{1 - \exp\left[-\frac{\left(t_i + \tau_r - \tau_p - \frac{2R}{c}\right)}{\tau_F}\right]\left[1 - \exp\left(-\tau_p/\tau_F\right)\right]\right\} \qquad (26)$$

The limits of integration are as given below.

Effective signal from Region III. – The governing equation is Equation (20) and the appropriate schematic is Figure 5G. The situation is one in which the recording interval is contained in the generating pulse and as R increases moves from the rear of the generating pulse to the front. The transformation necessary is to simply replace t_i by $(t_i - 2R/c)$. The effectiveness factor then becomes:

$$E(R) = U_o\left[\frac{\tau_F}{\left(t_i - \frac{2R}{c}\right)} - \frac{\tau_F}{\left(t_i - \frac{2R}{c}\right) + \tau_r} + \frac{\tau_F}{\left(t_i - \frac{2R}{c}\right) + \tau_r}\right.$$

$$\left. X\ \exp\left(-\frac{\left(t_i - \frac{2R}{c}\right) + \tau_r}{\tau_F}\right) - \frac{\tau_F}{\left(t_i - \frac{2R}{c}\right)}\exp\left(-\frac{\left(t_i - \frac{2R}{c}\right)}{\tau_F}\right)\right]. \qquad (27)$$

The limits of integration are as given above.

Effective signal from Region IV.– The governing equation and schematic is Equation (21) and Figure 5I. In the present case, however, the effective "τ_r" to get into the recording interval t_i to

$t_i + \tau_r$ changes from τ_r to 0 in the altitude regime. This is achieved by replacing τ_r by $\tau_r + (t_i - 2R/c)$. The efficiency factor at height R then becomes

$$E(R) = U_o \left\{ 1 - \frac{\tau_F}{\tau_r + (t_i - \frac{2R}{c})} \left[1 - \exp\left(- \frac{\tau_r + t_i - \frac{2R}{c}}{\tau_F} \right) \right] \right\} \quad (28)$$

The appropriate limits of integration are as given earlier.

Evaluation of total signal ($\tau_p > \tau_r$). - The total signal then is the sum of four integrals.

$$S = S_I + S_{II} + S_{III} + S_{IV} \quad (29)$$

where

$$S = \int_0^{\frac{ct_i}{2} - \frac{c\tau_p}{2}} B(R) \frac{\tau_F}{\tau_p} [1 - \exp(-\tau_r/\tau_F)] [\exp(\tau_p/\tau_F) - 1] \exp\left(- \frac{t_i - \frac{2R}{c}}{\tau_F} \right) dR$$

$$+ \int_{\frac{ct_i}{2} - \frac{c\tau_p}{2}}^{\frac{ct_i}{2} - \frac{c\tau_p}{2} + \frac{c\tau_r}{2}} B(R) \left\{ \left[\frac{\tau_F}{(t_i - \frac{2R}{c})} - \frac{\tau_F}{\tau_p} + \frac{\tau_F}{\tau_p} \exp(-\tau_p/\tau_F) - \frac{\tau_F}{(t_i - \frac{2R}{c})} \right.\right.$$

$$\left. \exp\left(- \frac{t_i - \frac{2R}{c}}{\tau_F} \right) \right] + \frac{\tau_F}{\tau_p} \left[1 - \exp\left(- \frac{t_i + \tau_r - \tau_p - \frac{2R}{c}}{\tau_F} \right) \right]$$

$$\left. \left[1 - \exp(-\tau_p/\tau_F) \right] \right\} dR \quad (30)$$

$$+ \int_{\frac{ct_i}{2} - \frac{c\tau_p}{2} + \frac{c\tau_r}{2}}^{\frac{ct_i}{2}} B(R)\left\{ \frac{\tau_F}{(t_i - \frac{2R}{c})} - \frac{\tau_F}{(t_i - \frac{2R}{c}) + \tau_r} + \frac{\tau_F}{(t_i - \frac{2R}{c}) + \tau_r} \right.$$

$$\exp\left(- \frac{(t_i - \frac{2R}{c}) + \tau_r}{\tau_F} \right) - \frac{\tau_F}{(t_i - \frac{2R}{c})}$$

$$\left. X \ \exp\left(- \frac{t_i - \frac{2R}{c}}{\tau_F} \right) \right\} dR$$

$$+ \int_{\frac{ct_i}{2}}^{\frac{ct_i}{2} + \frac{c\tau_r}{2}} B(R)\left\{ 1 - \frac{\tau_F}{\tau_r + (t_i - \frac{2R}{c})} \left[1 - \exp\left(\frac{\tau_r + (t_i - \frac{2R}{c})}{\tau_F} \right) \right] \right\} dR$$

2. Analysis for complete scattering for situation $\tau_p < \tau_r$ and $\tau_F > 0$. — The complete scattering analysis breaks down into the integration over four altitude regimes similar to that for $\tau_p > \tau_r$ and $\tau_F > 0$. The various regions are described below:

Region	Altitude Designation in Figure	Limits of Integration
I	OB′	0 to $\frac{ct_i}{2} - \frac{c\tau_p}{2}$
II	B′A	$\frac{ct_i}{2} - \frac{c\tau_p}{2}$ to $\frac{ct_i}{2}$
III	AC′	$\frac{ct_i}{2}$ to $\frac{ct_i}{2} + \frac{c\tau_r}{2} - \frac{c\tau_p}{2}$
IV	C′D′	$\frac{ct_i}{2} + \frac{c\tau_r}{2} - \frac{c\tau_p}{2}$ to $\frac{ct_i}{2} + \frac{c\tau_r}{2}$

The nature of the signal from each of these regions into t_i to $t_i + \tau_r$ is analyzed below.

Effective signal from Region I. - The analysis and the resulting parameter and integral is the same as the case for $\tau_p > \tau_r$.

Effective signal from Region II. - The analysis and the resulting parameters and integral are the same (although the limits are different) as for the case where $\tau_p > \tau_r$.

Effective signal from Region III. - The governing equation is Equation (24) and the schematic representation is given in Figure 5K. The transformation necessary to apply to the atmospheric case is to replace τ_r by $\tau_r - (2R/c - t_i)$. The efficiency factor then becomes:

$$E(R) = U_o \left\{ 1 - \frac{\tau_F}{\tau_p} \left[1 - \exp\left(-\tau_p/\tau_F\right) \right] + \frac{\tau_F}{\tau_p} \left[1 - \exp - \frac{\left(\tau_r - \tau_p \left[\frac{2R}{c} - t_i\right]\right)}{\tau_F} \right] \right.$$
$$\left. \left[1 - \exp\left(-\tau_p/\tau_F\right) \right] \right\} \qquad (31)$$

The limits of integration have been given above.

Effective signal from Region IV. - The governing equation is Equation (21) and the schematic representation is given in Figure 5K and is the same as is the case for $\tau_r < \tau_p$ except for the limits of integration.

In the interest of completeness, although three out of the four integrals are the same as in the case for $\tau_r < \tau_p$, there is recorded below the value of the integral.

Evaluation of total signal for $\tau_r > \tau_p$. - The total signal then is

$$S = S'_I + S'_{II} + S'_{III} + S'_{IV} \tag{32}$$

$$S'_I = \int_0^{\frac{ct_i}{2} - \frac{c\tau_p}{2}} B(R)\,\frac{\tau_F}{\tau_p}\,[1 - \exp(-\tau_r/\tau_F)]\,[\exp(\tau_p/\tau_F) - 1] \exp\left(-\frac{t_i - \frac{2R}{c}}{\tau_F}\right) dR \tag{33}$$

$$S'_{II} = \int_{\frac{ct_i}{2} - \frac{c\tau_p}{2}}^{\frac{ct_i}{2}} B(R)\left\{\left[\frac{\tau_F}{(t_i - \frac{2R}{c})} - \frac{\tau_F}{\tau_p} + \frac{\tau_F}{\tau_p}\exp(-\tau_p/\tau_F) - \frac{\tau_F}{(t_i - \frac{2R}{c})}\exp\left(-\frac{t_i - \frac{2R}{c}}{\tau_F}\right)\right] + \frac{\tau_F}{\tau_p}\left[1 - \exp\left(-\frac{t_i + \tau_r - \tau_p - \frac{2R}{c}}{\tau_F}\right)\right][1 - \exp(-\tau_p/\tau_F)]\right\} dR$$

$$S'_{III} = \int_{\frac{ct_i}{2}}^{\frac{ct_i}{2} + \frac{c\tau_r}{2} - \frac{c\tau_p}{2}} B(R)\left\{1 - \frac{\tau_F}{\tau_p}[1 - \exp(-\tau_p/\tau_F)] + \frac{\tau_F}{\tau_p}\left[1 - \exp\left(-\frac{\tau_r - \tau_p - (\frac{2R}{c} - t_i)}{\tau_F}\right)\right][1 - \exp(\tau_p/\tau_F)]\right\} dR$$

$$S'_{IV} = \int_{\frac{ct_i}{2} + \frac{c\tau_r}{2} - \frac{c\tau_p}{2}}^{\frac{ct_i}{2} + \frac{c\tau_r}{2}} B(R)\left\{1 - \frac{\tau_F}{\tau_r + (t_i - \frac{2R}{c})}\left[1 - \exp\left(-\frac{\tau_r + (t_i - \frac{2R}{c})}{\tau_F}\right)\right]\right\} dR \ .$$

Comments on analysis. – First it must be said that while the final mathematical results appear forbidding [Equations (30) and (33)], this is essentially true because the mathematical apparatus was constructed to cover a relatively broad gamut of possibilities. For specific cases where one of the parameters is much less than the others, considerable simplification can result. Additionally, if τ_F is extremely large and τ_p and τ_r small for an appropriate distribution of n(R) the first integral may be dominant.

For the more complex situations, numerical evaluation will have to be resorted to particularly since the integral contains complex exponential terms and where the concentration of scattering centers n(R) or the quenching factor Q(R) are strongly altitude dependent. Finally, it should be noted that the complete analysis has been predicated on a square wave optical pulse as a reasonable approximation to the actual laser probe.

IV. ATMOSPHERIC RAMAN PROBING BY LASER

A. Spontaneous Atmospheric Raman Scattering

The employment of laser atmospheric probes for the observation of Raman scattered radiation offers numerous advantages, but an important disadvantage involving the intensity, which varies between 10^{-3} and 10^{-2} that of the corresponding Rayleigh scattered light. However, it should be noted that Rayleigh scattering of laser energy in the atmosphere has been observed by Fiocco and Grams[42] using laser pulses of about 2 joules and by workers at GCA* using pulses of about 0.2 joules. This intensity loss can be compensated partially by employing higher energy outputs and operating at lower wavelengths.

The present purpose is a brief examination of the feasibility of atmospheric probing using Raman scattering and to explore both the advantages of the general approach and the expected results.

Raman scattered radiation is shifted by the frequency of the vibration or rotation energy. The higher cross section rotational (S_{00}) and vibration-rotational (Q_{01}) transitions in O_2 and N_2 are listed in Table 10 which were obtained from Reference 43 as calculated from the molecular constants in Reference 44.

---

*Using a neodymium laser harmonic Raman (stimulated) shifted to the barium resonance line at 5535Å, laser probe resonance scattering has been observed of rocket released barium clouds at 103, 185, and 225 km. "Background" return from intermediate regions was consistent with density-resonance-Rayleigh cross section ratio and laser line width. Similar results, though not as conclusive, were observed with a laser tuned to the sodium resonance line used to probe for the natural sodium layer at about 90 km.

TABLE 10

STRONG ROTATIONAL AND VIBRATIONAL RAMAN TRANSITIONS IN ATMOSPHERIC OXYGEN AND NITROGEN

O_2 RAMAN TRANSITION FREQUENCIES IN cm^{-1}			N_2 RAMAN TRANSITION FREQUENCIES IN cm^{-1}		
J	$S_{00}(J)$	$Q_{01}(J)$	J	$S_{00}(J)$	$Q_{01}(J)$
1	14.38	1556.36	0	12.0042	2330.712
3	25.88	1556.20	1	20.0070	2330.674
5	37.37	1555.92	2	28.0098	2330.600
7	48.86	1555.51	3	36.0126	2330.488
9	60.34	1554.97	4	44.015	2330.338
11	71.81	1554.31	5	52.018	2330.151
13	83.27	1553.52	6	60.020	2329.927
15	94.71	1552.60	7	68.023	2329.665
			8	76.026	2329.366
			9	84.029	2328.029
			10	92.032	2328.655
			11	100.035	2328.244

Since optical measurements of wavelength are performed at essentially constant dispersion, this means that at the lower wavelength region of the spectrum the separation in wavelength of the exciting line (or Rayleigh scattered line) and the Raman scattered line is less than at the longer wavelengths. The higher cross section Raman lines would appear as shown in Table II if excited by a ruby laser harmonic. It can be seen that separating the rotational structure from the Rayleigh line would be possible only with a relatively narrow band (and hence lossy) filter or moderately high dispersion spectrograph. Likewise, there would result some overlapping of N_2 and O_2 rotational structure. The vibrational Raman lines of O_2 and N_2 are separated by approximately 200Å and 300Å, respectively from the Rayleigh line or rotational Raman lines as well as about 100Å separating the Raman lines themselves. This indicates that one of the distinct advantages of observing Raman scattering involves the fact that the shifted radiation is characteristic of the scatterer and as distinguished from the Rayleigh, dust, or aerosol scattering. The "noise" present will be that due to normal night airglow or intrinsic to the detector. A number of atmospheric constituents may be monitored simultaneously if the receiver has a dispersion capability and is used with several detectors.

Temperature can be determined by comparing the intensity of the Stokes lines with those of the anti-Stokes lines. In general, the Raman scattering intensity can be expressed as[45]

$$I = N_m \frac{64\pi^2}{3c^2} (\nu_o - \Delta\nu)^4 [P]^2_{nm} \qquad (34)$$

TABLE 11

WAVELENGTHS OF RAMAN SHIFTED RADIATION IN O_2 AND N_2 EXCITED BY 3471Å RADIATION.

Element	Transition	Shift cm^{-1}	Anti Stokes (Å)	Laser	Stokes (Å)
O_2	$S_{00}(11)$	71.81	3462.26	3471.0	3479.68
	$Q_{01}(9)$	1554.97	3293.20	3471.0	3669.09
N_2	$S_{00}(8)$	76.026	3461.86	3471.0	3480.19
	$Q_{01}(6)$	2329.927	3211.22	3471.0	3776.51

where N_m is the total number of molecules in the initial state, ν_o the frequency of the incident light, $\Delta\nu$ the Raman frequency shift and P_{nm} is the transition probability for $n \rightarrow m$ transitions given by

$$[P]^2_{nm} = \frac{(n+1)}{8\pi^2\Delta\nu} \frac{E^2}{45} \{[45\ (\alpha')^2 + 7(\gamma')^2]\ (1 + \cos^2\theta) + 6(\gamma')^2 \sin^2\theta\} \quad (35)$$

where $\alpha' = \partial\alpha/\partial Q$ and $\gamma' = \partial\gamma/\partial Q$ are the derivatives of the isotropic and anistropic portions of the polarizability tensor, respectively and where Q is the intermolecular vibration coordinate. (For intensities of individual rotation levels of these vibrational transitions see Reference 43.) For spontaneous Raman vibration transitions, the total band intensity is of interest rather than that of individual rotational transitions. In stimulated Raman scattering, the rotational structure of these vibrational transitions is important. Under the simplifying assumptions that $\gamma' = 0$ (not true for N_2 or O_2 but true for CH_4), then $I_o = cE^2$ so that scattering will be in the backward direction, and taking into account the temperature dependence of Raman scattering, the result is

$$[P]^2_{nm} = \frac{(n+1)\alpha'}{8\pi^2 c\ \Delta\nu} I_o \quad (36)$$

$n = 0$ for ground state, and

$$I = N \frac{8\ (\nu_o - \Delta\nu)^4\ \alpha'^2}{3c^3\ \Delta\nu\ [1 - \exp(-h\Delta\nu/kT)]} \quad (37)$$

where N is the total number of molecules present (let $\tilde{\nu} = \nu/c$ to compare Rayleigh scattering expression). The ratio of Raman to Rayleigh intensities (for symmetrical vibration of the total band) is

$$\frac{I\ (\text{Raman})}{I\ (\text{Rayleigh})} = \left(\frac{\nu_o - \Delta\nu}{\nu_o}\right)^4 \left(\frac{\alpha'}{\alpha}\right)^2 \frac{h}{8\pi^2\ \Delta\nu\ [1 - \exp\ (-\ h\Delta\nu/kT)\ ]} \qquad (38)$$

where ν is in frequency units.

The vibrational band intensity of the anti-Stokes radiation is of the same form as that of the Stokes intensity with $-\Delta\nu$ changed to $+\Delta\nu$, namely:

$$I_{AS} = N \frac{8(\nu_o + \Delta\nu)^4\ \alpha'^2}{3c^3\ \Delta\nu\ [1 - \exp\ (h\Delta\nu/kT)\ ]} \qquad (39)$$

The ratio of anti-Stokes radiation to Stokes radiation is then given by

$$\frac{I_{AS}}{I_S} = \left(\frac{\nu_o + \Delta\nu}{\nu_o - \Delta\nu}\right)^4 \exp\ (-\ h\Delta\nu/kT) \qquad (40)$$

From this it follows that

$$T = \frac{h\Delta\nu}{k}\ \ell n^{-1} \left\{\frac{I_S}{I_{AS}} \left[\frac{\nu + \Delta\nu}{\nu - \Delta\nu}\right]^4\right\} \qquad (41)$$

and

$$\frac{\Delta \frac{I_{AS}}{I_S}}{\frac{I_{AS}}{I_S}} = \frac{h\Delta\nu}{kT} \cdot \frac{\Delta T}{T} \qquad (42)$$

Unfortunately, for a vibrational transition in N_2 with $\Delta\nu = 2330\ cm^{-1}$, $\exp\ (-\ h\Delta\nu/kT)$ is approximately 10^{-5} for $T = 300^oK$. The situation is not so limited, however, if pure rotational structure is used. For S_{00} transition:[44,46]

$$\frac{I_{AS}}{I_S} = \frac{2J + 5}{2J + 1} \exp\ (- h\Delta\nu/kT) \qquad (43)$$

where $\Delta\nu = 4B\ (J + 3/2)$ (B is the moment of inertia constant). From this it follows that

$$T = \frac{h\Delta\nu}{k} \ell n^{-1} \left[\frac{2J + 1}{2J + 5} \frac{I_S}{I_{AS}}\right] \qquad (44)$$

and again

$$\Delta \frac{\frac{I_{AS}}{I_S}}{\frac{I_{AS}}{I_S}} \quad \frac{h\Delta\nu}{kT} \frac{\Delta T}{T} \qquad (42)$$

In this case for the S_{00} transition in N_2, $\exp\ (- h\Delta\nu/kT) = 0.694$ for $T = 300^{o}K$. The anti-Stokes lines and Stokes lines are comparable although the resolution problems noted above still exist.

Now some numerical values of the Raman/Rayleigh ratio are examined briefly for which α'-values are required. Some authors[47-49] quote a q-value defined as $\alpha' \times N^{-1/2} \times 10^{16}$ with the units of both q and α' being $cm^2\ gm^{-1/2}$. Others[43] cite a value more easily compared to the polarizability, namely

$$\frac{h\ \alpha'^2}{8\pi^2\ \Delta\nu\ [1 - \exp\ (- h\nu/kT)]}$$

If a term is now defined by $y = c\ \Delta\nu \times 10^{+3}$; i.e., y is the Raman shift in thousands of wavenumbers, then

$$\frac{h\ \alpha'^2}{8\pi^2\ \Delta\nu} = \frac{q^2}{y} \times 1.74 \times 10^{-50}\ cm^6$$

As an example of the ratio, consider methane (CH_4) at 300°K. The exponential is negligible, y ≈ 2.916 for the strong C-H stretching vibration, q is given[45] as 2.08 and α is 26.0×10^{-25} cm^3. As such,

$$\frac{I_{RAM}\ (CH_4)}{I_{RAY}\ (CH_4)} = \left(\frac{28.8 - 2.99}{28.8}\right)^4 \frac{\left(\frac{h\alpha'^2}{8\pi^2\ \Delta\nu}\right)}{\alpha^2} = 0.64 \times 0.0038 = 0.0024$$

For the $Q_{01}(6)$ transition in N_2, the line strength is given[43] as approximately 3×10^{-52} cm^6. However, since there are a total of 11 transitions listed (for 11 J values) a total band strength of approximately 3×10^{-51} cm^6 is assumed. With α (N_2) being 17.6×10^{-25} cm^6 the approximate Raman/Rayleigh ratio for N_2 is 0.001. The S_{00} transitions are individually about a factor of 5 stronger.

B. Stimulated Raman Scattering

Stimulated Raman scattering in the atmosphere must be considered in two aspects. First, it could possibly limit the transmission of high power laser radiation by causing much of the radiation to be shifted to new frequencies. Some work on this aspect has been performed previously[49,50] to demonstrate that this would not constitute a problem for power densities below about 2000 megawatts/cm^2. The other possibility involves the use of the stimulated Raman process for investigative purposes.

The following equation describes Raman-Stokes intensity buildup[49]

$$\frac{dI_1}{dx} = \gamma\ I_o\ I_1 + \left(\frac{d\sigma}{d\Omega}\right) I_o\ d\Omega \qquad (45)$$

The first term describes the buildup by stimulated Raman scattering, characterized by a gain coefficient γ. The process is initiated by ordinary spontaneous Raman scattering characterized by the solid angle $d\Omega$, the cross section $(d\sigma/d\Omega)$, and dependent on the intensity of the incident light. A relation exists between the gain coefficient and the cross section much the same as that between the Einstein A and B coefficients, which when inserted yiel · the intensity at the Stokes frequency as a function of the distance down the beam x.

$$I_1(x) = \frac{h\omega_1 \Delta}{4} \frac{d\Omega}{\lambda_1^2} [\exp(\gamma I_o x) - 1] \tag{46}$$

where Δ is the width of the Raman transition, and ω_1 and λ_1 the radian frequency and wavelength of the Stokes line, respectively.

Overcoming threshold in the atmosphere may be difficult for N_2, but if one has already overcome threshold; i.e., the laser is a Raman laser such that it emits equal powers at both ν_o (the basic laser frequency) and at ν_1 (the Raman shifted frequency) then observations are possible. Re-examination of the equations (neglecting now the spontaneous scattering) yields

$$\frac{dI_1}{dx} = \gamma I_o I_1 \tag{47}$$

If it is assumed that $I_o(0) + I_1(0) = 2A$ (const) and $I_o(0) = I_1(0) = A$ and scattering out of the beam as well as diffraction are neglected, then

$$\frac{dI_1}{I_1 (2A - I_1)} = \gamma \, dx \tag{48}$$

so that it follows directly that energy is transferred from I_o to I_1 as the waves progress down their path. At any distance x

$$\frac{I_1 - I_o}{I_1 + I_o} = \frac{\exp\ (2A\gamma x) - 1}{\exp\ (2A\gamma x) + 1} \tag{49}$$

If A = 100 megawatts/cm^2 and γ is employed for the 2360 shift of N_2[43,49] then

$$\frac{I_1 - I_o}{I_1 + I_o} = 0.05 \text{ for } x \cong 15 \text{ meters}$$

so that it would appear quite feasible to search for and map abundant species by the above method. In N_2, the highest gain Raman transition depends on pressure as shown in Figure 6. This change occurs because the stimulated gain depends on both density and Raman line widths.

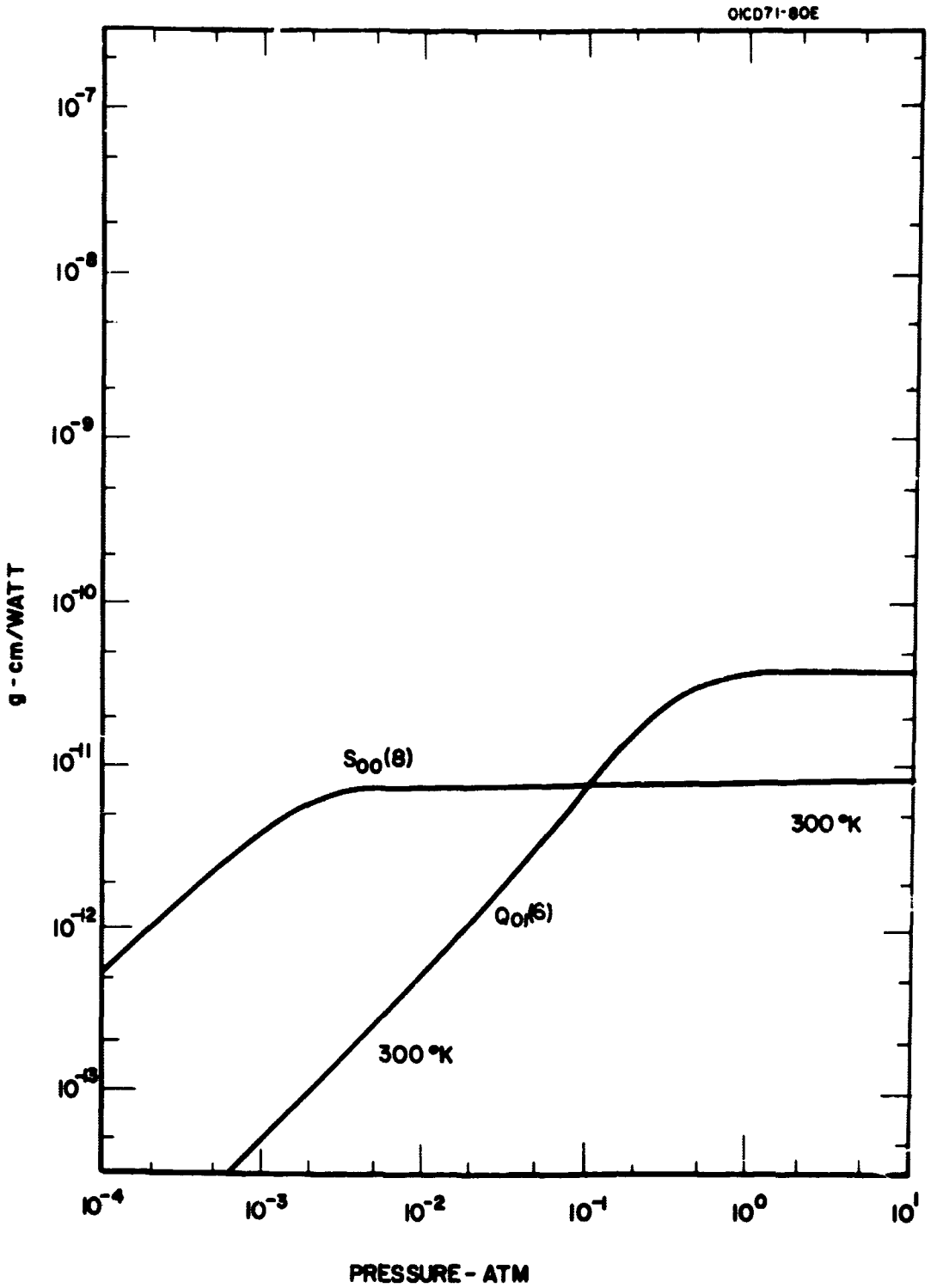

Figure 6. Normalized gain factors for stimulated Raman scattering in Nitrogen gas (adapted from Reference 43).

V. MEASUREMENT OF ISOTOPES BY LASER RESONANT SCATTERING IN THE ATMOSPHERE

The resonant scattering process is relatively attractive for laser atmospheric probing since by definition the cross-section for scattering (or absorption with subsequent re-emission) exhibits strong enhancement in a very confined frequency range. Thus, the scattering cross-section can exceed by over 10 orders of magnitude that of any other scattering process and can be easily validated by a small shift (~ 1Å) in the laser wavelength. The general theories of resonant scattering with particular application to laser atmospheric probing have been discussed numerous times.[51-54] In the present section, the evaluation of the line profiles of the resonance lines and the possible determination of relative isotopic abundances are of major interest. The initial evaluation involves the natually occurring isotopes of the alkali metals as discussed below.

A. Line Profiles and Preliminary Evaluation of Isotope Determination

The profiles of the spectrum of the D-lines of the alkali metals lithium, sodium, potassium, rubidium, and cesium are examined in detail. Although the evaluation has been limited to the naturally occurring isotopes of the species, the longer-lived radioactive isotopes of each element and those resulting from fission fragments will be noted.

Lithium. – The two naturally occurring isotopes of lithium are $_3Li^6$ (7.42 percent) and $_3Li^7$ (92.58 percent) with no long-lived radioactive isotopes. The effective contributions to the three peaks in the profile

(Figure 7) are due to a combination of the fine structure splitting and isotope shift.[55-57] It should be noted that equal abundances of Li-6 and Li-7 are assumed in Figure 7. The examined line is the 6708Å resonance line ($2p\ ^2P_{1/2,3/2} - 2s\ ^2S_{1/2}$ transition). There are two "lines" which are the classical D-lines of each isotope. The D_1 ($^2P_{1/2} - {}^2S_{1/2}$) line of Li-7 coincides (within the Doppler width) with the D_2 ($^2P_{3/2} - {}^2S_{1/2}$) line of Li-6 with the result that there are only 3 lines in the spectrum. (There is hyperfine structure - nuclear moment effect - as shown in Figure 8 but this is completely masked by the Doppler broadening.) The pair of lines due to one isotope is attributed to fine structure splitting and the shift of one pair with respect to the other pair is isotope shift. Since the three lines are separated by more than the Doppler width, they can be probed individually using a laser of sufficiently narrow spectral width. The problems involved in operation of a laser at this wavelength and obtaining the required narrow bandpass are discussed later in this report. The probing method would require tuning the laser to either one of the outer two components with no overlap into the central component. This is, of course, over-simplified; in practice, careful calculations of signal-to-noise must be made involving convolution integrals of the linewidth functions of the lithium lines and the laser probing line and of course weighted by the absorption cross-sections of the individual components.

Sodium. – There is only one naturally occurring isotope of sodium, namely $_{11}Na^{23}$. There is one realtively long-lived radioactive isotope $_{11}Na^{22}$ (β^+ 2.58 years) which does not occur in fission debris. A careful

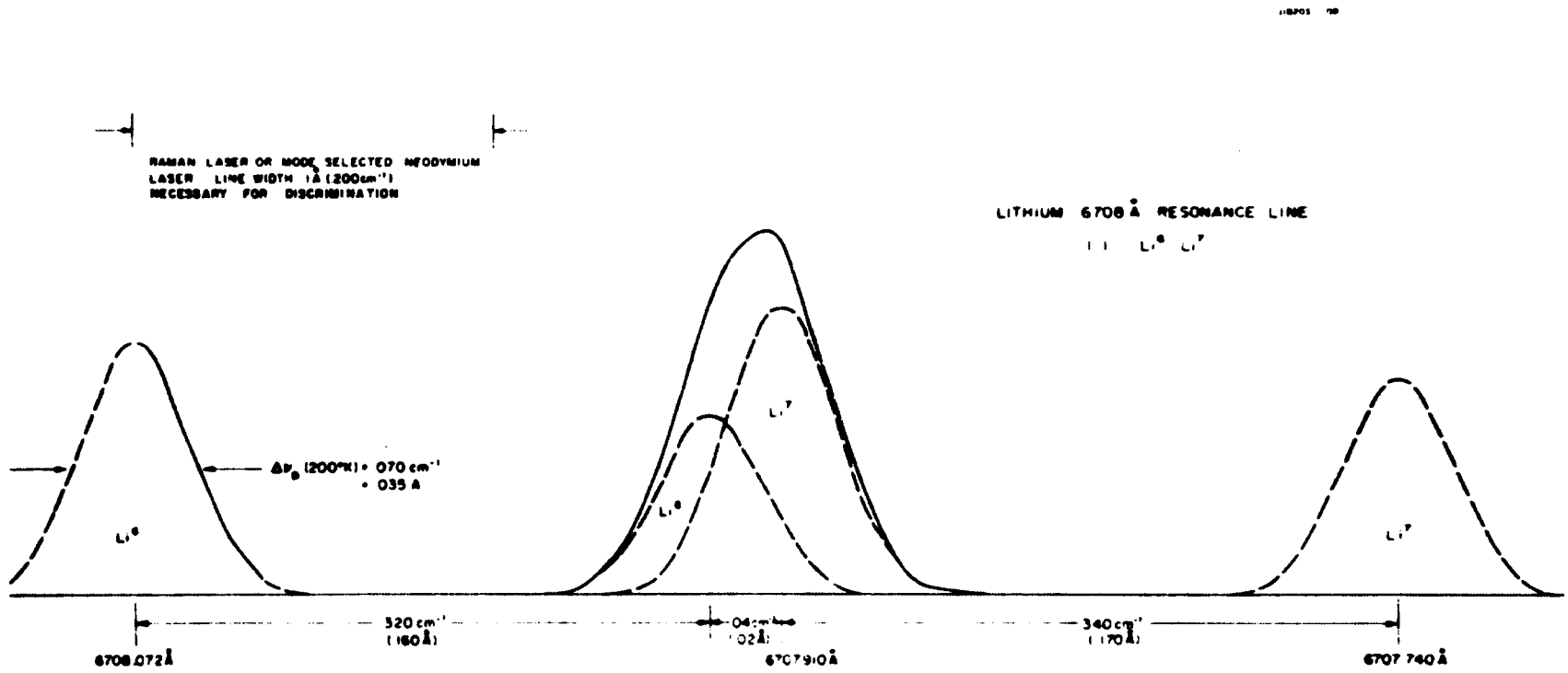

Figure 7. Lithium 6 and 7 natural resonance lines. Equal abundances of isotopes are assumed here.

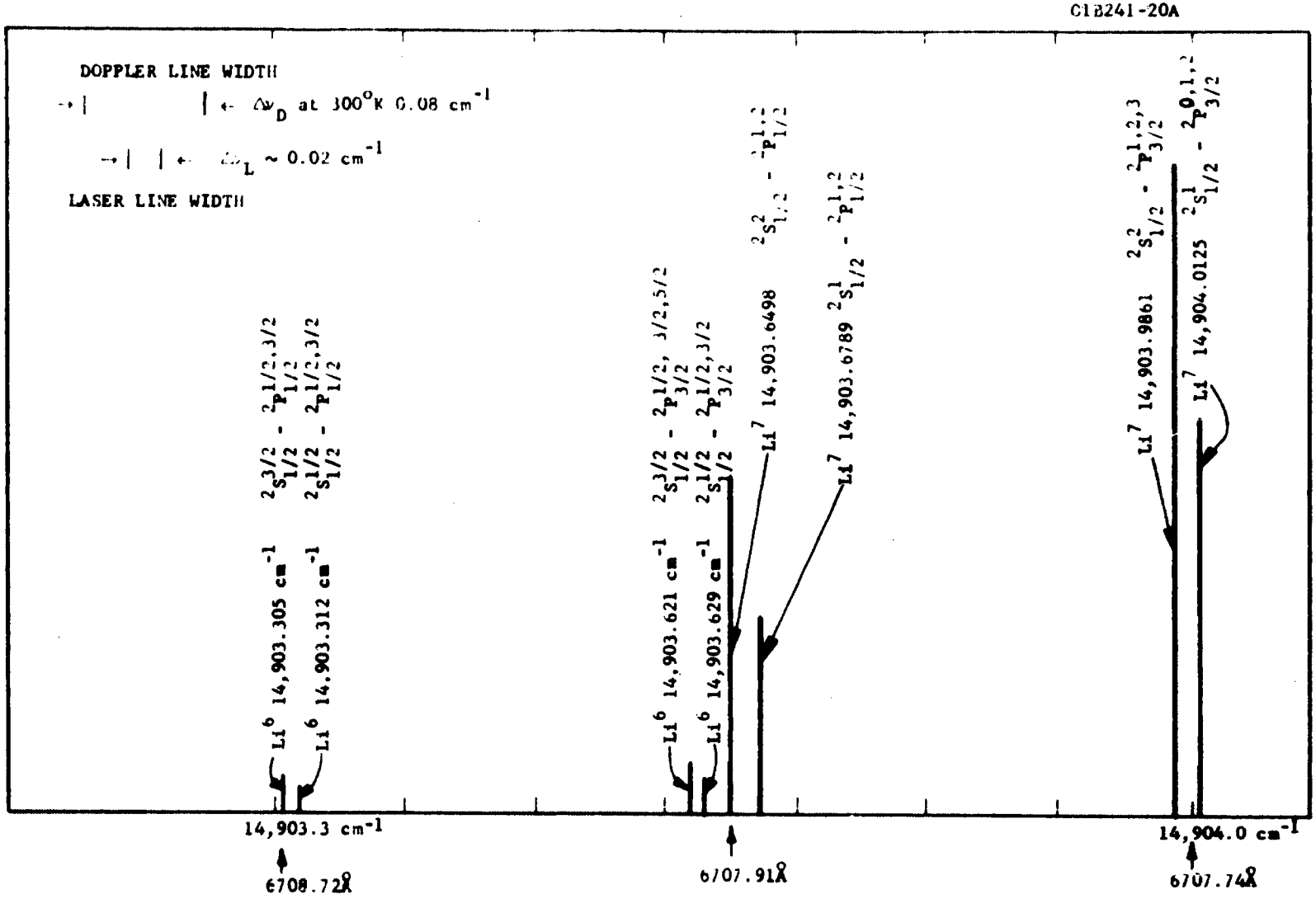

Figure 8. Structure of 6707.84Å resonance line of lithium showing fine structure, hyperfine structure and isotope shift. Superscripts indicate F levels. Height of lines show relative intensity in naturally occurring Li. Li^6(7.42%); Li^7(92.58%).

analysis of the hyperfine structure of Na^{23} is given in the energy level diagram of Figure 9 for the two D-line transitions.[57-60] From these data, the profiles of the D_1 line and D_2 line are presented in Figures 10 and 11. From these profiles drawn for a Doppler width at $0^{o}C$, it appears that the cross-section will not vary by more than a factor of 2 over a region of about 0.04Å. It should be noted here that even though the Doppler width is 0.04 cm^{-1}, the total effective useful probing line width is at least 3 times this width, so that the requirements on the laser are not overly stringent. Of course, with sodium no isotope discrimination is possible.

Potassium. – Of the naturally occurring potassium isotopes, two are stable $_{19}K^{39}$ (93.10 percent) and $_{19}K^{41}$ (6.88 percent) and one is radioactive $_{19}K^{40}$ (0.0118 percent, β^-, 1.3×10^9 yrs). There are no long-lived or fission product isotopes. The fine structure, hyperfine structure (moment effect), and isotope shift of the three naturally occurring potassium isotopes have been analyzed carefully under the current program. The energy level diagrams for each isotope for both the 5P - 4S and 4P - 4S transitions are shown in Figures 12, 13, and 14. The isotope shifts are shown with respect to K^{39} and the $5P_{3/2}$ level of each isotope (the isotope shifts should be shown with respect to the series limit; however, the isotope shift of the $5^2P_{3/2}$ level is negligibly small - if not zero - with respect to the information desired here). The K^{39} - K^{40} isotope shift is assumed to be one-half of the K^{39} - K^{41} isotope shift which is both reasonable and consistent with both observations of other isotope shifts and the formula for the mass dependent isotope shift. The

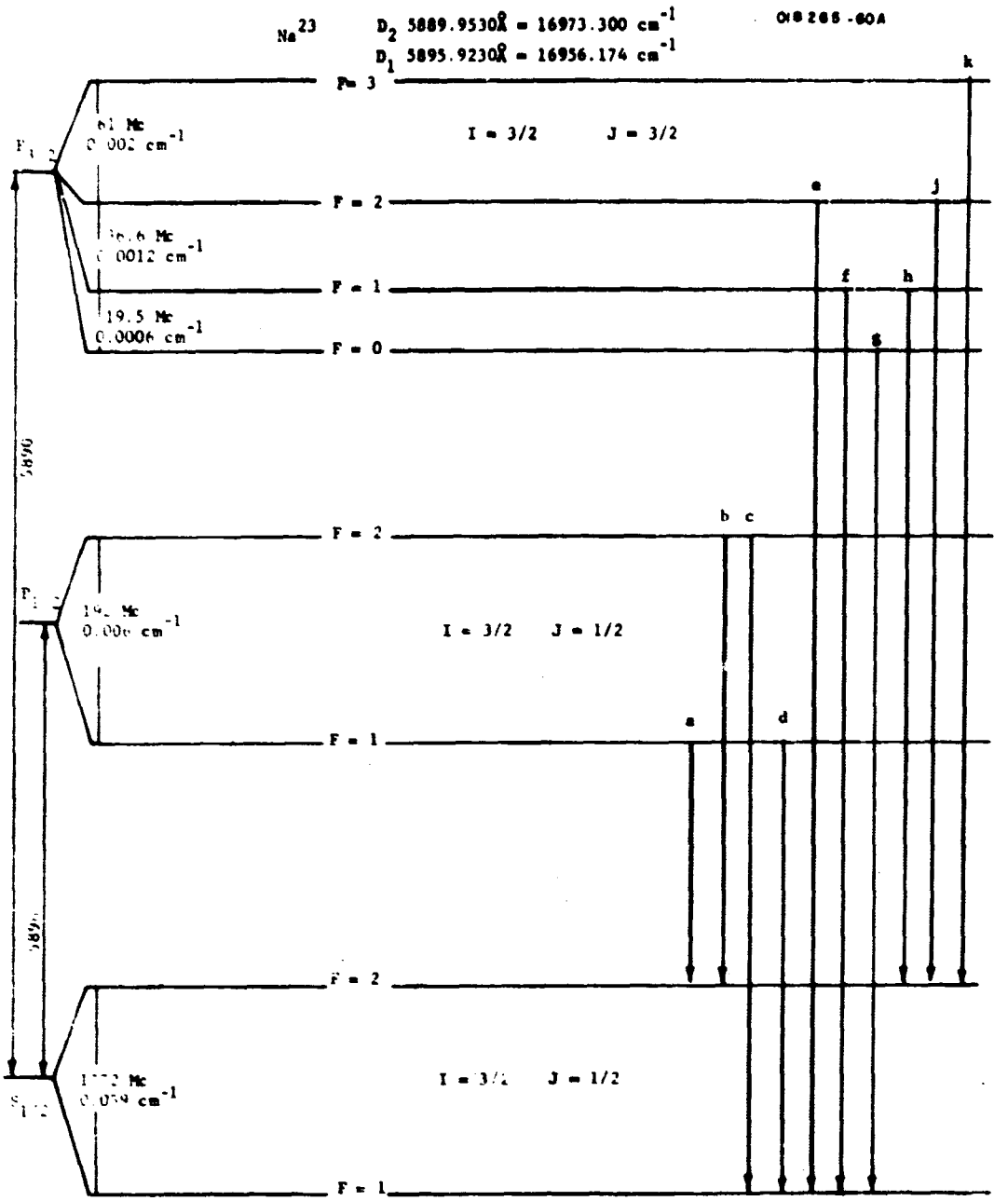

Figure 9. Energy level diagram showing transitions giving rise to D_1 and D_2 sodium resonance lines. Data on hyperfine structure splittings from Reference 60.

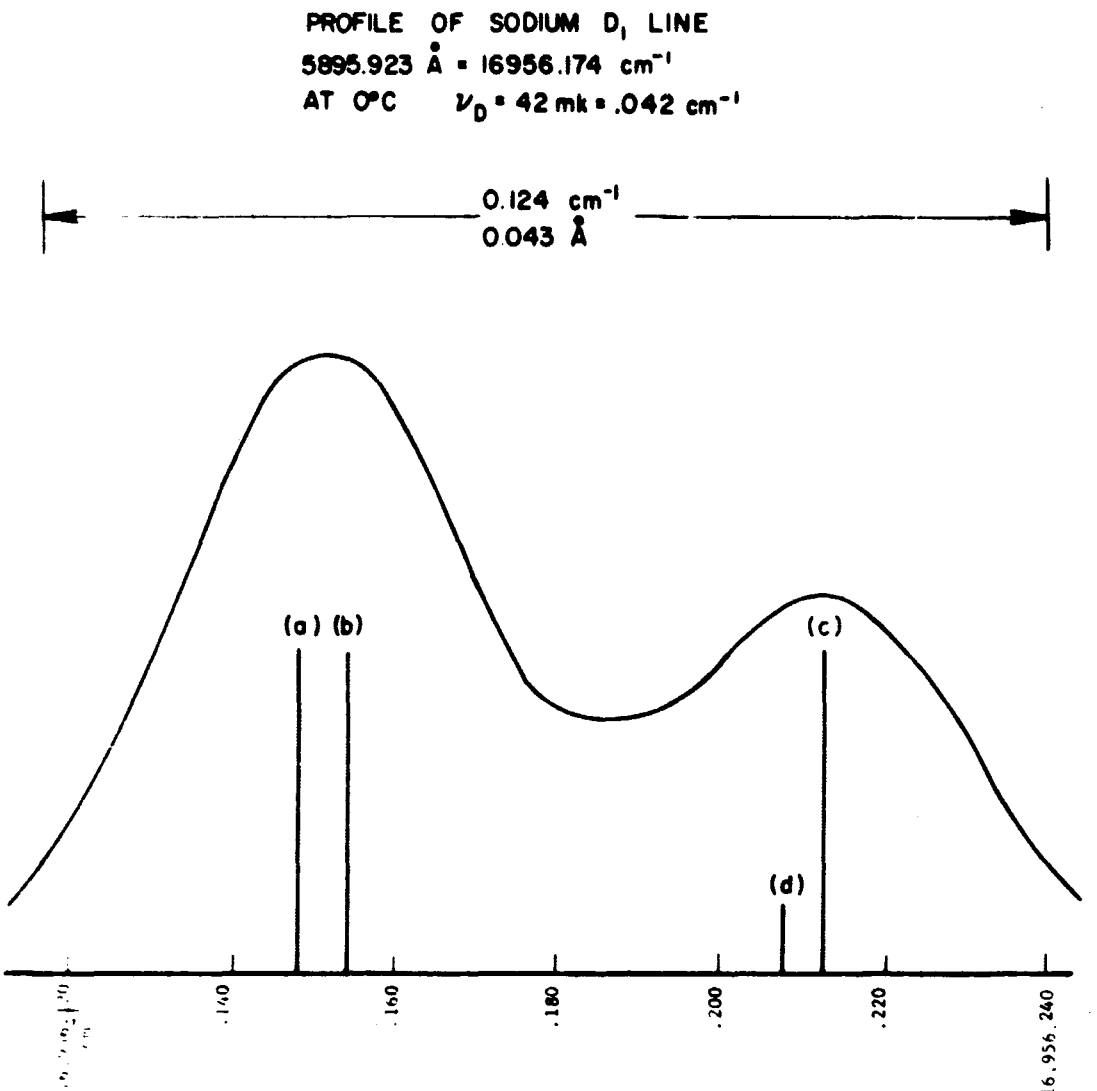

Figure 10. Profile of Na^{23} D_1 resonance line at 5896Å.

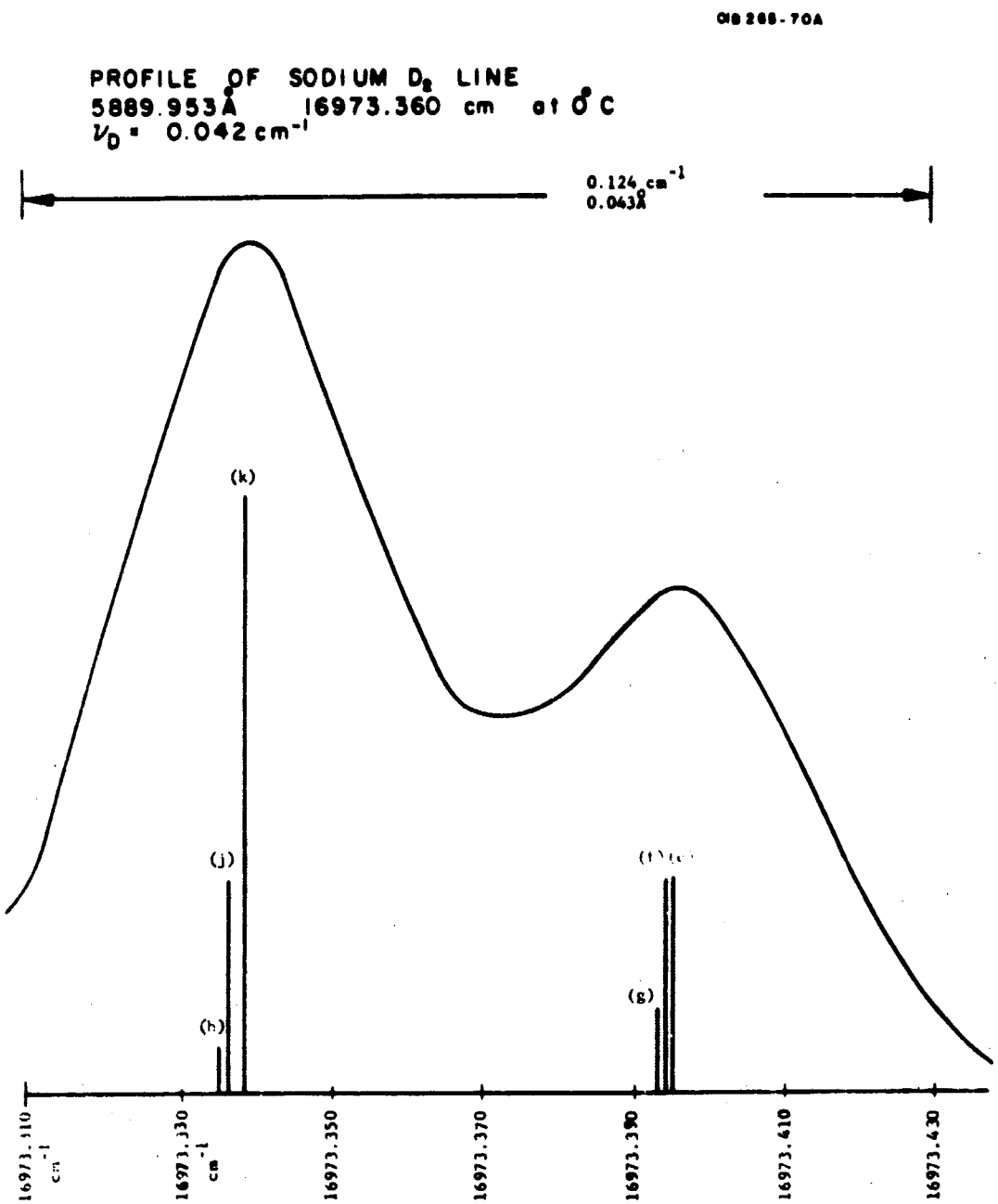

Figure 11. Profile of Na^{23} D_2 resonance line at 5890Å.

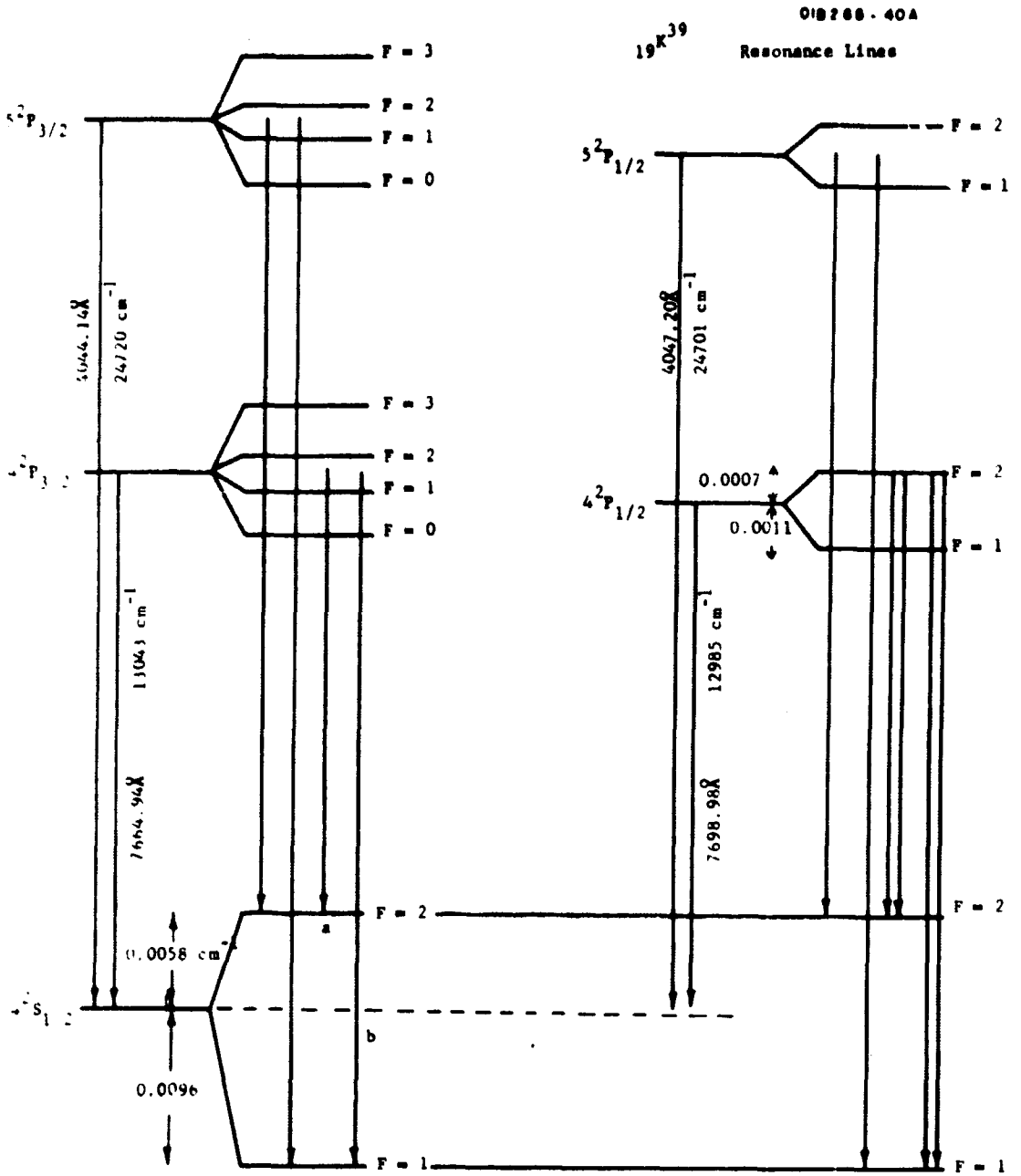

Figure 12. Energy level diagram showing transitions giving rise to resonance lines in potassium 39. Natural abundance 93.10 percent.

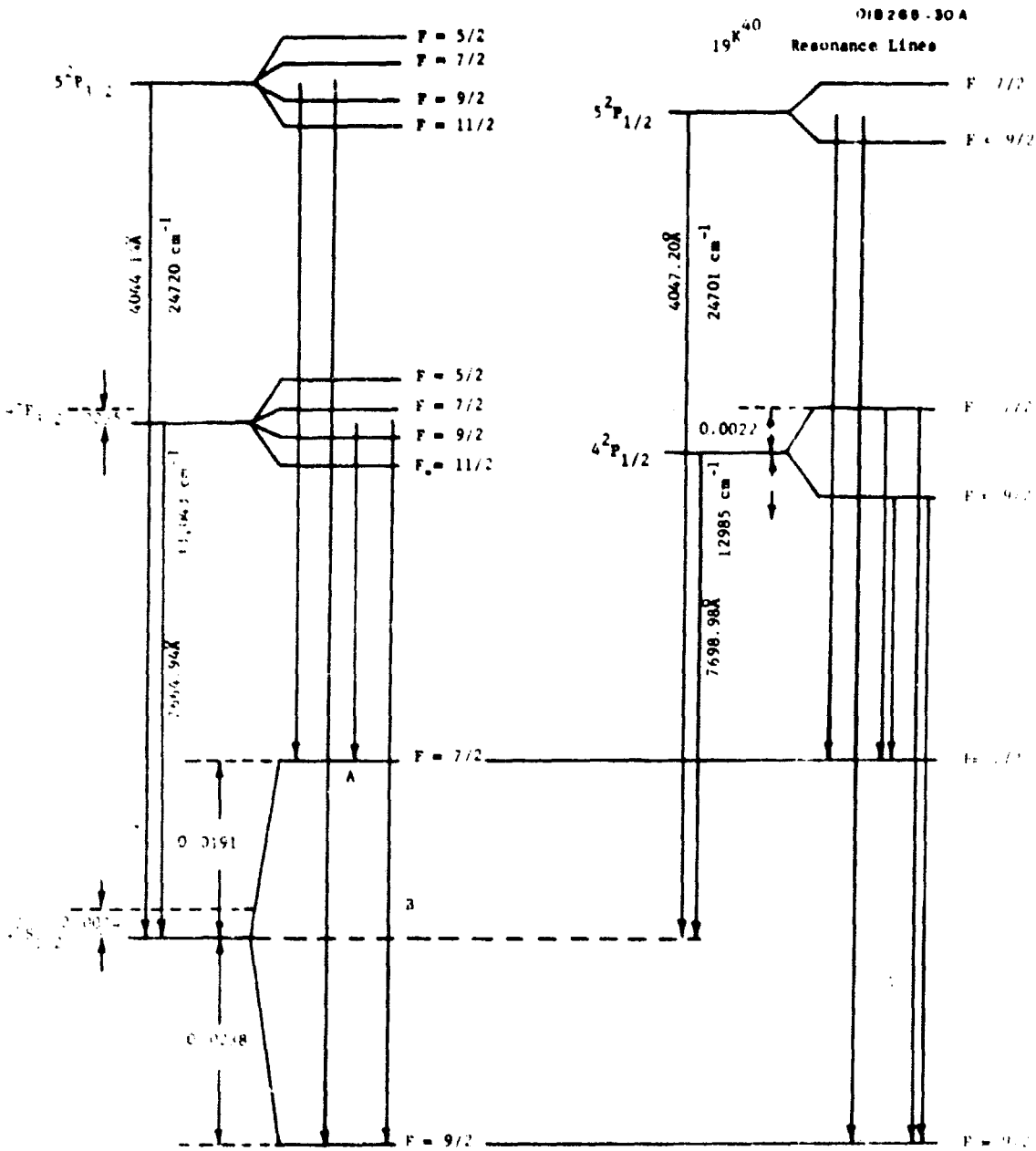

Figure 13. Energy level diagram showing transitions giving rise to resonance lines in Potassium 40. Natural abundance 0.0118 percent; radioactive β-emitter half life 1.3×10^9 years.

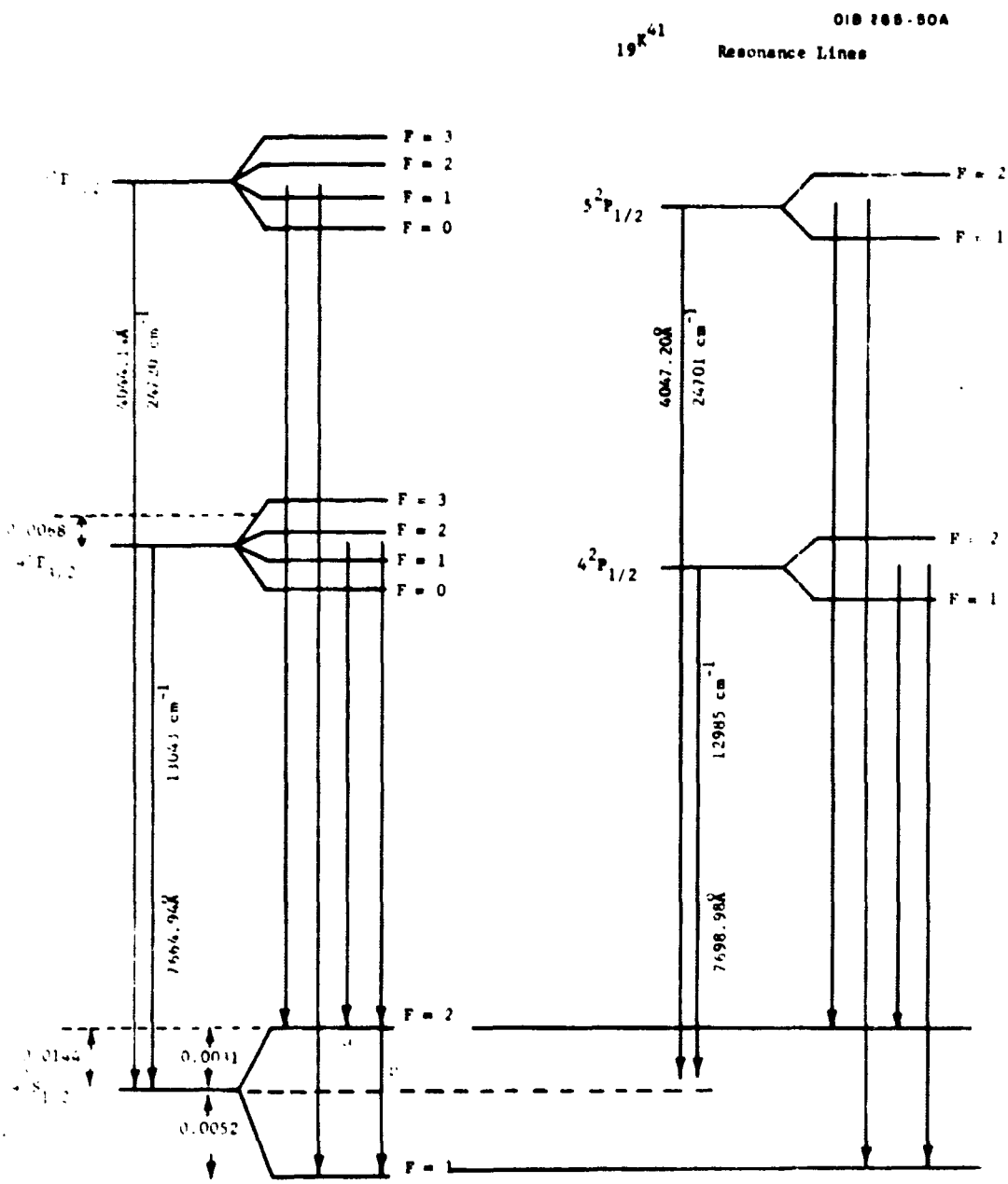

Figure 14. Energy level diagram showing transitions giving rise to resonance lines in potassium 41. Natural abundance 6.88 percent.

hyperfine structure of K^{40} is calculated on the basis of simple theory using the measured data of K^{39}, i.e.,

$$\Delta W_{I,J} = A\, C/2 \qquad (50)$$

where $C = F(F + 1) - I(I + 1) - J(J + 1)$

$$A = \frac{\mu_I \overline{H(0)}}{IJ}$$

and $\overline{H(0)}$, the average magnetic field at the nucleus produced by the electrons, is the same for both K^{40} and K^{39}. The various data have been extracted from References 57, and 61-64. The relative positions of the components (2 each for each isotope) of the 7665Å resonance line are shown in Figure 15. In this case, a Doppler width of 60°K for each component is shown separately so that a better indication of their relative positions can be obtained. In addition equal isotopic abundance has been assumed. An overall profile for natural abundance and 300°K Doppler width would result in essentially a single line distorted slightly toward higher frequencies. It would appear that no possibility exists for detection of individual isotopes of potassium.

Rubidium. – The two naturally occurring isotopes of rubidium, one radioactive, are $_{37}Rb^{85}$ (72.15 percent) and $_{37}Rb^{87}$ (27.85 percent, β^-, 4.7×10^{10} yrs). Of the longer lived other radio isotopes: $_{37}Rb^{83}$ (83 days), $_{37}Rb^{84}$ (33 days), $_{37}Rb^{86}$ (18.77 days) none are produced as fission products.[65] The isotope shift for rubidium is negligibly small since this is the mass region where the nuclear mass effect is just cancelled by the nuclear volume effect. Both the energy level diagrams and relative spectroscopic

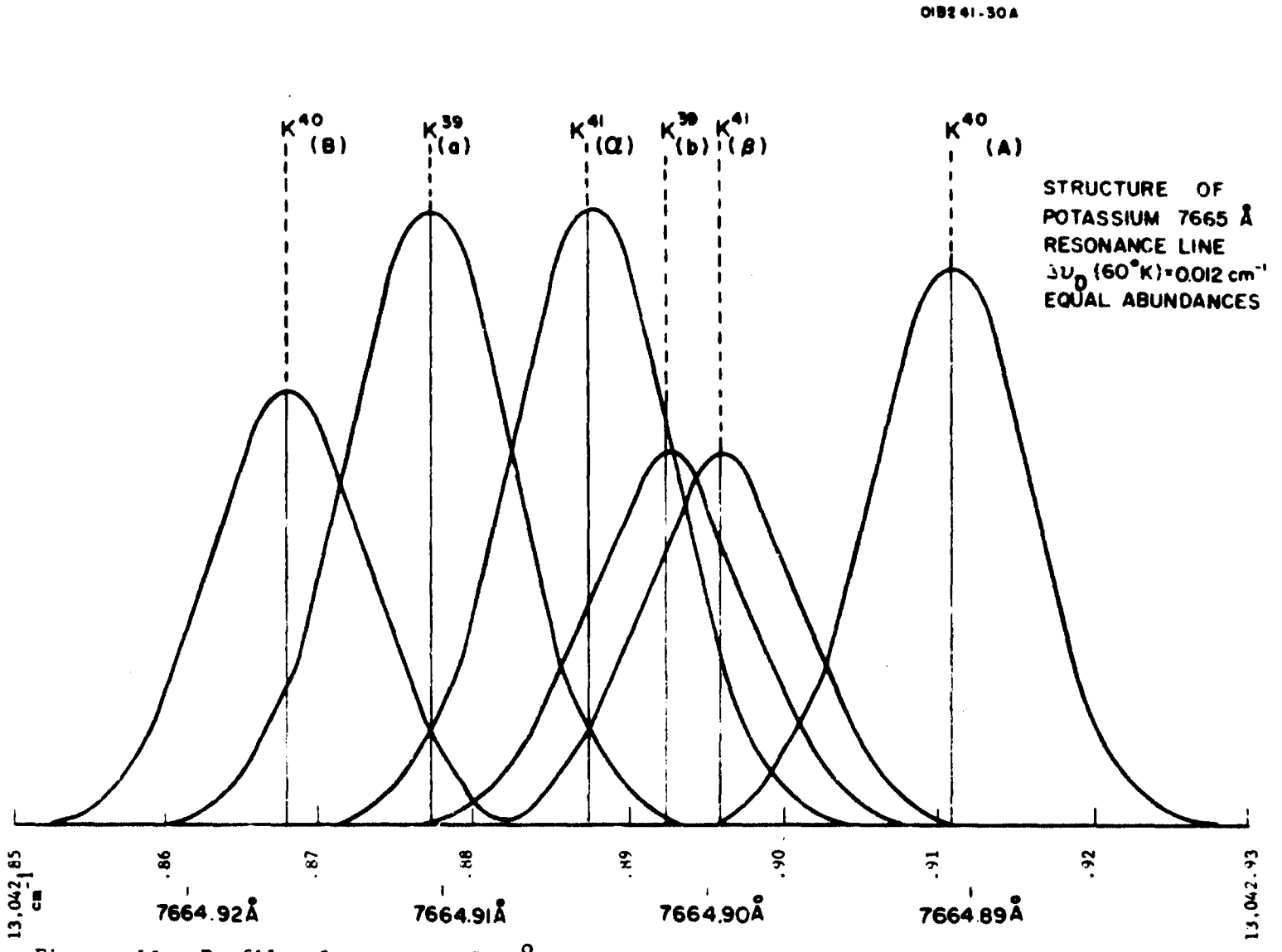

Figure 15. Profile of potassium 7665Å resonance line showing isotope shift and hyperfine structure of naturally occurring isotopes assuming equal abundance of each isotope. Actual abundances are K^{39} (93.10%), K^{40} (0.0118%), and K^{41} (6.88%). Profile of 7698.98Å line(D_1) resonance line and 4044.14Å and 4047.20Å resonance lines are similar. This figure represents each component separately. $\Delta\nu_D$ (300°K) = 0.025 cm^{-1}.

positions of components for the 7800Å resonance line are shown in Figure 16 where it has been assumed that no splitting occurs in the $P_{3/2}$ levels and also that equal abundances of the Rb^{85} and Rb^{87} isotopes[66-68] is appropriate. As can be seen, it is feasible in this case to probe independently for either of the two isotopes. For the B(b) components, the separation is five times the Doppler width at 300°K. Likewise, in probing for naturally occurring or artificially deposited rubidium, it is necessary to tune quite accurately to the (A) component of Rb^{85}.

Cesium. – The only naturally occurring isotope of cesium is $_{55}Cs^{133}$ while $_{55}Cs^{134}$ (2.17 yrs), $_{55}Cs^{135}$ (2.0×10^6 yrs), $_{55}Cs^{137}$ (30 yrs) are the longer-lived isotopes of which 135 and 137 are found in fission products. The hyperfine structure of the 8521.1Å resonance line is presented in Figure 17 with energy level diagram and profile.[69-71] For cesium therefore, it is imperative that this hyperfine structure be considered in probing experiments where, at 300°K, the separation is about 25 times the Doppler width.

B. Lasers for Generating Resonance Radiation

The application of lasers to atomic resonance probing requires detailed consideration of several aspects of laser capability:

(1) Time-energy considerations (CW or pulsed, pulse repetition rates, peak powers, total energy).

(2) Scattering cross-section, atmospheric transmission, signal-to-noise calculations.

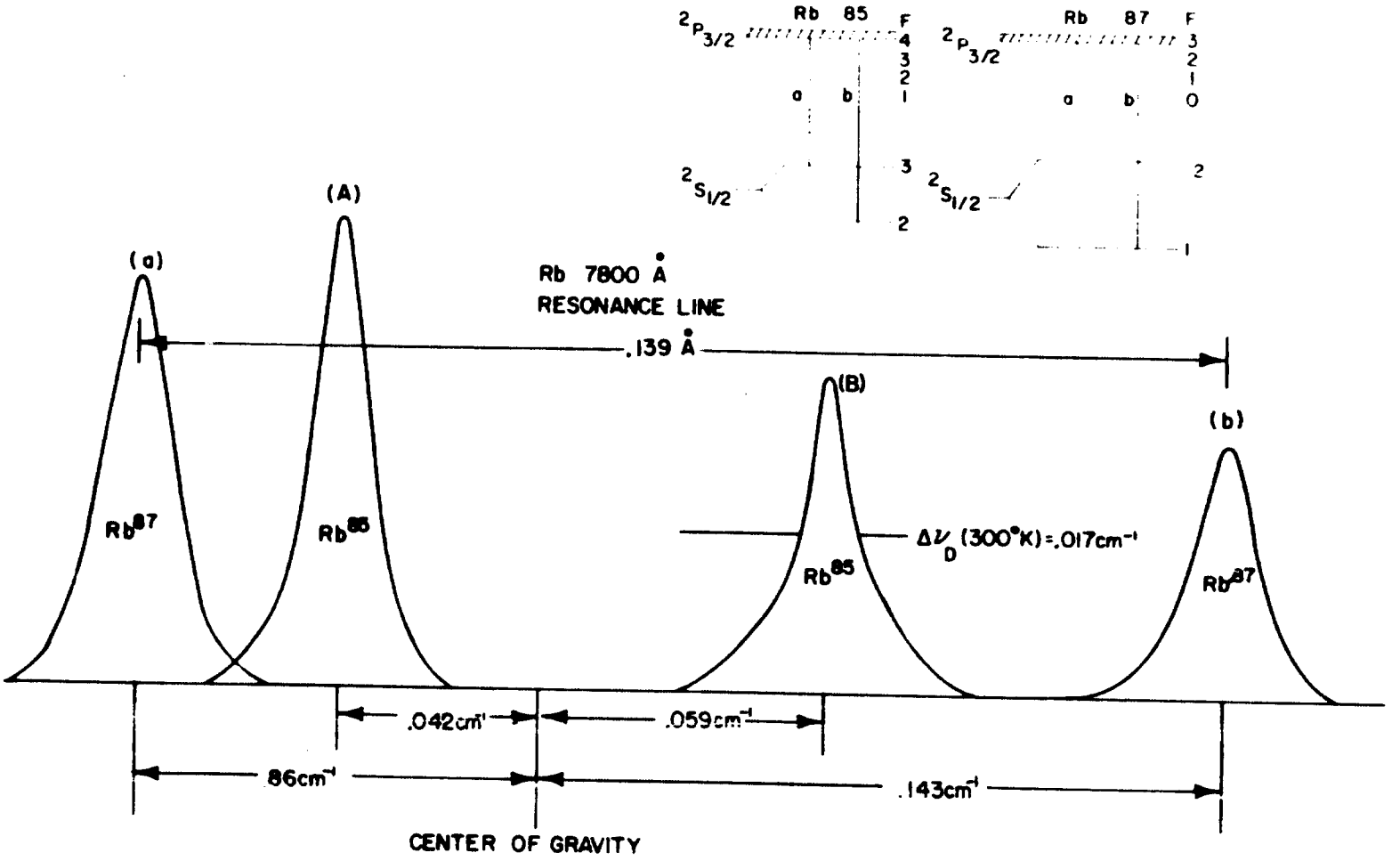

Figure 16 Profile of rubidium 7800Å. Resonance line showing isotope shift and hyperfine structure of naturally occurring isotopes assuming equal abundance of each isotope. Actual abundances are Rb^{85}(72.15%); Rb^{87}(27.85%). Profile of 7947.60Å (D_2) resonance line and of 4201.85Å and 4215.56Å resonance lines are similar. Rd^{87} is radioactive, β^-, half life $\sim 7 \times 10^{10}$ years.

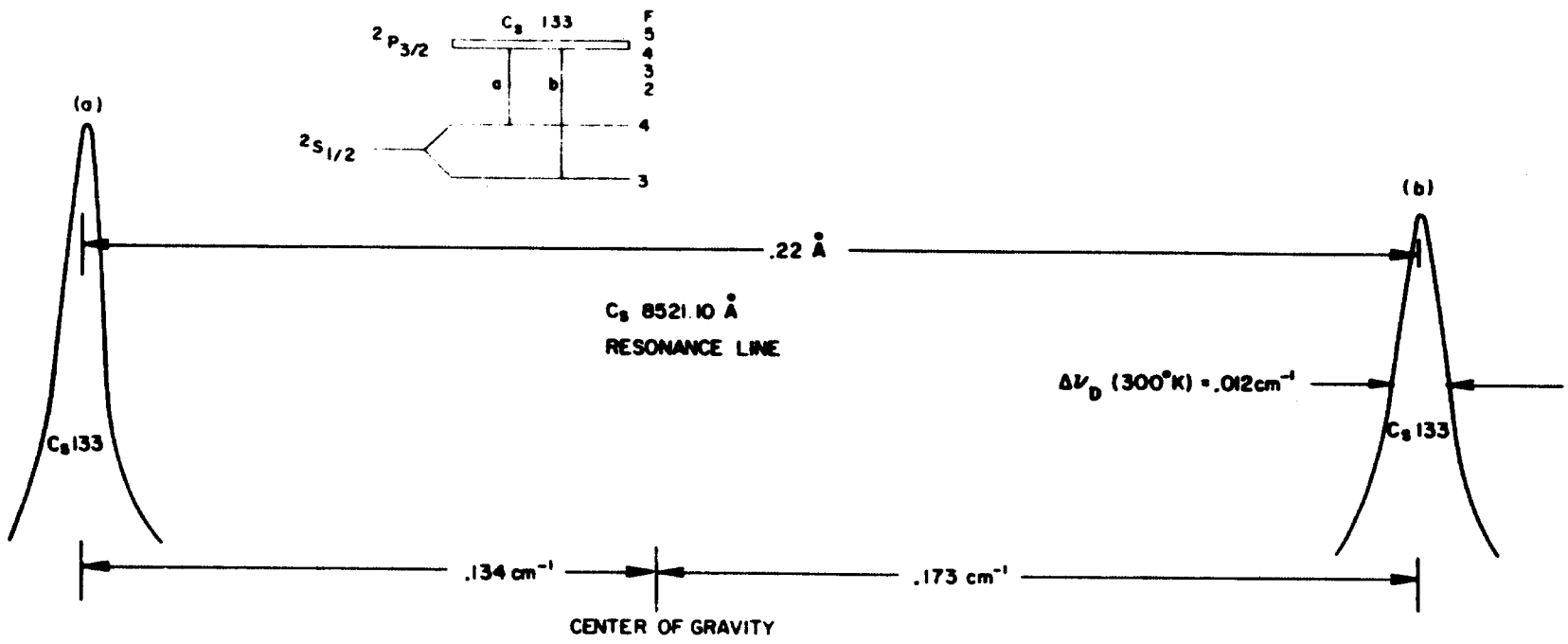

Figure 17. Profile of cesium 8521.10Å. Resonance line showing hyperfine structure of only naturally occurring isotope Cs-133. Profiles of 8943.50Å (D_2) resonance line and of 4555.36Å and 4593.18Å resonance lines are similar.

(3) Generation of laser radiation at the resonance line.

(4) Linewidth characteristics, requirements and methods of production for isotope discrimination and optimum matching.

Since many excellent discussions of the (1) and (2) items are available, the following analytical descriptions involve items (3) and (4).

Of the currently available lasers, only the dye laser offers the possibility of direct generation of the laser radiation at the resonance lines of these atoms. Over the past two years, work has progressed on laser pumped dye lasers[72-78] with considerable information becoming available on the characteristics of the dyes to be employed. The necessity of using one laser to pump another as well as the relatively broad spectral line width output leave something to be desired. Recently reported results of laser action in dyes directly pumped with special flash lamps[79] and the line narrowing (to 0.6Å) obtained in a laser pumped dye by using a grating as one of the reflecting surfaces[80] offer great encouragement for the ultimate application to laser resonance probing. The reported characteristics of the relatively fast rise time flash lamp pumped dye are: pulse energy, 0.2 joules; peak power, 1 megawatt; pulse duration, 200 nanoseconds. With higher pumping efficiency, 0.5 joule pulses are predicted. Since this is a liquid laser, higher repetition rates are possible than with a high efficiency Raman laser, for example, with PRF being limited mainly by the recovery rate of the lamp, PRF of the Tobe Deutschland capacitor used to discharge the lamp and the lifetime of the triplet states of the dyes. Similarly, since

the resonance line matching radiation is produced directly,no nonlinear processes are involved (harmonic generation or Raman shifting) and hence no requirement for high peak powers. The energy per pulse, which constitutes the important parameter for scattering represents the only necessary consideration.

The use of a grating does not reduce the laser linewidth sufficiently to meet the requirements outlined above for optimum line matching or for isotope discrimination. The reported narrowing is from 60Å in an all-dielectric reflector cavity to 0.6Å when the grating was employed. The required narrowing is at least another order of magnitude.

Resonant line matching using another laser system requires tuning for which several methods are known including (semiconductor lasers are neglected):

(1) harmonic generation[54, 81,82]

(2) parametric oscillation and amplification[82,83]

(3) stimulated Raman effect[54,84] (Raman laser)

(4) tuning by refractive index change[85-88]

(5) isotope substitution in vibrational lasers[89,90]

(6) magnetic tuning[91-93]

(7) temperature tuning[53]

(8) interferometric tuning[53]

(9) use of frequency broadening in stimulated Raman scattering[94]

(10) Doppler shifting directly.[95]

On the basis of current knowledge, the most effective mechanism or combination thereof for probing applications and high power long distance transmission investigation involve items (2), (3), (7), and (8), using ruby lasers or neodymium-in-glass lasers Q-switched. The ruby laser can be tuned by changing temperature from 6940.0Å (14405.2 cm^{-1}) at -50°C to 6945.3Å (14394.3 cm^{-1}) at +50°C. The neodymium-in-glass laser can be tuned such that its harmonic, which is more important for alkali atom probing, can cover the range from 5300Å (18,860 cm^{-1}) to 5312Å (18,820 cm^{-1}). With this tuning range in mind, some methods of generating laser outputs at some of the resonance lines of the alkali atoms are listed below:

Lithium 6708Å. –

(a) First antistokes line of $Sn(CH_3)_4$ [also $Zn(CH_3)_2$, C_2H_5I, or CHD_2I] generated by ruby laser.

(b) Second harmonic of 1.34μ neodymium-in-glass* laser output.

Sodium 5890Å or 5896Å. – Second Stokes line of C_6D_6 generated by neodymium-glass 1.06μ laser output.

Potassium 7665Å. – First Stokes line of 1,3-$FC_6H_4NO_2$ generated by ruby laser.

7699Å. – Third Stokes line of $BC\ell_3$ generated by ruby laser.

Rubidium 7800Å. – Second Stokes line of 1,4-Br $C_6H_4(CH_3)$ generated by ruby laser.

Cesium 8521Å. – Second Stokes line of 1-nitro naphthalene generated by ruby laser.

---

*Nd^{+++} has a fluorescence output from about 1.34μ to 1.38μ. Under a separate program successful normal mode laser output has been successfully demonstrated at GCA with the laser tunable throughout this spectral range. Quasi-Q-switched operation (pulse shortening) has been achieved using a "rotating pipe" full-scale Q-switching has not been attempted.

The use of the stimulated Raman effect is straightforward although the dye laser problem exists wherein the line is generally broader than the resonance line. In some cases, Raman laser lines are extremely broad extending over hundreds of angstroms.[96] These effects are observed most frequently when multimoded lasers or Raman materials are employed having large anisotopy and hence high beam focusing potential. Possible methods of avoiding the difficulties and deriving narrow lines involve the use of Raman oscillator amplifier configurations,[97] the use of gases[97,98] and the use of high Q Raman cavities.[99,100]

VI. EVALUATION OF LASER PROBING FOR SPECIFIC MOLECULES

A. Sample Calculations of Feasibility of Laser Probing for MgO

In the present section the detailed analysis of a specific molecule is considered instead of performing a general parametric analysis, since each molecule is characterized by its own unique problems. The case of MgO was selected since it represented a highly suspect meteoritically deposited specie in planetary atmospheres. The expected signal return MgO in the terrestrial upper atmosphere in the 90 to 95 km altitude range is calculated below.

The $B\ ^1\Sigma$ - $X\ ^1\Sigma$ transition of MgO is selected for analysis with the 0,0 band near 5000Å, as the best probable indicator for the presence of MgO. The pertinent molecular constants are, in cm^{-1} units:

	ω_e	$\omega_e x_e$	B
$B\ ^1\Sigma$ (upper state)	824.1	4.76	0.5822
$X\ ^1\Sigma$ (lower state)	785.1	5.18	0.5743

At 90 km the kinetic temperature is about 172^oK, and it is assumed that the MgO is in thermal equilibrium with the surrounding N_2 and O_2. The remaining pertinent questions involve the optimum wavelength for illumination and the number of molecules which will be excited.

In order to calculate the received (emitted) signal a treatment analogous to that for the solar-illuminated cloud situations is developed and applied. Thus, adding the subscripts ℓ to the laser-illuminated case, results in

$$\Phi_{\ell}\,\alpha_{\lambda} = P_{\ell} \tag{51}$$

and

$$\Phi_{o\ell} = P_{\ell} N_{\ell} \tag{52}$$

where the symbols are described below as they are evaluated numerically.

With respect to the N_{total} (available MgO molecules/cm^3) parameter, it should be noted that MgO has not been measured in the atmosphere. Narcisi and Bailey[101] measured a profile of Mg^+ (N at 84 km was 200, at 95 km was about 6000, and at 104 km was back down to 200 per cm^3). It should be noted, however, that since thermodynamic equilibrium among Mg^+, Mg, and MgO is not applicable, the above particle density distribution with altitude for Mg^+ was assumed pertinent to MgO. Thus, by vertical integration the column count for Mg^+ is 3.1×10^9 particles/cm^2 which is tentatively accepted as the MgO column count value.

If the total (and assumed) uniform spatial distribution) concentration is N_{total}/cm^3, recall[44] for the ground state

$$N_{J''}/N_{total} = \frac{hcB}{kT}\,(2J+1)\,\exp\,[-\,BJ(J+1)\,\frac{hc}{kT}] \tag{53}$$

and

$$J''_{max} = 0.5896\sqrt{\frac{T}{B}} - 0.5 \tag{54}$$

The J'' for the maximum population designated here as J''_{max} is shown in Figure 18 for three temperatures and as a function of the rotational

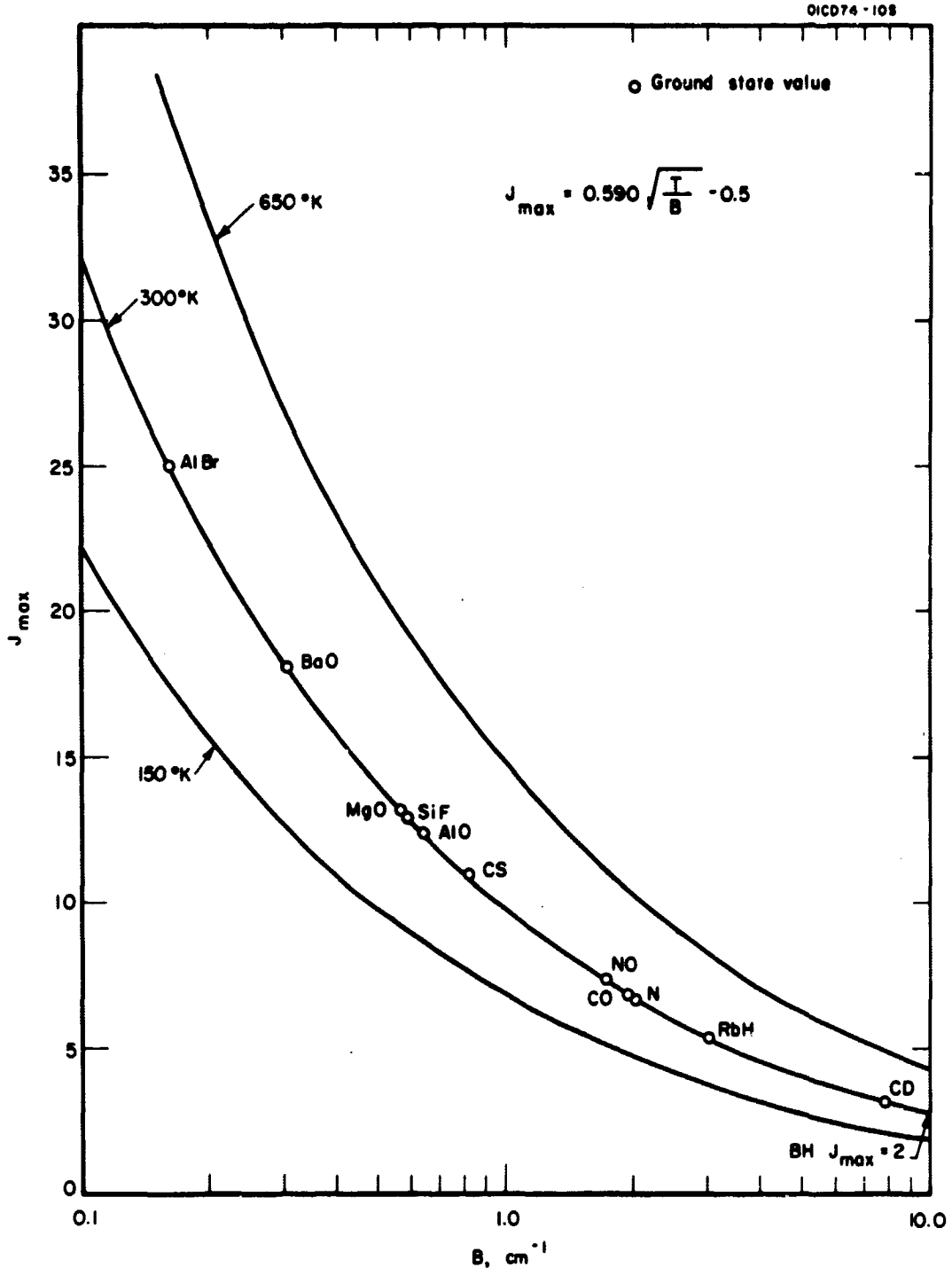

Figure 18. Calculation of J″ for maximum population (J''_{max}) as a function of rotational constant B for three temperatures.

constant B (so-called reciprocal moment of inertia). The above expressions yield $J''_{max} = 10$ (at 172°K) for B″ of 0.5743 cm^{-1}; $hcB''/kT = 4.81 \times 10^{-3}$ and $N_{J''=10}/N_{total}$ is $4.81 \times 10^{-3}(21)\{\exp[-110(0.481 \times 10^{-3})]\} = 4.81 \times 10^{-3}(21)(0.589)$ or 5.95×10^{-2}. Thus, it is expected that about 6 percent of the MgO molecules present in the volume illuminated will be excited. A related calculation shows that $N_{J''=10}/N_{J''=0}$ is 12.4, showing further there is appreciable rotational excitation even at this low temperature.

Now electing to start from J″ = 10, should the resonance be performed at J′ = 9 or 11? (Ignore J′ = 10 since $\Delta J = 0$ are not allowed in a $^1\Sigma - {}^1\Sigma$ transition; i.e., no Q-branch in this system.) Actually, it makes little difference since the ratio $S_J/2J+1 = \frac{J+1}{2J+1}$ in absorption for $\Delta J = +1$ (i.e., 10 → 11 in absorption) and is $J/2J+1$ for $\Delta J = -1$ (i.e., 10 → 9 in absorption).* Also the line spacings are about 2B (cm^{-1}) ≈ 1.2 cm^{-1} except near the band head and $\nu = 20000.0$ cm^{-1} for λ of 5000Å while $\nu = 20001.2$ cm^{-1} for λ of 4999.70Å so the wavelength for illumination is about the same. (In fact a problem in line matching may result in some wandering from one line to another (changing J″) if the laser wavelength drifts.) As such, illumination of the 10 → 11 line is assumed for which the resulting J′ = 11 → J″ = 12 and J′ = 11 → J′ = 10 emission lines will be monitored both of which will be within the bandpass of most filter-detector combinations.

*Keep in mind these S_J are for $\Delta\Lambda = 0$.

The next question is what are the line absorption f-values, $f_{mnJ'J''}$? If the band f-value $f_{mnv'v''}$ is accepted* for $v'v'' = 0,0$ of $f_{mn00} = 9.26 \times 10^{-3}$, then the $f_{mnJ'J''}$ given in Table 12 are obtained.

TABLE 12

LINE ABSORPTION f-VALUES FOR MgO, B $^1\Sigma$ - X $^1\Sigma$

$$f_{mnJ'J''} = \frac{S_{J''}}{2J+1} f_{mnv'v''}$$

$S_{J''} = J''+1$ for $\Delta J = 1$; $S_{J''} = J''$ for $\Delta J = -1$

J''	To	J	$\frac{S_{J''}}{2J''+1}$	$f_{mnJ'J''} \times 10^3$
10		11	11/21	4.85
10		9	10/21	4.41
20		21	21/41	4.74
5		6	6/11	5.05

The above is an example of how the sum of several $f_{mnJ'J''}$ can quickly exceed $f_{mnv'v''}$. The population weighting factor will be discussed subsequently.

Now typical α_λ will be calculated. For the J'' = 10 to J' = 11 transition the wavelength to which the laser must be tuned is $\lambda = 1/\nu$ where

*The band f-number is for an assigned transition moment of 1 Debye. However, recall the previous discussion of MgO so that the value is realistic.

$$\nu_{mm}{}_{10,11}\ (cm^{-1}) = 19984.0 + 824.1(1/2) - 4.76(1/4) + 0.5822(11)(12)$$

$$- [785.1(1/2) - 5.18(1/4) + 0.5743(10)(11)]$$

$$= 2001728\ cm^{-1} \text{ or } \lambda = 4995.68\text{Å}$$

Then

$$\alpha_\lambda = (8.84 \times 10^{-13})(4.85 \times 10^{-3})(4.9957 \times 10^{-5})^2$$

$$= 1.07 \times 10^{-23}\ cm^3 \text{ (at } J'' = 10,\ J' = 11)$$

This is the integrated absorption cross section per molecule for the specified transition. (It is about 1/200 of α_λ for the strongest resonance line of NaI at 5890Å.)

The next question of the laser illumination must be investigated. It is assumed that a laser is available at the desired wavelength, with the output collimated by a 16-inch diameter mirror so that the beam diverges by 1 milliradian (i.e., 1 km at 1000 km). Thus, at 95 km a circular field of 0.095 km in radius or area of $2.83 \times 10^8\ cm^2$ is illuminated. Since the MgO would be concentrated in a relatively narrow altitude range (thin disc) near 95 km, about $2.8 \times 10^8\ cm^2 \times 3.1 \times 10^9$ molecules/$cm^2 = 8.5 \times 10^{17}$ molecules will be illuminated and (recall earlier calculation for 6 percent of molecules in $J'' = 10$), there will be 5.0×10^{16} molecules that can resonate with $J'' = 10$ to $J' = 11$. Furthermore, it is assumed that the laser output is 20 millijoules/pulse, with a pulse duration of about 20 nsec so that there are 5.0×10^{16} $\frac{\text{photons}}{\text{pulse}}$. Thus, there are just enough photons to excite the molecules

that can resonate with the chosen transition; the exact agreement is sheer coincidence. In practice, the beam will undergo some attenuation and scatter before interception by the "target" MgO region. Also, of course, the MgO concentration is quite uncertain. The most important factor is the α_λ value.

The laser illumination is now expressed in terms of the flux Φ_ℓ for substitution in Equation (51). The laser and molecular line width comparison is now made. For the latter, recall that the half-width b of a level is, by the uncertainty principle, $b = h/2\pi\tau$. Thus, the greater the mean lifetime, τ of a state, the small is the level width. Only the upper state of MgO is of interest here, since the lower level is the ground state for which the corresponding lifetime is very long and the energy level width vanishingly small.

Thus, for a line near 5000Å and with τ (MgO B state) about 1 μs, b is 10^{-21} ergs, the transition energy E is 10^{-15} ergs, so that $b/E = 10^{-6}$. The natural line width for this example is then 0.02 cm^{-1} or 0.05Å. This is comparable to the natural line widths of 0.001 to 0.01Å quoted by Herzberg[44] for strong transitions. However, the Doppler broadening is usually a factor of 10 greater than the natural line width so the actual line width is about 0.01 to 0.1Å. The additional effect of pressure broadening will be neglected since this is important only above about 5-mm pressure, which exceeds that in most contemplated upper atmosphere experiments.

The present laser art, using solid rods permits output pulses with line widths of 0.1 to 0.2Å. Thus, the laser line width is near to, or greater than, the width of the Doppler-broadened line. The 0.2Å value is employed in the following estimation exercise.

$$\text{The laser flux } \Phi_\ell = \frac{\text{photons/pulse}}{(\text{illuminated area})(\text{pulse duration})(\text{laser line width})}$$

$$= \frac{5.0 \times 10^{16} \text{ photons}}{(2.8 \times 10^{8} \text{ cm}^2)(2.0 \times 10^{-8} \text{ sec})(0.2\text{Å})}$$

$$\Phi_\ell = 4.5 \times 10^{16} \text{ photons/cm}^2\text{-sec-Å}$$

This is the laser flux converted to a continuous (CW) basis. It is about 800 times the solar flux at the top of the atmosphere, at 5000Å. Thus

$$\Phi_\ell \alpha_\lambda = \left(4.5 \times 10^{16} \frac{\text{photons}}{\text{cm}^2\text{-sec-Å}}\right)(1.1 \times 10^{-23} \text{ cm}^3)(10^8 \text{Å/cm})$$

or $P_\ell = 50$ photons/sec-excited molecule (CW basis). Also, correcting the integrated column count for the 6 percent population factor developed earlier,

$$N_\ell = (3.1 \times 10^{9} \text{ molecules/cm}^2)(0.06)$$

$$= 1.9 \times 10^{8} \text{ excited molecules/cm}^2 \text{ in total vertical path or column}$$

Then

$$\Phi_{o\ell} = P_\ell N_\ell = \left(\frac{50 \text{ photons}}{\text{sec-molecule}}\right)\left(1.9 \times 10^{8} \frac{\text{molecules}}{\text{cm}^2\text{-column}}\right)$$

$$= 9.0 \times 10^{9} \frac{\text{photons}}{\text{sec-cm}^2\text{-column}} \text{ (CW basis)}$$

Now return to a per-pulse basis and compute the total number of photons per pulse. Using the target illuminated area, pulse duration, and the expectation that the scattered (emitted) signal is isotropic, the following emission is obtained:

$$\left(9 \times 10^{9} \frac{\text{photons}}{\text{sec-cm}^2\text{-column}}\right)(2.8 \times 10^{8}\ \text{cm}^3)\left(2.0 \times 10^{-8} \frac{\text{sec}}{\text{pulse}}\right)$$

$$= 5.0 \times 10^{10} \frac{\text{photons}}{\text{pulse-}4\pi\text{-sterad}}$$

or 4.0×10^{9} photons/steradian-pulse.

If the same laser optics are used for collection (i.e., 16-inch diameter mirror) and the average range of this optically thin source is 95 km, the solid angle for collection is $\frac{\pi(8'')^2}{(95\ \text{km})^2} = 1.44 \times 10^{-11}$ sterad. Then the signal collected from the entire illuminated area is about 0.06 photons/pulse.

This appears to be a somewhat pessimistic value, but the situation should be examined further. First, a cooled photomultiplier has a dark current of about 50 counts per second at the cathode. For the MgO system examined here the spontaneous radiative lifetime is about 1 μs, so it is assumed that the detector is gated to receive the expected 0.06 photon from each pulse over a 5-μs period; 5 lifetimes is adequate for complete depopulation of the emitting state. In 5 μs the average dark

count is then about 2.5×10^{-4} counts, 4×10^{-3} that of the expected MgO signal. Hence, the expected intrinsic signal/noise is favorable. This ignores any background signal, which, being a slowly varying or steady signal, could be processed out in data reduction. Probably, for night operation, the system would be signal-level limited.

Also, it was assumed previously that the MgO concentration was the same as the known Mg^+ concentration. This may be unrealistic, with the MgO probably being greater than Mg^+ although further speculation on this matter is pure conjecture. In addition, a 1-megawatt pulse and relatively small (16-inch diameter) collector mirror were assumed. Doubling the receiver mirror diameter and increasing the laser power to 5 megawatts (still collimated by a 16-inch diameter transmitter mirror) would yield a factor of 20 improvement in expected signal; i.e., to about 1 photon/pulse which is close to the detection threshold of realistic systems.

One situation that is promising is an artificially created cloud of AℓO. This is treated below.

B. Analysis of Laser Probing Possibilities for Trimethyl Aluminum Release

Introduction. – The purpose of the following discussion is to assess the possibility of probing TMA (trimethyl aluminum) clouds with an appropriately selected laser. A considerable amount of investigation has been performed regarding the employment of AℓO released clouds for the determination of winds under both twilight resonance conditions

(AℓO band spectrum) and nighttime chemiluminescent conditions (continuum spectrum). Most of the research interest has centered on the determination of ambient atmospheric temperature by means of the analysis of the vibrational structures of the $A\ ^2\Sigma^+ - X\ ^2\Sigma^+$ electronic transition and also the analysis of the rotational P transitions of the (0,0) vibrational band.[101-107]

While the $\Delta v = \pm 1$ bands have received the most attention, it is the (0,0) band which is by far the most prominent feature of the resonance spectrum. The $\Delta v = \pm 1$ bands have been analyzed in detail because of their strong temperature dependence. However, the purpose of the present study is to determine the capability of detecting and locating the AℓO molecules in space in a chemical release experiment rather than the previous type of temperature determination experiments.

Analysis of (0,0) band absolute scattering properties. – The purpose of the following discussion is to determine the spectroscopic properties of the (0,0) band, in particular, the absolute transition probabilities as expressed in terms of a cross section for the band and various rotational lines. Further, the population expected to be present in the (0,0) band and the various rotational levels will be examined.

To document the choice of the (0,0) band, the relative band intensities calculated by Armstrong[108] have been reviewed. It is evident from these calculations that for temperatures from 400 to 1000°K the (0,0) band is stronger by a factor of at least four than the (0,1) system and five to six than the (1,1) system and much larger for the other bands.

This theoretical estimate is borne out by two spectra from Authier[106] from grenade release experiments. In addition, a third spectrum from Rosenberg[107] from a trimethyl aluminum release supports this contention. Consequently, both the theory and field observations support the choice of the (0,0) band for laser probing. This choice has been predicated on the assumption that in the spectral region λλ 4000-6000Å there is little substantial difference in the power of pulsed lasers.

Spectroscopic properties of the (0,0) band of the $A\ ^2\Sigma^+ - X\ ^2\Sigma^+$ electronic transition of AℓO. – The relevant spectroscopic properties of the (0,0) band are discussed below including: (1) rotational line width, (2) spacing and location of rotational lines and band-head, and (3) absolute strength of rotational line and cross section for scattering.

(1) Rotational line width. – The line width is determined by the Doppler line width $\Delta\nu_D$ which is larger than the natural line width, $\Delta\nu_n$:

$$\Delta\nu_n = (2\pi\tau)^{-1} \tag{55}$$

where $\tau > 10^{-8}$ seconds so that $\Delta\nu < 10^9$ seconds^{-1}. The Doppler line width $\Delta\nu_D$ is given by $\Delta\nu_D = (\nu/c)\sqrt{2RT/\mu}$ where μ is the molecular weight (43 for AℓO). R the gas constant, c the velocity of light, and T the absolute temperature. For T of approximately 600°K and converting to wavelengths, where $\delta\lambda = \lambda^2 \frac{\delta\nu}{c}$ there is obtained

$$\Delta\nu_D \sim 2 \times 10^{-2}\text{Å}$$

(2) Spacing and location of rotational lines and band-head. – The pertinent spectroscopic properties of AℓO are presented in Table 13. There exist some variations in the estimate of the location of the band-head. Authier[106] quotes a figure of 4842.3Å. Using the value of 2.5Å given by Best[102] as the difference between the band-head and origin quoted as 4844.7Å, a value of 4842.2Å is obtained. Jevons[109] quotes 4842.1Å while Tyte and Nicholls[110] employ 4842.18Å as the band-head and 4846.09Å for the band origin. A band-head of 4842.2Å is selected as optimum.

The actual frequency of the laser is subject to some uncertainty and under operational conditions, a shifting in wavelength may occur. While the frequency given above is the desired one, some adjustment may be necessary under field operating conditions.

(3) Absolute strength of line and equivalent cross section. – The basic problem is that of obtaining the absolute transition probability for the rotational lines of the (0,0) band. Wentink[111] has calculated the f-number of the (0,0) band as 3.55×10^{-3}. Vanpee, et al.[112] have calculated this f-number as 2.7×10^{-3} for the (0,0) band. Johnson, et al.[103] on the basis of observations of the radiant output of grenade glow clouds in the lower thermosphere, calculates $\varepsilon \sigma = 3 \times 10^{-14}$ cm^2 or $f = 0.005$ for the rotational line transition. This value is based not only on the absolute radiance of the cloud but also on a radiance profile of the cloud particularly the transition from optically thick to optically thin and hence constitutes a two-fold basis. Authier,[106] using the

TABLE 13

SPECTROSCOPIC MOLECULAR CONSTANTS FOR AlO

Author	State	T_e	ω_e	$\omega_e x_e$	B_e	α_e	D_e	β_e	r_e(Å)	ν_{oo}
Pomeroy[1]	A $^2\Sigma$		866[1]	3.75[4]	0.6019[3]	0.00453[3]	-1.1630×10^{-6}	$+0.0059\times10^{-6}$	1.665	20635.27
	X $^2\Sigma$		969[1]	7.00	0.6386	0.00575	-1.1094×10^{-6}	-0.0087×10^{-6}	1.617	---
Jevons[2]	A $^2\Sigma$	20686.9	868.15	3.76	0.6019	0.00453			1.663	20635.3
	X $^2\Sigma$		977.0	7.00	0.6386	0.00575			1.614	
Sen[3]	A $^2\Sigma$				0.60417		-1.1660×10^{-6}		1.664	
	X $^2\Sigma$				0.64148		-1.1050×10^{-6}		1.615	
Roy[4]	A $^2\Sigma$	20699.25	870.0	3.80						
	X $^2\Sigma$		978.2	7.12						
Herzberg[5]	A $^2\Sigma$	20699.2	870.0	3.80	0.60417	0.00453			1.6667	20635.3
	X $^2\Sigma$		978.2	7.12	0.64148	0.00575	-1.114×10^{-6}	0.0087×10^{-6}	1.6176	
Lagerqvist[6]	A $^2\Sigma$	20688.95	870.05	3.52	0.60408	0.00447	-1.16×10^{-6}		1.6668	20635.18
	X $^2\Sigma$		979.23	6.97	0.64136	0.00580	-1.08×10^{-6}	-0.02×10^{-6}	1.6176	

1. Pomeroy, W. C., "The Quantum Analysis of the Band Spectrum of Aluminum Oxide (λ5200-λ4650)," Phys. Rev. 29, 59 (1927).

2. Jevons, W., "Report on Band Spectra of Diatomic Molecules," The Phys. Soc. (1932).

3. Sen, M. K., "Spin Doubling in $^2\Sigma$ States in AlO," Indian J. Phys. 11, 251 (1937).

4. Roy, D , "New Measurements of Aluminum Monoxide Bands," Indian J. Phys. 13, 231 (1939).

5. Herzberg, G , "Molecular Spectra and Molecular Structure I - Spectra of Diatomic Molecules," second ed., Van Nostrand, New York (1950).

6. Lagerqvist, A., Nilsson, N. E. L. and Barrow, R. F., "Rotational Analysis of the $^2\Sigma$ - $^2\Sigma$ System of AlO," Arkiv for Fysik 12, 543 (1957).

radiance of grenade clouds, calculates from the ratio of solar input to the cloud radiance $K\ell = 0.15$ where $\ell = 20$ km (2×10^6 cm) is the diameter of the cloud. Since $K\ell = \sigma N$ where σ is the scattering cross section and N is the concentration per cm^3. N is estimated at approximately 10^6 although it could be as low as 10^5. For $N = 10^6$

$$\sigma = 5 \times 10^{-14}$$

for $N = 10^5$, $\sigma = 5 \times 10^{-13}$.

The relation between f and σ is given by:

$$\sigma = \frac{\pi e^2}{mc} \frac{f}{\delta \nu} \tag{56}$$

Both the Authier and Johnson twilight evaluation assumed that effectively all the AℓO molecules were scattering under solar radiation in one rotational line window of 2×10^{-2}Å. This calculational device is appropriate since, if it is assumed that I_o is the photon flux over a rotational line, then the solar flux is relatively constant over the (0,0) band-head, or

$$I = \sum I_o \, \sigma_{k''} \, N_{k''} \tag{57}$$

Moreover, σ_k is relatively constant over large values of k since the rotational transition factor is given by

$$S_R = \frac{K'}{2K'+1} \sim \frac{1}{2}$$

for K large. Consequently,

$$I = I_o \, \sigma \sum N_{k''} \quad \text{and} \quad \sum N_{k''} \sim N_t$$

where N_t is the total number of molecules.

The various estimates of the f-numbers and equivalent cross sections are summarized in Table 14.

A head is formed in the R branch if $B_{v'} - B_{v''} < 0$ and the band is degraded toward the red which is the case for AℓO. For AℓO, $B_{v'} - B_{v''} < 0$, the heads are formed in the R branches, and the bands are degraded toward the red. It was found that the tuning point occurs at about K = 17, and is about 2.5Å away from the band origin.

It can be shown that the separation of the rotational lines is given by

$$\frac{d\lambda}{dm} \text{ (Å)} = 0.31141 - 0.01865 \text{ m}$$

Thus, the separation of lines of low rotational quantum number is about 0.3Å, and at K = 15 in the P branch it is about 0.6Å. At K = 17 in the R branch the line spacing is about 0.02Å which is equivalent to the rotational line width. Consequently, approximately five rotational lines at the band-head can be assumed to be covered by a laser line width of 0.1Å. The close spacing at the band-head is also advantageous in that there are fewer holes for the laser line to filter through without being scattered.

Population of (0,0) band. – One of the factors in the strength of the laser signal return is the population of the lower resonant state. The atmospheric temperature in the region 90 to 170 km where TMA clouds are released varies between approximately 200°K and 1000°K. It is

TABLE 14

VARIOUS ESTIMATES OF f-NUMBERS FOR A $^2\Sigma^+$ - X $^2\Sigma^+$ AlO TRANSITION FOR (0,0) BAND AND ROTATIONAL TRANSITIONS

f-Number	Transition	Equivalent σ	Basis
3.55×10^{-3}	(0,0) band	2.12×10^{-14}	Wentink [111]
2.7×10^{-3}	(0,0) band	1.6×10^{-14}	Vanpee [112]
5.0×10^{-3}	rotational line at (0,0) band head	3×10^{-14}	Johnson, et al. [103]
8.5×10^{-3}	rotational line at (0,0) band head	5×10^{-14}	Calculated from Authier data [105]

known that the vibrational population of the v″ = 0 level ranges from 100 to 70 percent of the total number of AℓO molecules for the temperature range given above.

Owing to th .er rotational energies, the rotational distribution is spread significantly. As indicated in the spectroscopic analysis, a laser frequency at the band-head will be employed because of the smaller spacing of rotational lines. In the previous discussion, a band-head occurring at K″ = 17 was indicated. At 200°K, the population for this band-head line is about 5 percent while at 1000°K the population is about 2.5 percent of the total in the vibrational population. The effective population for scattering then depends upon the number of rotational lines within the laser line width as determined by the exact placement of the laser line in the band-head.

C. Signal Calculations

In the following discussion, the order of magnitude of photons scattered to a receiver by an existing GCA-type laser probing a trail release of TMA will be calculated.

The laser system is assumed to have a power level of 5 MW, a pulse width of 30 nanoseconds with a receiving area of 10^3 cm^2. The energy of the pulse is 0.15 joules or 4×10^{17} photons at 4842.3Å. The receiver time is assumed to be equal to the transit time of the pulse through the scattering cloud. This effectively means the receiver time is adjusted to receive in one recording interval all the photons scattered by the cloud.

The scattered photons (omitting atmospheric and optical transmission lasers) is given by

$$S = \frac{P_\tau \, \tau_T n\ell \, \sigma \, A_r}{4\pi r^2} \tag{58}$$

where P_τ = transmitted power

τ_T = pulse width

n = concentration of $A\ell O$ molecules per cm^2

ℓ = path length through cloud

A_r = area of receiver

Using a range of 100 km for R, then

$$S \cong 4 \times 10^5 \, n\ell \, \sigma$$

Reasonable value estimates of $n\ell\sigma$ will now be obtained using a usual TMA payload of about 10 pounds. For a molecular weight of 72 this represents about 4×10^{25} molecules. It can be assumed that one-half the payload vaporizes while the other half of the released TMA is in the solid aluminum oxide form. Assume that this amount of $A\ell O$ is distributed over a trail 60 km long. Then the line density per cm, $n\ell = 1.5 \times 10^{18}$ molecules cm^{-1}.

In time, this trail will expand in width. In Table 15 there is calculated (for the above line density) for cylinders of radius r, the concentration per cm^3, the path length $n\ell$ (actually 2 rn) and the scattered photons S. The concentration is simply $\frac{n\ell}{\pi r^2}$ assuming all the material is within a radius r. The integrated concentration transverse to the trail

TABLE 15

CALCULATION OF OPACITY AND PHOTONS SCATTERED AS A FUNCTION OF TRAIL RADIUS

r (km)	n (cm^{-3})	2 rn (cm^{-2})	2 rnσ	S (photons/pulse)
1	5.1×10^{7}	1.0×10^{13}	2×10^{-1}	8×10^{4}
5	1.6×10^{6}	1.6×10^{12}	3.2×10^{-2}	1.2×10^{4}
10	4.1×10^{5}	8.2×10^{11}	1.6×10^{-2}	6.4×10^{3}
20	1.3×10^{5}	5.2×10^{11}	1.0×10^{-2}	4.0×10^{3}
50	1.6×10^{4}	1.6×10^{11}	3.2×10^{-3}	1.3×10^{3}
100	5.1×10^{3}	1.0×10^{11}	2.0×10^{-3}	8.0×10^{2}

$\sigma = 2 \times 10^{-14}$

is 2 rn while the opacity is 2 rnσ which is equivalent to the fractional scattering. The scattering S, total number of photons scattered into the laser receiver, has been discussed previously.

The time required to reach the various radii as a function of time is an important operational parameter which involves two processes. The first is a rapid process in which the released material achieves a radius r_o equal to the ambient density. The ambient density n_o, the initial radius r_o, and the diffusion coefficient D as a function of altitude over the relevant regime are presented in Table 16. The values of r_o are determined from

$$r_o = \left(\frac{n\ell}{\pi n_a}\right)^{1/2} \tag{59}$$

In cylindrical diffusion the value of the $\frac{1}{e}$ point (the Gaussian half width) is given by

$$r^2 = r_o^2 + 4\,Dt \tag{60}$$

For the values of r in Table 15, $r_o^2 \ll r^2$ consequently r_o may be omitted and

$$r^2 = 4\,Dt$$

or

$$t = \frac{r^2}{4D} \tag{61}$$

is the equation employed in calculating Table 17.

TABLE 16

ATMOSPHERIC CONCENTRATION AND DIFFUSION COEFFICIENT

H (km)	n_o (cm^{-3})	r_o (cm)	D ($cm^2\ sec^{-1}$)
80	5×10^{14}	3.2×10	5×10^4
100	10^{13}	2.3×10^2	10^6
120	5×10^{11}	3.2×10^3	6×10^7
140	7×10^{10}	2.7×10^3	5×10^8
160	3×10^{10}	4.2×10^3	10^9
180	1.5×10^{10}	5.9×10^3	2×10^9

TABLE 17

TIME (SECONDS) TO REACH RADIUS r AT VARIOUS ALTITUDES H

r	S	H					
		80	100	120	140	160	180
1	8×10^4	2.0×10^5	1.0×10^4	1.6×10^2	2.0×10	10	5
5	1.2×10^4	5.0×10^6	2.5×10^5	4.0×10^3	5.0×10^2	2.5×10^2	1.2×10^2
10	6.4×10^3	2.0×10^7	1.0×10^6	1.6×10^4	2.0×10^3	10^3	5×10^2
20	4.0×10^3	8.0×10^7	4.0×10^6	6.4×10^4	8.0×10^3	4×10^3	2.0×10^3
50	1.3×10^3	5.0×10^8	2.5×10^7	4.0×10^5	5.0×10^4	2.5×10^4	1.2×10^4
100	8.0×10^2	2.0×10^9	1.0×10^8	1.6×10^6	2.0×10^5	10^5	5.0×10^4

While molecular diffusion coefficients were employed, at altitudes below 100 km, eddy diffusion may be expected to increase the rate of growth. However, for the long times available laser probing is still of interest. The optical path length selected has been transverse to the trail. However, under conditions in which the optical path is oblique the scattering will increase by the cosecant of the angle to the normal.

Signal-to-noise considerations. – Since the photomultiplier can be cooled, internal noise is not a severe constraint. The airglow likewise is not an important consideration. The background of importance is the Aℓ0 solar scattered radiation under twilight conditions or the radiation from chemiluminescence of Aℓ0. The chemiluminescence radiation of night releases is lower per unit surface of the cloud by one order of magnitude than under twilight conditions. Hence, if it can be shown that under twilight conditions the signal-to-noise ratio is favorable, then under night conditions the situation must be even more favorable. The case is now examined where the divergence of the laser beam is 1 millirad so that at 100 km, the subtended area is approximately 10^{-2} km^2. The total projected area of the cloud when r is 1 km is 60 x 4 = 240 km^2. Of the total number of molecules available then (some 10^{25}) only $\frac{10^{-2}}{240} = 4 \times 10^{20}$ are in the field of view. At the rate of emission of 10^{-1} photons/molecule/sec, the receiver records 8×10^7 photons/sec (at 100 km range). For the trail transit time of 7 microseconds some 5.6×10^2 photons will arrive at the detector. The criterion for performance is the fluctuation ratio of the electron $\bar{n}_s \sqrt{2\bar{n}_n}$. For the above case $\frac{\bar{n}}{\sqrt{2\bar{n}_n}} = \frac{8 \times 10^4 Q}{\sqrt{1.1 \times 10^3 Q}} \sim$ $2 \times 10^3 Q^{1/2}$ which is a favorable ratio for reasonable values of Q, the

quantum efficiency of the detector in electrons per photon, e.g., if $Q = 0.2$ then

$$\frac{\bar{n}_s}{\sqrt{2\bar{n}_n}} \sim 10^3$$

for an $r = 1$ km situation. As the cloud grows in diameter the laser signal and the background solar signal decrease inversely with the radius (once the field of view of the laser receiver is filled) and

$$\frac{\bar{n}_s}{\sqrt{2\bar{n}_n}} \sim \frac{1}{r^{\frac{1}{2}}}$$

Consequently, when the trail radius has increased from 1 km to 100 km the signal-to-noise ratio decreases by $\frac{1}{10}$ and

$$\frac{\bar{n}_s}{\sqrt{2\bar{n}_n}} \sim 10^2$$

The above preliminary analysis indicates that for the realistic situation assumed herein (a 10-pound TMA release 60 km in length), a laser probe at 4842Å operating at the 5-MW power level with pulse width of 30 nanoseconds should be adequate for detection of the AℓO molecule for reasonable periods of time.

VII. EVALUATION OF TECHNIQUE FOR CALCULATION OF WINDS FROM LASER DENSITY DATA

A. Introduction

The slanting of the laser optical axis to perform density measurements not only vertically, but also over a broad area leads to a new possibility for the measurement of winds. Knowing the density at a fixed altitude and using the hydrostatic equation, one can obtain from the density distribution the vertical pressure distribution and, additionally, the temperature distribution. The hydrostatic equation is:

$$dp = - \rho g dz \tag{62}$$

In ordinary meteorological usage, the wind field is computed from the pressure by the geostrophic field equations:

$$v = \frac{1}{f\rho} \frac{\partial p}{\partial x} \quad \text{and} \quad u = \frac{-1}{f\rho} \frac{\partial p}{\partial y} \tag{63}$$

where f = Coriolis, constant = $2\Omega \sin \Phi$; Ω = earth's rotation rate, Φ = latitude.

v = east-west wind velocity component

u = north-south wind velocity component

ρ = density

p = pressure

There is now examined to the first order the requirements that such a system is feasible. First, the necessary pressure gradient for a specific wind velocity is determined for a specific height and compared with the

average pressure to determine the variation in pressure (or density equivalent). For an altitude of 50 km, the constants are:

$$\rho = 9.7 \times 10^{-7} \text{ gm/cm}^3, \ \Omega = 7.3 \times 10^{-5} \text{ rad/sec}$$

$$P = 0.76 \text{ mb} = 7.6 \times 10^{2} \text{ dynes/cm}^2$$

Using the geostrophic equation and a separation distance, delta X = 200 km with a v = 100 mph, a delta p ~ 7 dynes/cm^2 or a 1 percent variation is obtained. Consequently, the accuracy of the laser measurement of a density must be at least 1 percent for this situation. Because of the similar exponential behavior of ρ and P, this percentage variation of the variable to be measured is relatively constant with height. Performing the measurement at higher altitudes is advantageous since a larger area is available over which the density gradient can be measured. It is disadvantageous because the returned signal is smaller so that the measurement requirement to 1 percent accuracy is more difficult.

A possible instrumental setup is that for splitting the beam by a half-reflecting mirror and differencing the returns electronically at the receiver.

Another source of error that must be considered is due to height errors. By comparing the error in pressure due to a small change in dZ and that expected from the earlier analysis due to a pressure gradient of 1 percent, it is found that a 1-percent error in dp is due to height errors of 100 meters. Owing to the great resolution capability of a laser pulse of the order of a nanosecond, the height error is not considered to be important.

TABLE 18

SEPARATION OF LASER BEAMS AT DIFFERENT ALTITUDES FOR DIFFERENT ZENITH ANGLES, θ

h (km) \ θ	30°	45°	60°	75°
30	35	60	102	222
40	46	80	126	294
50	58	100	170	368
60	69	120	204	444
70	81	140	238	516

TABLE 19

PERCENTAGE VARIATION OF PRESSURE NECESSARY TO GIVE WIND VELOCITY FOR VARIOUS HORIZONTAL SEPARATION ΔX AT DIFFERENT LATITUDES

Velocity Miles/Hr	Velocity Km/Hr	ΔX Lat.	100 Km		200 Km		300 Km		400 Km		500 Km		1000 Km		2000 Km	
			30°	60°	30°	60°	30°	60°	30°	60°	30°	60°	30°	60°	30°	60°
30	50		0.1	0.3	0.3	0.5	0.5	0.9	0.6	1.5	0.7	1.8	1.4	3.6	2.8	7.2
60	100		0.3	0.5	0.6	1.0	0.9	1.6	1.2	2.1	1.5	2.5	3.0	5.0	6.0	10.0
90	150		0.45	0.8	0.9	1.6	1.35	2.4	1.8	3.1	2.25	4.8	2.5	8.0	5.0	16.0
120	200		0.6	1.0	1.2	2.1	1.8	3.1	2.4	4.2	3.0	5.0	6.0	10.6	12.0	21.0
180	300		0.9	1.6	1.8	3.1	2.7	4.8	3.6	6.3	4.5	8.0	9.0	16.0	18.0	32.0
240	400		1.2	2.1	2.4	4.2	3.6	6.3	4.8	8.3	6.0	10.5	12.0	21.0	24.0	42.0

Alternatively, while a single laser site is probably restricted to measurements of the pressure gradient over a horizontal distance of less than 500 km, a network or grid of lasers spaced 1000 to 2000 km apart could yield larger distances over which to measure the horizontal variation.

B. Calculations

1. Order-of-magnitude requirements. — The horizontal spreads in km for two laser beams inclined at a zenith angle θ and at 180-degree azimuth separation are presented in Table 18. The percentage variations of pressure necessary to give various wind velocities for various horizontal separations ΔX for different latitudes are shown in Table 19. The calculated numbers are independent of altitude because of the exponential covariation of pressure and density. There is a variation with latitude due to the occurrence of the sin Φ latitude factor in the Coriolis constant.

It is noted in Table 18 that, for a single station laser site, one only obtains reasonable separation 300 to 500 km for inclinations θ of 75 degrees and for altitudes above 40 km. Larger separations would be achieved by lasers operating at separate sites 1000 to 2000 km apart. The results of Table 19 indicate that the larger pressure differentials occur for more northerly latitudes, higher wind velocities, and larger separations. What must be assessed then is the possibility for measuring the basic parameters of atmospheric density or molecular concentration (since the molecular weight is constant) within the desired accuracy.

2. Two alternate variations for measuring winds. — Two major conditions must be fulfilled if this system is to be implemented. The first condition is that the returned signal must be large enough so that variations of 1 percent can be detected at the altitudes of interest (30 to 70 km) and the signal-to-noise ratio be adequate for this purpose. The second condition is that the signal must be of such a nature that the Rayleigh scattering component can be separated from the Mie component. This is essentially the problem of whether atmospheric density or dust or a combination of both is being observed in the scattering volume.

Calculations for the geostrophic wind technique. — As noted previously, a measurement of the horizontal pressure gradient of sufficient accuracy can be employed to determine the winds by the geostrophic Equation (63). However, only the relative density is measured because of the variable attenuation in the lower atmosphere so that the actual light intensity at the scattering volume is not known. Certainly the transmission will vay either diurnally or seasonally by a few percent. Consequently, since the scattered power is proportional to the product of the scattering centers and the light intensity, these cannot be separated.

However, if at a point free from Mie scattering, the density is determined by some alternate technique, this would constitute an absolute calibration of the laser scattering measurements of density. The most direct approach would be to employ measurements of pressure and temperature from a routine radiosonde balloon at a 10-mb pressure altitude or approximately 31.2 km. Pressure and temperature can be measured to that degree of accuracy. It can be assumed that the light intensity remains relatively

constant to within 1 percent above 31 km. Since at this altitude the molecular concentration is $2 \times 10^{17}/cm^3$ with a scale height of 6 km, the integrated column count is approximately 10^{23} molecules/cm^2. With a Rayleigh scattering coefficient of $\beta = 2 \times 10^{-27}$/molecule at 0.7 microns and $\beta = 0.35 \times 10^{-27}$/molecule at 1.1 micron, the additional attenuation above 31 km is satisfactorily less than the arbitrary 1-percent criterion.

In order to obtain the pressure values, use is made of

$$T_q = T_o \frac{\rho_o}{\rho_q} + \frac{GM}{R\rho_q} \int_{h_o}^{h_q} \rho(h)\, dh \qquad (64)$$

where the symbols have their standard meanings. This equation has been analyzed in great detail by Minzner and Sauerman.(113)

The percentage errors in temperature at different altitudes for different assumed errors in the base temperature which is assumed to be 300°K are presented in Table 20. The increase in error is due to the nature of Equation (64) in which errors in T_i are propagated upward by the ratios of ρ_o/ρ_q where ρ_o is the density for the lowest or laser altitude, whereas ρ_q is the altitude at the upper level. Middleton has estimated the error in measurement of temperature by high altitude radiosonde as being 0.2°K due to the effect of radiation under carefully controlled conditions. Additionally, the use of Equation (64) in a single gas downward integrated form estimating the temperature at 70 km yields an error of approximately 0.25°K for the temperature at 31 km. To obtain the temperature at 31 km, the temperature at 70 km is first estimated. It is considered that an

TABLE 20

ERRORS IN TEMPERATURE FROM EQUATION (14) FOR ERRORS IN BASE MEASUREMENT OF TEMPERATURE FOR SINGLE GAS UPWARD CALCULATION

H (km)	ρ (kg/m^3)	$\frac{\rho_o}{\rho}$	T (^oK)	Error					
				0.2°K		0.3°K		1.0°K	
				Abs.	%	Abs.	%	Abs.	%
31	1.60×10^{-2}	1.0	227	0.2	0.1	0.5	0.25	1.0	0.5
40	3.85×10^{-3}	4.8	251	1.0	0.5	2.5	1.0	5.0	2.0
50	1.02×10^{-3}	15.0	270	3.0	1.5	7.5	3.7	15.0	7.4
60	2.85×10^{-4}	57.0	254	11.0	5.7	27.0	14.0	55.0	28.0
70	7.80×10^{-3}	204.0	216	41.0	20.4	102.0	31.0	205.0	62.0

NOTE: Density and temperature taken from U.S. Standard Atmosphere, 1962

error in estimate of only $50^{o}K$ may occur because this regime is relatively stable. This error is diminished by ρ_o/ρ_q where now $\rho_o = \rho(71\ km)$ and $\rho_q = \rho(31\ km)$.

An evaluation can now be made as to the range of possibilities for this system still subject to the two limitations to be discussed below.

(1) Relative absence of Mie scattering above 30 km.

(2) Signal adequate to be analyzed to 1-percent accuracy.

The range of velocities which can be measured for an error of $0.2^{o}K$ in the base temperature for various horizontal separations at a latitude of $60^{o}N$ is indicated in Table 21. Basically, a comparison has been made between percent error figures for temperature in Table 20 and the percentage variation of pressure (temperature) for various horizontal separations required to generate winds of different intensity. Because of the varying horizontal separation with altitude for the single-station laser, a separate table (Table 22) has been prepared to show what wind velocities can significantly be measured. Tables 23 and 24 represent parallel tabulations for the case of a base temperature error of $1^{o}K$.

The calculations indicate that for a $0.2^{o}K$ base error in temperature all winds greater than 50 km/hr can be measured for horizontal separations greater than 400 km for altitude between 30 and 40 km. For stronger winds, the altitude range over which wind measurements are significant becom s larger, extending to higher altitudes of approximately 60 km. Consequently, the indications are good for the laser network associated with a radiosonde network as a complementary tool for achieving wind measurements to higher

TABLE 21

HEIGHT RANGE (KM) IN WHICH WINDS OF VELOCITY, V, CAN BE MEASURED FOR HORIZONTAL SEPARATION ΔX, FOR LATITUDE 60°N AND FOR ERROR 0.2°K IN MEASUREMENT OF BASE TEMPERATURE

Velocity Miles/Hr	Km/Hr	ΔX Km: 100	200	300	400	500	1000	2000
30	50	None	None	31-35	31-40	31-50	31-50	31-60
60	100	None	None	31-40	31-50	31-50	31-50	31-60
90	150	None	31-40	31-50	31-50	31-50	31-60	31-60
120	200	31-40	31-40	31-50	31-50	31-50	31-60	31-60
180	300	31-40	31-40	31-50	31-60	31-60	31-60	31-60
240	400	31-40	31-40	31-60	31-60	31-60	31-60	31-60

TABLE 22

GEOSTROPHIC WIND TECHNIQUE

CAPABILITY FOR MEASURING WINDS OF VELOCITY, V, FOR SINGLE-STATION LASER SLANTED AT ZENITH ANGLE 75° WITH ASSUMED BASE ERROR OF 0.2°K AT 31 KM FOR 60°N LATITUDE

H (km)	ΔX (Separation, km)	δT^* Percentage Temperature Error (%)	Capability for Measuring Wind (km/hr)
31	222	0.1	
40	294	0.5	> 25
50	368	1.5	> 100
60	444	5.7	> 200
70	516	20.4	> 400

*This is percentage error calculated from Equation (14) assuming absolute error of 0.2°K in measurement at 31 km.

TABLE 23

HEIGHT RANGE (KM) IN WHICH WINDS OF VELOCITY, V, CAN BE MEASURED FOR HORIZONTAL SEPARATION, ΔX (KM) FOR LATITUDE 60°N AND FOR ERROR 1.0°K IN MEASUREMENT OF BASE TEMPERATURE

Velocity Miles/Hr	Km/Hr	ΔX Km 100	200	300	400	500	1000	2000
30	50	None	None	31-35	31-35	31-35	31-45	31-45
60	100	None	None	31-35	31-40	31-40	31-50	31-50
90	150	None	None	31-40	31-45	31-40	31-50	31-53
120	200	None	None	31-40	31-45	41-45	31-50	31-55
180	300	None	None	31-40	31-45	31-50	31-55	31-60
240	400	30-40	30-40	31-40	31-50	31-50	31-55	31-60

TABLE 24

GEOSTROPHIC WIND TECHNIQUE

CAPABILITY FOR MEASURING WINDS OF VELOCITY, V, FOR SINGLE-STATION LASER SLANTED AT ZENITH ANGLE 75° WITH ASSUMED BASE ERROR OF 1.0°K AT 31 KM FOR 60°N LATITUDE

H (km)	ΔX (Separation, km)	δT^* Percentage Temperature Error (%)	Capability for Measuring Wind (km/hr)
31	222	0.5	> 50
40	294	2.0	> 100
50	368	7.4	> 300
60	444	28.0	> 400
70	516	62.0	Not possible

*This is percentage error calculated from Equation (14) assuming absolute error of 1.0°K in measurement at 31 km.

altitudes, since in such a form, the necessary horizontal separation can be achieved. The lack of adequate horizontal separation for a single laser station even for a zenith angle of 75 degrees limits the utility of wind measurements to predominantly below 40 km.

A larger base temperature error of $10^{o}K$ imposes greater restrictions on the region of significant wind measurement. However, for a ΔX value (horizontal separation) of 460 km, significant winds can be measured for velocities greater than 50 km/hr between 31 and 35 km. The altitude region increases to 45 km for a ΔX value of 2000 km. For higher velocity winds, the altitude regime of applicability is increases to 50 km for a 200 km/hr wind for a ΔX of 500 km. The single station technique is more limited and is basically applicable only between 30 and 40 km, since for higher altitudes only winds of velocity greater than 10 km/hr can be measured.

Thermal wind technique calculations. – This technique has for its basic requirement not only the measurement of temperature and pressure at approximately 30 km, but also the measurement of winds at 30 km by radar measurements. Using the thermal wind equations, Δu and Δv are calculated to yield the wind at altitudes above 30 km. The major problem to be evaluated is the question of the errors in the values of the temperature determined by the laser measurements due to the propagation of errors by Equation (64).

The governing equations for the thermal wind equation are:

$$\frac{\partial v}{\partial Z} = \frac{g}{fT}\frac{\partial T}{\partial X} \qquad \text{and} \qquad \frac{\partial u}{\partial z} = \frac{-g}{fT}\frac{\partial T}{\partial y} \tag{65}$$

where the symbols have their usual meaning. The ΔT values for various separations ΔX are calculated in Table 24 to give the thermal wind Δu over a 10-km vertical interval for latitudes 30 and 60°N. It is the ΔT's in this table (absolute values) which when compared with the δT's, the errors in the measured and extrapolated value from Equation (64) of temperature, that determine the region of validity for measuring Δu. The geometrical altitudes and the wind velocities, within which significant measurements can occur, are presented in Tables 25 through 29 for base temperature errors of 0.2°K and 1.0°K.

For a base temperature error of 0.2°K, two laser stations separated by a distance exceeding 300 km can perform significant thermal wind measurements for Δu relatively small (of the order of 10 km/hr/10 km). At 1000 to 2000 km separation distances, the altitude region of significance increases to 55 km for the previously quoted value of Δu. A single laser site with a zenith angle slanting capability of 45 degrees can measure Δu of 10 to 40 km/hr/10 km in the region up to 40 km altitude. Thereafter the thermal wind must be significantly higher to be measured at higher altitudes.

For a base temperature error of 1.0°K, two laser stations separated again by 300 km can perform significant thermal wind measurements for Δu greater than 30 km/hr/10 km in the altitude region 31 to 35 km. When the separation ΔX increases as indicated in Table 28, the measurable Δu decreases to 10 km/hr/10 km in the altitude region 31 to 35 km. Stronger wind changes of the order of 50 km/hr/10 km can be measured up to 45 km

TABLE 25

ΔT REQUIRED TO GIVE VELOCITY CHANGE Δu OVER A TEN KILOMETER VERTICAL INTERVAL FOR VARIOUS HORIZONTAL SEPARATIONS ΔX AT DIFFERENT LATITUDES

ΔX km / Δu Km/Hr/10 km	100 km		200 km		300 km		400 km		500 km		1000 km		1200 km		2000 km	
	30°	60°	30°	60°	30°	60°	30°	60°	30°	60°	30°	60°	30°	60°	30°	60°
1	6×10^{-3}	10^{-2}	10^{-2}	2×10^{-2}	0.02	0.03	0.02	0.04	3×10^{-2}	5×10^{-2}	6×10^{-2}	0.1	0.06	0.12	0.1	0.2
10	6×10^{-2}	0.1	0.1	0.2	0.2	0.3	0.2	0.4	0.3	0.5	0.6	1.0	0.6	1.2	1.2	2.0
20	0.1	0.2	0.2	0.4	0.3	0.6	0.4	0.8	0.6	1.0	1.2	2.0	1.2	2.4	2.4	4.0
40	0.25	0.4	0.5	0.8	0.75	1.2	1.0	1.6	1.2	2.0	2.4	4.0	3.0	4.8	4.8	8.0
50	0.3	0.5	0.6	1.0	0.9	1.5	1.2	2.0	1.5	2.5	3.0	5.0	3.6	6.0	6.0	10.0
80	0.5	0.8	1.0	1.6	1.5	2.4	2.0	3.2	2.4	4.0	4.8	8.0	6.0	9.6	9.6	16.0
100	6×10^{-1}	1.0	1.2	2.0	1.8	3.0	2.4	4.0	3.0	5.0	6.0	10.0	7.2	12.0	12.0	20.0
200	1.2	2.05	2.4	4.2	3.6	6.15	4.8	8.4	6.0	10.5	12.0	21.0	14.4	25.2	24.0	42.0
300	1.8	3.0	3.6	6.0	5.4	9.0	7.2	12.0	9.0	15.0	18.0	30.0	21.6	36.0	36.0	60.0
400	2.4	4.1	4.8	8.4	7.2	12.3	9.6	16.8	12.0	21.0	24.0	42.0	24.8	504.0	48.0	84.0

TABLE 26

THERMAL WIND CALCULATIONS

HEIGHT RANGE (KM) IN WHICH VERTICAL WIND CHANGE Δu (KM/HR/10 KM) CAN BE SIGNIFICANTLY MEASURED FOR HORIZONTAL SEPARATION ΔX, FOR LATITUDE 60°N AND FOR ERROR 0.2°K IN MEASUREMENT OF BASE TEMPERATURE

ΔX km / Δu Km/Hr/10 km	100	200	300	400	500	1000	1200	2000
	60°	60°	60°	60°	60°	60°	60°	60°
1	None	None	None	None	None	None	None	None
10	None	None	31-35	31-35	31-35	31-40	31-40	31-55
20	None	31-35	31-35	31-35	31-40	31-45	31-45	31-55
40	31-35	31-35	31-40	31-40	31-45	31-50	31-50	31-50
50	31-35	31-40	31-40	31-40	31-45	31-50	31-50	31-55
80	31-35	31-40	31-45	31-50	31-50	31-55	31-55	31-60
100	31-40	31-50	31-50	31-55	31-55	31-60	31-65	31-70
200	31-45	31-50	31-50	31-55	31-60	31-65	31-65	31-70
300	31-45	31-50	31-55	31-60	31-65	31-65	31-70	31-70
400	31-50	31-55	31-55	31-60	31-65	31-70	31-70	31-70

TABLE 27

CAPABILITY FOR MEASURING THERMAL WIND OF VELOCITY Δu (KM/HR/10 KM) FOR A SINGLE-STATION LASER SLANTED AT 75° ZENITH ANGLE WITH ASSUMED BASE TEMPERATURE ERROR OF 0.2°K FOR 60°N LATITUDE

H (km)	ΔX (Separation, km)	δT Absolute Temperature Error	Capability For Measuring Thermal Wind (km/Hr/10 km)
31	222	0.2	> 10
40	294	1.0	> 40
50	368	3.0	> 50
60	444	11.0	> 200
70	516	41.0	

TABLE 28

THERMAL WIND CALCULATIONS
HEIGHT RANGE IN WHICH VERTICAL WIND CHANGE Δu (KM/HR/10 KM) CAN BE SIGNIFICANTLY MEASURED FOR HORIZONTAL SEPARATION ΔX, FOR LATITUDE 60°N, AND FOR ERROR 1.0°K IN MEASUREMENT OF BASE TEMPERATURE

ΔX km / Δu Km/Hr/10 km	100	200	300	400	500	1000	1200	2000
	60°	60°	60°	60°	60°	60°	60°	60°
1	None	None	None	None	None	None	None	None
10	None	None	None	None	None	None	None	31-33
20	None	None	None	None	None	31-33	31-33	31-35
40	None	None	None	31-33	31-33	31-37	31-37	31-45
50	None	None	31-33	31-33	31-33	31-40	31-40	31-45
80	None	31-35	31-35	31-35	31-37	31-42	31-42	31-50
100	None	31-35	31-35	31-37	31-40	31-45	31-45	31-55
200	31-35	31-35	31-40	31-40	31-50	31-52	31-52	31-57
300	31-35	31-40	31-45	31-45	31-50	31-55	31-55	31-60
400	31-35	31-45	31-45	31-50	31-53	31-60	31-57	31-62

TABLE 29

CAPABILITY FOR MEASURING THERMAL WIND OF VELOCITY Δu (KM/HR/10 KM) FOR A SINGLE-STATION LASER SLANTED AT 75° ZENITH ANGLE WITH ASSUMED BASE TEMPERATURE ERROR OF 1.0°K FOR 60°N LATITUDE

H (km)	ΔX (Separation, km)	δT Absolute Temperature Error	Capability For Measuring Thermal Wind (km/Hr/10 km)
31	222	1.0	> 50
40	294	5.0	> 100
50	388	15.0	> 300
60	444	55.0	
70	516	205.0	

altitude. The slanted laser single station calculations (Table 29) indicate capability for measuring thermal winds Δu of 50 to 100 km/hr/10 km. As the geometrical altitude increases, only winds of considerably higher velocity can be measured.

Evaluation of magnitude of laser signal returns. – In the use of the areal laser technique, it is necessary, although not a sufficient condition, that the signal be large enough so that it can be measured to approximately 1-percent accuracy. This requirement can also be stated by insisting that the signal-to-noise ratio be of the order of 100. This criterion should be satisfied up to the altitude of approximately 70 km. The signal return is given by:

$$C = \left(\frac{n\rho_R}{h^2}\right) \frac{\pi D^2 \, c \, N_o \, T^2 \, Q \, \tau_r}{8} \tag{66}$$

where n = number density of molecules,

ρ_R = Rayleigh back-scattering function,

h = range,

D = mirror diameter,

τ_r = integration time,

c = velocity of light,

N_o = number of photons in single pulse,

T = fraction of light transmitted by the atmosphere,

Q = quantum efficiency of photomultiplier.

As an indication of the capability of present laser probing setups, the equipment of Chemesha, et al [114] is described. These equipment characteristics are:

$D = 0.5$ m

$\tau_r = 10^{-5}$ sec

$\beta_R = 1.98 \times 10^{-32}$ m^2 $sterad^{-1}$

$N_o = 1.0 \times 10^{19}$ photons

$T^2 = 0.3$

$Q = 0.03$.

For a single pulse this equipment yields a count of 2 photons at an altitude of 60 km. At lower altitudes, the count rises exponentially and accurate measurements can be performed. Integration may be performed over a large number of pulses, e.g., 100. This results in relatively long integration time and decreases the statistical fluctuations, since even at present, ten pulses per minute is achievable. The Clemesha group is presently expanding the mirror diameter D to approximately 5 m (actually 4.5 m) by constructing a mosaic of smaller mirrors. This should increase the signal by some two orders of magnitude.

The noise background is fundamentally statistical noise of the signal itself. Sky noise during the night (and the preceding discussion has been restricted to the night) is mainly wide-band and can be reduced to negligible proportions by using even a 2-millimicron filter. The noise from the photomultiplier itself can be reduced significantly by cooling the photocathode. It is considered that with this increase in mirror diameter by

a factor of 100, summing over a large number of pulses approximately 300, and increase of energy to a small extent (say a factor of 3), the signal-to-noise ratio $S/N = N/\sqrt{N} = 100$ for altitudes in the neighborhood of 70 km. It is considered that with the above suggested parameters, which are within the current state-of-the-art, accuracies of less than 1 percent in density measurements can be achieved.

Magnitude of Mie scattering in the mesosphere. – As noted previously, a basic requirement is that the scattering in the region 30 to 70 km must be Rayleigh scattering. Moreover, this requirement is rather stringent in that the Mie scattering component must account for less than 1 percent of the total scattering.

In general, atmospheric Mie scattering diminishes with height. Layers are observed at 20 km[115] and at 70 km[116] and at higher altitutdes above 100 km, presumably due to meteoritic impact. Also in general, the Mie scattering in the region 30 to 70 km is substantially less than that of Rayleigh scattering. This is the fundamental basis upon which even relative measurements of density in the mesosphere are meaningful. Measurements by optical radar in the 30 to 70 km region have systematically followed the standard atmosphere curve. However, it would appear at present that there is insufficient data to characterize this region as a Rayleight scattering region to within 1 percent.

C. Conclusions and Recommendations

(1) The wind measuring technique outlined above is best suited to laser stations separated by distances of 1000 to 2000 km. This is due to the temperature errors as extrapolated upward from Equation (64), so that a large horizontal spread is required to overcome the aforementioned temperature error.

(2) There is a basic uncertainty in the system due to the lack of knowledge of Mie scattering to the 1-percent level in the mesosphere. This necessary precision would be difficult to achieve even utilizing multiple frequencies and multiple sites.

(3) Perhaps the most effective procedure to check the suggested techniques would be to have two lasers each operating at a weather radiosonde site which are widespread throughout the United States. A site in the North American rocket launching network which is in between the radiosonde sites or close by should be selected. Then wind measurements (chaff) by rockets and by the laser geostrophic wind technique should be compared over a reasonable number of trails.

REFERENCES

1. Wentink, T., Jr., Isaacson, L. and Spindler, R. J., "Research on the Opacity of Low Temperature Air: Oscillator Strengths, etc.," Air Force Weapons Laboratory Report AFWL-TR-65-139 (December 1965).

2. Wentink, T., Jr., Isaacson, L. and Marram, E. P., "Research on the Opacity of Low Temperature Air: Oscillator Strengths, etc.," Air Force Weapons Laboratory Report AFWL-TR-67-6 (January 1967).

3. Wentink, T., Jr., Isaacson, L., Marram, E. P. and Spindler, R. J., "Experimental Determination of Molecular Oscillator Strengths," Air Force Weapons Laboratory Report AFWL-TR-67-30 (February 1967).

4. Nicholls, R. W., Ann. de Geophysique 20, 144 (1964).

5. Dalby, F. W., "Encyclopedia of Physics," Vol. XXVII, p. 460, ed. by S. Flugge, Springer-Verlag, Berlin (1964).

6. Soshnikov, V. N., Usp. Fiz. Nauk. 74, 61 (1961); translated in Soviet Physics Uspekhi 4, 425 (1961).

7. Lofthus, A., "Molecular Spectrum of Nitrogen," Spectroscopic Report No. 2 of Dept. of Physics, University of Oslo, Blindern, Norway (in English) (December 1960).

8. Tilford, S. G., Wilkinson, P. G., Franklin, V. B., Naber, R. H., Benesch, W. and Vanderslice, J. T., Ap. J. Supplement Series No. 115, XIII, 31 (1966) and numerous references therein.

9. Tanaka, Y., Namioka, T. and Jursa, A. S., Can. J. Phys. 39, 1138 (1961); see also J. Chem. Phys. 39, 2629 (1963) and numerous references therein.

10. Krupenie, P. H., "Band Spectrum of CO," National Bureau of Standards NSRDS-NBS-5 (July 1966).

11. Informal Meeting of IDA Atomic and Molecular Panel, Institute for Defense Analysis (8 December 1967).

12. Main, Roger P., (Heliodyne Corp.), Unpublished, "Survey on Oscillator Strengths of Metallic Oxides, etc." and presented at the Informal Meeting of IDA Atomic and Molecular Panel (8 December 1967).

13. Main, R. P., Carlson, D. J. and DuPuis, R. A., JQRST 7, 805 (1967).

14. Brewer, L., University of California at Berkeley (private communication).

15. Vanpee, M., Kineyko, W. R. and Caruso, R., Thiokol (Denville, N. J.), Semiannual Report on ARPA Order No. 553, Contract No. DA-31-124-ARO-D-441 (October 1967).

16. Johnson, E. R., Lloyd, K. H., Low, C. H. and Sheppard, L. M., Australian Defence Scientific Service, Weapons Research Establishment Report HSA-23 of June 1967 (Adelaide, S. Australia).

17. Main. R. P., Morsell, A. L. and Hooker, W. J., unpublished work on SiO, to be submitted to JQSRT in early 1968.

18. Wentink, T., Jr., Isaacson, L., Marram, E. P. and Spindler, R. J., Air Force Weapons Laboratory, "Ablative Material Spectroscopy," AFWL-TR-67-30, Vol. I (November 1967).

19. Kivel. B. and Camm, J., Avco-Everett (AERL) Research Note 374 of 1958, edited and reissued July 1963).

20. Sauermann, G. O. and Schultz, E. D., "Resonant Scattering Parameters for the Elements," GCA Technology Division Report GCA-653 (1965).

21. Walsh, R. M., University of California (Berkeley), Ph.D. Thesis (1965). See also University of California Radiation Laboratory Report UCRL-11927 (1965).

22. Herzberg, G., Electronic Spectra of Polyatomic Molecules, D. Van Nostrand Co., Inc., Princeton, N. J. (1966).

23. Herzberg, G., Proc. Roy. Soc. (London) 262A, 291 (1961).

24. Wentink, T., Jr., Isaacson, L., Marram, E. P. and Spindler, R. J., Avco Report issued by Air Force Weapons Laboratory, Kirtland Air Force Base, New Mexico, AFWL-TR-67-30 (July 1967).

25. Fink, E. H. and Welge, K. H., J. Chem. Phys. 46, 4315 (1967).

26. Linevsky, M. J., General Electric MSD Project Glow Report 66SD9175, (November 1966). To be published in J. Chem. Phys.

27. Bennett, R. G. and Dalby, F. W., J. Chem. Phys. 32, 1716 (1960).

28. Spindler, R. J., JQSRT 5, 165 (1965).

29. Nicholls, R. W., JQSRT 5, 647 (1965).

30. Main, R. P. and Bauer, E., JQSRT 7, 527 (1967).

31. Ortenberg, F. S. and Antropov, E. G., Soviet Phys. Usp 9, 717 (1967); issued first in Usp, Fiz. Nauk. 90, 237 (1966).

32. Nicholls, R. W., J. Res. Natl. Bureau Std. (U.S.) 65A, 451 (1961).

32a. Childs, D. R., JQSRT 4, 283 (1964).

33. Ortenberg, F. S., Opt. Spectry. (USSR) 9, 82 (1960).

34. Pathak, A. N. and Masheshwari, R. C., Indian J. Pure Appl. Phys. 5, 138 (1967).

35. Spindler, R. J. (unpublished work).

36. Vanderslice, J. T., Mason, E. A. and Lippincott, J. Chem. Phys. 30, 129 (1959).

37. Benesch, W., Vanderslice, J. T., Tilford, S. G. and Wilkinson, P. G., Astrophys. J. 143, 236 (1966).

38. Stern, O. and Volmer, M., Physik Z. 20, 183 (1919).

39. Bennett, R. G. and Dalby, F. W., J. Chem. Phys. 40, 1414 (1964).

40. Wentink, R., Jr. and Isaacson, L., J. Chem. Phys. 46, 822 (1967).

41. Arnold, J. S., Brown, R. J. and Ogryzlo, E. A., Photochem. and Photobiology 4, 963 (1965).

42. Fiocco, G., and Grams, G. W., "Optical Radar Observations of Mesospheric Aerosols in Norway During the Summer of 1966," Quarterly Progress Report, Research Laboratory for Electronics, M.I.T. No. 86, p. 59 (July 15, 1967); see also other references therein.

43. Minch, R. W., Hagenlocker, E. E., and Rado, W. G., "Consideration and Evaluation of Factors Influencing the Stimulated Optical Scattering in Gases," Ford Scientific Laboratory Report of 23 March 1966.

44. Herzberg, G., Molecular Spectra and Molecular Structure, Vol. I, Spectra of Diatomic Molecules, D. Van Nostrand Co., Princeton, N. J. (1950).

45. Hester, R. E., "Raman Intensities and the Nature of the Chemical Bond," in Raman Spectroscopy, H. Szymanski, Plenum Press, New York, (1967) p. 101.

46. Stoicheff, B. P., "High Resolution Raman Spectroscopy," in Advances in Spectroscopy, Vol. I, ed. by H. W. Thompson, Interscience Publishers, Inc., New York (1959) p. 91.

47. Yoshino, T., and Berstein, H. J., "Intensity on the Raman Effect: The Mean Polarizability Derivatives of Hydrocarbon Molecules," Spectro. Chemica Acta 14, 127 (1959).

48. Yoshino, T., and Berstein, H. J., "Intensity in the Raman Effect VI and VII," J. Mol. Spectroscopy 2, 213-252 (1958).

49. Glass, A., ONR, ARPA Laser Physics Conference, Des Plaines, Ill. (March 22, 1965).

50. Glass, A., "Propagation Effects at High Power," Laser Propagation in the Atmosphere, Ohio State University, August 1-11, 1967.

51. Hirono, M., J. Radio Research Lab., (Japan) 11, 251 (1964).

52. Vassiliadis, A. and Battelle, R. B., Final Report on Contract No. DA-49-146-XF-324 (Standford Research Institute)(January 1965).

53. Moore, H. R., Final Report on Contract AF33(657)-13801, "Electro-Optical Systems," (April 1965).

54. Atwill, W., et al., Final Report on Contract No. DA-49-146-XF-350, GCA Technology Division (December 1965).

55. Kopfermann, H., Nuclear Moments, Academic Press, New York (1958) pp. 73, 166, 451, 455.

56. Meissner, K. W., Mundie, L. G. and Stelson, P. H., "Structure of the ^2D Terms of the Arc Spectrum of Lithium," Phys. Rev. 74, 932 (15 October 1948).

57. Kusch, P. K. and Taub, H., Phys. Rev. 75, 1477 (1949).

58. Kopfermann, H., ibid., pp. 73, 441, 451.

59. Logan, R. A. and Kusch, P., Phys. Rev. 81, 280 (1951).

60. Sagalyn, P. L., "The Hyperfine Structure of the $^3P_{3/2}$ state of Na^{23}," Phys. Rev. 94, 885 (15 May 1954).

61. Kopfermann, ibid., pp. 73, 92, 166, 441, 451.

62. Ochs, S. A., Logan, R. A. and Kusch, P., Phys. Rev. 78,184 (1950).

63. David, L., Nagle, D. and Zacharias, J. R., Phys. Rev. 76, 1068 (1949).

64. Jackson, D. A. and Kuhn, H., "Hyperfine Structure, Zeeman Effect and Isotope Shift in the Resonance Lines of Potassium," Proc. Roy. Soc. A165, 303 (5 April 1938).

65. Data on Fission Products are taken from General Electric Chart of the Nuclides.

66. Kopfermann, H., ibid., pp. 73, 102, 166, 441, 451.

67. Kopfermann, H. and Kruger, H., Z. Phys. 103, 315 (1956).

68. Senitzky, I. R. and Rabi, I., Phys. Rev. 103, 315 (1956).

69. Kopfermann, H., ibid., pp. 73, 441, 452.

70. Essen, L., Perry, J. V. L. and Bullard, E. C., Nature 176, 280, 284 (1955).

71. Stroke, H. H., Jaccarino, V., Edmonds, D. S. and Weiss, R., Phys. Rev. 105, 590 (1957).

72. Sorokin, P. P. and Lankard, J. R., "Stimulated Emission Observed from an Organic Dye, Chloro-Aluminum Phthalocyanine," IBM J. of Res. and Dev. 10, 162 (March 1966).

73. Spaeth, M. L. and Bortfeld, D. P., "Stimulated Emission from Polymethine Dyes," Appl. Phys. Letters 9, 179 (1 September 1966).

74. Schafer, F. P., Schmidt, W. and Volze, J., "Organic Dye Solution Laser," Appl. Phys. Letters 9, 306 (15 October 1966).

75. Sorokin, P. P., Culver, W. H., Hammond, E. C. and Lankard, J. R., "End-pumped Stimulated Emission from a Thiacarbocyanine Dye," IBM J. of Res. and Dev. 10, 401 (September 1966).

76. Sorokin, P. P., Lankard, J. R., Morizzi, V. L. and Hammond, E. C., "Organic Dye-Stimulated Emission Spectra," Bull. Am. Phys. Soc. 12, 90 (January 1967).

77. Schafer, F. P., Schmidt, W. and Marth, K., "New Dye Lasers Covering the Visible Spectrum," Phys. Letters 24A, 280 (27 February 1967).

77a. Sorokin, P. P., Lankard, J. R., Hammond, E. C. and Morizzi, V. L., "Laser-pumped Stimulated Emission from Organic Dyes: Experimental Studies and Analytical Comparisons," IBM J. of Res. and Dev. 11, 130 (March 1967).

78. McFarland, B. B., "Laser Second-Harmonic-Induced Stimulated Emission of Organic Dyes," Appl. Phys. Letters 10, 208 (1 April 1967).

79. Sorokin, P. P. and Lankard, J. R., "Flashlamp Excitation of Organic Dye Lasers: A Short Communication," IBM J. of Res. and Dev. 11, 148 (March 1967).

80. Soffler, B. H. and McFarland, B. B., "Continuously Tunable, Narrow Band Organic Dye Lasers," Appl. Phys. Letters 10, 266 (15 May 1967).

81. Bloembergen, N., Non-Linear Optics, W. A. Benjamin, Inc., New York (1965).

82. Minck, R. W., Terhune, R. W. and Wang, C. C., "Non-Linear Optics," Proc. IEEE 54, 1357 (October 1966).

83. Giordmaine, J. A. and Miller, R. C., Appl. Phys. Letters 9, 298 (15 October 1966).

84. Eckhardt, G., "Selection of Raman Laser Materials," IEEE J. Quant. Elec. QE-2, 1 (January 1966).

85. Kupper, F. P. and Funfer, E., "Doppler Shift of Ruby Laser Light by Means of a Kerr Cell Traveling Wave Line," Phys. Letters 19, 486 (1 December 1965).

86. Duguay, M. A., Hargrove, L. E. and Jefferts, K. B., "Optical Frequency Translation of Mode-Locked Laser Pulses," Appl. Phys. Letters 9, 287 (15 October 1966).

87. Garrett, C. G. B. and Guguay, M. A., "Theory of the Optical Frequency Translator," Appl. Phys. Letters 9, 374 (15 November 1966).

88. Teller, E., "The Photon Accelerator," Bull. Am. Phys. Soc. 12, 629 (May 1967).

89. Wieder, I. and McCurdy, G. B., "Isotope Shifts and the Role of Fermi Resonance in the CO_2 Infrared Maser," Phys. Rev. Letters 16, 565 (28 March 1966).

90. McCurdy, G. B. and Wieder, I., "Generation of New Infrared Maser Frequencies by Isotopic Substitution," IEEE J. Quant. Elec. QE-2, 385 (September 1966).

91. Fork, R. L. and Patel, C. K. N., Proc. IEEE 52, 208 (February 1964).

92. Brunet, H., "High Resolution Spectroscopy by Zeeman Tuned Infrared Laser," IEEE J. Quant. Elec. QE-2, 382 (September 1966).

93. Fork, R. L., Sargent, M. and Lamb, W. E., "Measurement of Atomic Parameters Using Magnetic Field Tuned Optical Masers," Bull. Am. Phys. Soc. 12, 89 (January 1967).

94. Carman, R., "Wide-Range Continuously Tunable High Power Sum Frequency Generation," Bull. Am. Phys. Soc. 12, 668 (May 1967).

95. Singer, J. R., "Tunable Ion Lasers," Bull. Am. Phys. Soc. 12, 668 (May 1967).

96. Garmire, E., Stimulated Raman Emission Ion Liquids, Proc. of Physics of Quantum Electronics Conference, San Juan, Puerto Rico (June 28-30, 1965) ed. P. E. Tannewald, P. L. Kelley and B. Lax, McGraw-Hill, N.Y., p. 167 (January 1966).

97. Glass, A., "Design Considerations for Raman Lasers," IEEE J. Quant. Elec. QE-3, 249 (June 1967).

98. Bloembergen. N., Bret, G., Lallemand, P., Pine, A. and Simova, P., "Controlled Stimulated Raman Amplification and Oscillation in Hydrogen Gas," IEEE J. Quant. Elec. QE-3, 197 (May 1967).

99. Avizonis, P. V., "Observations on Stimulated Raman Scattering in Hydrogen," Bull. Am. Phys. Soc. 12, 629 (May 1967).

100. Tannewald, P. E., "Mode Structure in a Resonant Raman Oscillator," Bull. Am. Phys. Soc. 12, 662 (May 1967).

101. Narcisi, R. A. and Bailey, A. D., J. Geophys. Res. 70, 3687 (1965).

102. Best, G., "Upper Atmosphere Temperature Determination Using AlO Bands Excited by the Sun at Twilight," GCA-TR-67-7-N, Contract NASW-1083 (May 1967).

103. Johnson, E. R., et al., "The Radiant Output of Grenade Glow Clouds in the Lower Thermosphere," Report HSAB, Dept. of Supply, Ans-Dif. Sci. Serv., Wea. Res. Establ. (June 1967).

104. Harang, O., "AlO Resonant Spectrum for Upper Atmospheric Temperature Determination," AFCRL-66-314, Envir. Res. Paper No. 192 (May 1966).

105. Authier, B., et al., Ann. de Geophys. 20, 342 (1964).

106. Authier, B., ibid, 353.

107. Rosenberg, N. W., et al., J. Geophys. Res. 69, 7 (1 April 1964).

REFERENCES (continued)

108. Armstrong, E., PASS II, 733-742 (1963).

109. Pearse, R. W. B. and Gayden, A. G., Identification of Molecular Spectra, 3rd ed., Chapman and Hall, London (1963).

110. Tyte, D. C. and Nicholls, R. W., Identification Atlas of Molecular Spectra, 1. The AlO A $^2\Sigma$ - X $^2\Sigma$ Blue-Green System, Univ. of Western Ont. (March 1962).

111. Wentink, T., Jr., private communication (December 1967).

112. Vanpee, M., Kineyko, W. R. and Caruso, R., "Study of Reentry Observables," Thiokol Chem. Corp. Report of October 24, 1967 on ARPA Order No. 553, DA-31-124-ARO-D-441.

113. Minzner, R. and Sauermann, G., "Temperature Determination of Planetary Atmosphere," GCA Technical Report 66-6-N, Contract No. NASW-1225 (1966).

114. Clemesha, R., et al., J. Appl. Meteor. 6, 386.

115. Junge, C. E. and Mairson, J. E., Geophys. Res. 66, 2163 (1961).

116. Fiocca, G. and Smullin, L. D., Nature 199, 1275 (1963).

APPENDIX A

COMPILATION OF KNOWN FRANCK-CONDON FACTORS AND r-CENTROIDS

The following compilation of sources of $q_{v'v''}$ and $\bar{r}_{v'v''}$ matrices should be considered preliminary and will be revised as required.

In the tables, references to the original arrays are listed for approximately 50 diatomic molecules and in some cases additionally their ions or isotopic modifications, and some 165 separate band systems. The matrix size (extent in maximum v' and v'' covered) is given, whether it is based on the Morse or RKR (more realistic, tabular) potential assumption, and if the known calculation included an equivalent r-centroid array. The $q_{v'v''}$ and/or $\bar{r}_{v'v''}$ may not be published but are listed it they are retrievable.

Judgements have not been made regarding best array. In general, the largest $q_{v'v''}$ matrix size, especially is accompanied by a $\bar{r}_{v'v''}$ matrix, is an indication that modern large computers have been employed so that it probably represents a best choice. This is particularly true if an RKR potential well was used. An important exception, based on experience, is Reference F-5 for NO(?); Reference W-7 is recommended instead.

The 96 references employed herein in Table 1 have been typed by an IBM printer directly from punched cards. This approach was selected to facilitate present and future editing,and subsequent printings of an anticipated expanded reference list.

KEY TO TABLE 1

a: Includes some modification of potential such as Morse-Pekeris.

b: Rydberg-Klein-Rees or alternative experimentally determined potential.

c: Matrix size given means maximum valve of v′ and v″; e.g., 4 x 9 covers v′ = 0 through 4 and v″ = 0 through 9. In many publications, the arrays are not complete, and often $\sum_{v''} q_{v'v''}$ or $\sum_{v'} q_{v'v''}$ are less than unity. 0 x 0 means only v′ = 0, v″ = 0 data given.

d: ( ) indicates unpublished data but usually available on request.

e: [ ] indicates reference for potentials used in calculation of RKR arrays.

f: N-11 quoted as unpublished in Reference N-10.

g: Data of Reference S-8 for D-A of MgO are applicable to a good approximation to C-A since the vibrational constants of C and D are so similar.

h: $q_{v'v''}$ not given explicitly.

TABLE 1

SOURCES OF FRANCK-CONDON FACTORS AND r-CENTROIDS FOR DIATOMIC MOLECULES

Molecule	System Name	Transition		Morse Potential[a]			RKR Potential[b]		
		Upper State	Lower State	$q_{v'v''}$ (Note c,d)	$r_{v'v''}$ (Note c,d)	Reference	$q_{v'v''}$ (Note c,d)	$r_{v'v''}$ (Note c,d)	Reference (Note e)
AlO	Green	A $^2\Sigma^+$	X $^2\Sigma^+$	7 x 7		N-1	9 x 9	9 x 9	S-6 [5-6]
B_2		A $^3\Sigma_u^-$	X $^3\Sigma_g^-$	0 x 0		H-1			
				2 x 3		N-2			
BH		B $^1\Sigma^+$	A $^1\Pi$	0 x 0		H-1			
				2 x 2		N-2			
BCl		A $^1\Pi$	X $^1\Sigma$	4 x 8	(4 x 8)	W-5			
BBr		A $^1\Pi$	X $^1\Sigma$	(3 x 5)	(3 x 5)	S-4			
BF		A $^1\Pi$	X $^1\Sigma$	4 x 9	(4 x 9)	W-5			
		b $^3\Sigma^+$	a $^3\Pi$	3 x 3	3 x 3	P-1			
BN	Violet	A $^3\Pi$	X $^3\Pi$	0 x 0		H-1			
				3 x 4		N-2			
				(?)		(N-11) N-10[f]			
BO	Alpha	A $^2\Pi_i$	X $^2\Sigma^+$	0 x 0		H-1			
				8 x 8		N-2			
				5 x 5		N-3			
				(4 x 10)	(4 x 10)	S-4			
	Beta	B $^2\Sigma^+$	X $^2\Sigma^+$	0 x 0		H-1			
				4 x 8		N-2			
				(4 x 15)	(4 x 15)	S-4			
	(Combination)	B $^2\Sigma^+$	A $^2\Pi_i$	0 x 0		H-1			
				5 x 5		N-2			

TABLE 1 (continued)

Molecule	System Name	Transition		Morse Potential[a]			RKR Potential[b]			
		Upper State	Lower State	$q_{v'v''}$ (Note c,d)	$r_{v'v''}$ (Note c,d)	Reference	$q_{v'v''}$ (Note c,d)	$r_{v'v''}$ (Note c,d)		
BaO		$A\ ^1\Sigma$	$X\ ^1\Sigma$	14 x 13		O-5				
				6 x 6		O-7				
				(?)	(?)	(N-11) N-10				
				(10 x 5)	(10 x 5)	S-4				
PeO		$A\ ^1\Pi$	$X\ ^1\Sigma^+$	(?)	(?)	(N-11) N-10				
	Blue-green	$B\ ^1\Sigma^+$	$X\ ^1\Sigma^+$	4 x 4	4 x 4	D-1				
				4 x 4		N-3				
				4 x 4		O-7				
	(Combination Band)	$B\ ^1\Sigma^+$	$A\ ^1\Pi$	(?)	(?)	(N-11) N-10				
C_2	Swan	$A\ ^3\Pi_g$	$X'\ ^3\Pi_u$	7 x 7		F-1	8 x 15	(8 x 15)	W-4	[S-2]
				3 x 6		H-1				
				14 x 14		H-2				
				4 x 5		N-2				
				13 x 13		N-13				
				4 x 4	4 x 4	N-21				
				5 x 9		O-1				
				9 x 13	(9 x 13)	S-1	9 x 13	(9 x 13)	S-1	[S-2, J-1]
				5 x 8	5 x 8	J-1	5 x 8	5 x 8	J-1	[S-2, R-2]
	Ballik-Ramsay	$A'\ ^3\Sigma_g^-$	$X'\ ^3\Pi_u$	6 x 6		H-1				
				4 x 13		N-13				
	Fox-Herzberg	$B\ ^3\Pi_g$	$X'\ ^3\Pi_u$	10 x 8		H-1	2 x 16	(2 x 16)	W-5	[R-1]

TABLE I (continued)

Molecule	System Name	Transition: Upper State	Transition: Lower State	Morse Potential[a]: $q_{v'v''}$ (Note c,d)	Morse Potential[a]: $r_{v'v''}$ (Note c,d)	Morse Potential[a]: Reference	RKR Potential[b]: $q_{v'v''}$ (Note c,d)	RKR Potential[b]: $r_{v'v''}$ (Note c,d)	RKR Potential[b]: Reference (Note)
C_2	Fox-Herzberg (continued)	$B\ ^3\Pi_g$	$X'\ ^3\Pi_u$	8 x 8		N-2			
				4 x 13		N-13			
				4 x 8	4 x 8	J-1	4 x 8	4 x 8	J-1 [J-1], [R-2]
	Phillips	$b\ ^1\Pi_u$	$x\ ^1\Sigma_g^+$	8 x 6		H-1	(10 x 10)	(10 x 10)	S-3 [ ]
				6 x 10		N-2			
				8 x 5		N-13			
				12 x 9		O-1			
				9 x 10		S-1	9 x 10		S-1 [S-1]
	Deslandres-d'Azambuja	$c\ ^1\Pi_g$	$b\ ^1\Pi_u$	5 x 6		H-1	3 x 11		W-5 [R-1]
				6 x 5		N-2			
				6 x 8		N-13			
	Mulliken	$d\ ^1\Sigma_u^+$	$x\ ^1\Sigma_g^+$	4 x 4		H-1	(?)	(?)	S-3 [R-1]
				8 x 8		N-2			
				5 x 5		N-13			
	Freymark	$e\ ^1\Sigma_g^+$	$b\ ^1\Pi_u$	6 x 6		H-1	3 x 13		W-S [R-1]
				5 x 8		N-13			
CH and CD	4300Å	$A\ ^2\Delta$	$X\ ^2\Pi$	6 x 7		C-1			
				2 x 2		H-1			
				2 x 3	2 x 4	P-1			
	3900Å	$B\ ^2\Sigma^-$	$X\ ^2\Pi$	6 x 7		C-1			
				3 x 2		H-1			
	3143Å	$C\ ^2\Sigma^+$	$X\ ^2\Pi$	0 x 4		H-1			
				(3 x 5)	(3 x 5)	S-4			
CH^+		$A\ ^1\Pi$	$X\ ^1\Sigma^+$	? x 2		N-3, N-11			

TABLE 1 (continued)

Molecule	System Name	Transition: Upper State	Transition: Lower State	Morse Potential[a]: $q_{v'v''}$ (Note c,d)	Morse Potential[a]: $r_{v'v''}$ (Note c,d)	Morse Potential[a]: Reference	RKR Potential: $q_{v'v''}$ (Note c,d)	RKR Potential: $r_{v'v''}$ (Note c,d)	RKR Potential: Reference (Note [illegible])
CF		$A\ ^2\Sigma^+$	$X\ ^2\Pi$	2 x 13	(2 x 13)	W-3			
		$B\ ^2\Sigma^+$	$X\ ^2\Pi$	2 x 7	(2 x 7)	W-3			
$C\ell_2$		$A\ ^3\Pi_u$	$X\ ^1\Sigma_g^+$	0 x 0		H-1			
CN	Red	$A\ ^2\Pi_i$	$X\ ^2\Sigma^+$	6 x 6		N-1			
				8 x 5		H-1			
				9 x 8		N-2			
				19 x 18		N-4			
				15 x 18		S-1	18 x 18	(?)	S-1 [F-6]
				8 x 8		W-1			
					10 x 13	W-5			
	Violet	$B\ ^2\Sigma^+$	$X\ ^2\Sigma^+$	3 x 3		F-1			
				2 x 2		F-2			
				8 x 6		H-1			
						J-2			
				3 x 3		N-2			
				19 x 18		N-4			
				3 x 3	3 x 3	N-21			
				15 x 18		S-1	18 x 18	(?)	S-1 [F-6]
CO	Fourth Positive	$A\ ^1\Pi$	$X\ ^1\Sigma^+$	10 x 8		H-1			
				7 x 7	7 x 7	J-3			
				18 x 24		N-5			
				13 x 7		O-1			
				(17 x 24)	(17 x 24)	S-3	(17 x 24)	(17 x 24)	S-3 [ ]
	Hopfield-Birge	$B\ ^1\Sigma^+$	$X\ ^1\Sigma^+$						
	Angstrom	$B\ ^1\Sigma^+$	$A\ ^1\Pi$	1 x 6		N-3			
				11 x 13		O-1			

TABLE I (continued)

Molecule	System Name	Transition: Upper State	Transition: Lower State	Morse Potential[a]: $q_{v'v''}$ (Note c,d)	Morse Potential[a]: $r_{v'v''}$ (Note c,d)	Morse Potential[a]: Reference	RKR Potential[b]: $q_{v'v''}$ (Note c,d)	RKR Potential[b]: $r_{v'v''}$ (Note c,d)	RKR Potential[b]: Reference (Note ·)
CO (con'd)	Hopfield-Birge	C $^1\Sigma^+$	X $^1\Sigma^+$						
	Herzberg	B $^1\Sigma^+$	A $^1\Pi$						
	Cameron	a $^3\Pi$	X $^1\Sigma^+$	9 x 6 6 x 6 7 x 24		H-1 J-7 N-5			
	Hopfield-Birge-a	a' $^3\Sigma^+$	X $^1\Sigma^+$	8 x 8 10 x 24 (?)		H-1 N-5 (N-11) N-10			
	Asundi	a' $^3\Sigma^+$	a $^3\Pi$	10 x 8 12 x 2		H-1 J-7	9 x 10	9 x 10	W-5 [illegible]
	Third-Positive	b $^3\Sigma^+$	a $^3\Pi$	1 x 7 10 x 13		N-3 O-1			
	Hopfield-Birge-b	b $^3\Sigma^+$	X $^1\Sigma^+$	1 x 24		N-5			
	Triplet	d $^3\Delta$	a $^3\Pi$	10 x 15	10 x 15	W-5			
CO^+	Comet-tail	A $^2\Pi_i$	X $^2\Sigma^+$	8 x 8 8 x 7 10 x 13	 10 x 13	H-1 J-7 N-6			
	First-Negative	B $^2\Sigma^+$	X $^2\Sigma^+$	6 x 6 10 x 13 10 x 13	 10 x 13	H-1 N-5 N-6			
	Baldet-Johnson	B $^2\Sigma^+$	A $^2\Pi_i$	6 x 6 10 x 10	 10 x 10	H-1 N-6			
CO^+-CO		X $^2\Sigma$	X $^1\Sigma^+$	(?) 10 x 0		(N-11) N-10 W-2			

TABLE 1 (continued)

Molecule	System Name	Transition: Upper State	Transition: Lower State	Morse Potential[a]: $q_{v'v''}$ (Note c,d)	Morse Potential[a]: $r_{v'v''}$ (Note c,d)	Morse Potential[a]: Reference	RKR Potential[b]: $q_{v'v''}$ (Note c,d)	RKR Potential[b]: $r_{v'v''}$ (Note c,d)	RKR Potential[b]: Reference (Note c)
$CO^+ \rightarrow CO$ (Con'd)		A $^2\Pi_i$	X $^1\Sigma^+$	10 x 10		W-2			
		B $^2\Sigma^+$	X $^1\Sigma^+$	10 x 10		W-2			
CP	(like CN-red)	A $^2\Pi_i$	X $^2\Sigma^+$	5 x 5	5 x 5	S-4			
	(like CN-violet)	B $^2\Sigma^+$	X $^2\Sigma^+$	5 x 10	5 x 10	S-4			
		B $^2\Sigma^+$	A $^2\Pi_i$	5 x 5	5 x 5	S-4			
CS		A $^1\Pi$	X $^1\Sigma^+$	8 x 8	8 x 8	F-7			
CaH	6946Å	A $^2\Pi$	X $^2\Sigma$	3 x 3		O-7			
		B ?	X $^2\Sigma$	3 x 4	3 x 4	P-5			
CaO	Second-Infrared	? $^1\Sigma$	(X) $^1\Sigma$	6 x 6 11 x 9		O-7 O-5			
CrO		A ?	X ?	6 x 6	6 x 6	M-1			
CsH		A $^1\Sigma^+$	X $^1\Sigma^+$	0 x 0		H-1			
D_2 (see H_2)									
GaI		(?) A $^3\Pi_o$	X $^1\Sigma^+$	(?)		(N-11) N-10			
H_2	Lyman	B $^1\Sigma_u^+$	X $^1\Sigma_g^+$	10 x 8 14 x 14 13 x 14		H-1 H-2 N-17	36 x 14 20 x 0	0 x 0 20 x 0	S-7 [S-7] G-2 [N-23]
HD				10 x 8		H-1			
HT				10 x 8		H-1			
D_2				10 x 8 14 x 14		H-1 H-2			

Molecule	System Name	Transition		Morse Potential[a]			RKR Potential[b]		
		Upper State	Lower State	$q_{v'v''}$ (Note c,d)	$r_{v'v''}$ (Note c,d)	Reference	$q_{v'v''}$ (Note c,d)	$r_{v'v''}$ (Note c,d)	Reference (Note e)
H_2		$B'\,^1\Sigma_u^+$	$X\,^1\Sigma_g^+$	10 x 7		H-1	9 x 14	0 x 0	S-7[S-7]
HD				10 x 7		H-1			
D_2				10 x 7		H-1			
H_2	Werner	$C\,^1\Pi_u$	$X\,^1\Sigma_g^+$	10 x 6		H-1	14 x 14 12 x 0	0 x 0 12 x 0	S-7[S-7] G-2[N-23]
HD				10 x 6		H-1			
HT				10 x 6		H-1			
D_2				10 x 6		H-1			
H_2		$D\,^1\Pi_u$	$X\,^1\Sigma_g^+$	10 x 5		H-1	15 x 14	0 x 0	S-7 [S-7]
HD				10 x 5		H-1			
D_2				10 x 5		H-1			
H_2		$E\,^1\Sigma_u^+$	$B\,^1\Sigma_u^+$				9 x 36	0 x 0	S-7 [S-7]
		$G\,^1\Sigma_g^+(1)$	$B\,^1\Sigma_u^+$				13 x 36	0 x 0	S-7 [S-7]
		$G\,^1\Sigma_g^+(2)$	$B\,^1\Sigma_u^+$				20 x 36	0 x 0	S-7 [S-7]
		$I\,^1\Pi_g$	$B\,^1\Sigma_u^+$				14 x 36	0 x 0	S-7 [S-7]
		$d\,^3\Pi_u$	$a\,^3\Sigma_g^+$				17 x 18	0 x 0	S-7 [S-7]
		$h\,^3\Sigma_g^+$	$c\,^3\Pi_u$				18 x 20	0 x 0	S-7 [S-7]
		$k\,^3\Pi_u$	$a\,^3\Sigma_g^+$				19 x 18	0 x 0	S-7 [S-7]

TABLE 1 (continued)

Molecule	System Name	Transition: Upper State	Transition: Lower State	Morse Potential[a]: $q_{v'v''}$ (Note c,d)	Morse Potential[a]: $r_{v'v''}$ (Note c,d)	Morse Potential[a]: Reference	RKR Potential[b]: $q_{v'v''}$ (Note c,d)	RKR Potential[b]: $r_{v'v''}$ (Note c,d)	RKR Potential[b]: Reference (Note c)
$H_2^+ \rightarrow H_2$		$X\ ^2\Sigma_g^+$	$X\ ^1\Sigma_g^+$	(?)		N-11			
I_2		$B\ ^3\Pi_{ou}^+$	$X\ ^1\Sigma_g^+$	Graphs		N-18			
KH (and KD)		$A\ ^1\Sigma^+$	$X\ ^1\Sigma^+$	0 x 0		H-1			
Li_2		$A\ ^1\Sigma_u^+$	$X\ ^1\Sigma_g^+$	0 x 0		H-1			
LiH (and LiD)		$A\ ^1\Sigma^+$	$X\ ^1\Sigma^+$	0 x 0		H-1			
LaO	Red	$A\ ^2\Pi$	$X\ ^2\Sigma$	7 x 7		0-5			
		$B\ ^2\Sigma$	$X\ ^2\Sigma$	8 x 8		0-5			
MgH		$A\ ^2\Pi_i$	$X\ ^2\Sigma^+$	2 x 2		H-1			
				(?)		(N-11) N-10			
		$C\ ^2\Pi$	$A\ ^2\Pi$ or $X\ ^2\Sigma^+$	4 x 4		0-7			
				(?)		(N-11) N-10			
MgO		$B\ ^1\Sigma$	$X\ ^1\Sigma^+$	7 x 7		N-1			
				8 x 8		0-5			
				3 x 3		0-6,0-7			
				(2 x 5)	(2 x 5)	S-4			
		$B\ ^1\Sigma$	$A\ ^1\Pi$	7 x 7		N-1			
				(3 x 5)	(3 x 5)	S-4			
		$A\ ^1\Pi$	$X\ ^1\Sigma^+$	(4 x 5)	(4 x 5)	S-4			
		$D\ ^1\Delta$	$A\ ^1\Pi$	3 x 4	3 x 4	S-8			
		$C\ ^1\Sigma$	$A\ ^1\Pi$	(3 x 4)	(3 x 4)	Note g			

Molecule	System Name	Transition: Upper State	Transition: Lower State	Morse Potential[a]: $q_{v'v''}$ (Note c,d)	Morse Potential[a]: $r_{v'v''}$ (Note c,d)	Morse Potential[a]: Reference	RKR Potential[b]: $q_{v'v''}$ (Note c,d)	RKR Potential[b]: $r_{v'v''}$ (Note c,d)	RKR Potential[b]: Reference (Note c)
N_2	Vegard-Kaplan	$A\ ^3\Sigma_u^+$	$X\ ^1\Sigma_g^+$	14 x 14		H-2	13 x 20		B-1 [B-2]
				9 x 20		J-4	9 x 20		Z-1 [Z-1]
				16 x 27		N-5			
				16 x 27		N-7			
					2 x 14	N-22			
		$B\ ^3\Pi_g$	$X\ ^1\Sigma_g^+$				17 x 20		B-1 [B-2]
	Ogawa-Tanaka-Wilkinson	$B'\ ^3\Sigma_u^-$	$X\ ^1\Sigma_g^+$				18 x 20		B-1 [B-2]
	IR-Afterglow	$B'\ ^3\Sigma_u^-$	$B\ ^3\Pi_g$				18 x 17		B-3 [B-2]
	Tanaka	$C\ ^3\Pi_u$	$X\ ^1\Sigma_g^+$				4 x 20		B-1 [B-2]
							4 x 15		Z-1 [Z-1]
	First-Positive	$B\ ^3\Pi_g$	$A\ ^3\Sigma_u^+$	6 x 6		F-4,J-4	17 x 13		B-3 [B-2]
				4 x 6	5 x 5	F-8		2 x 4	J-8 [F-1]
				14 x 14		H-2			
				12 x 12		J-5			
					5 x 5	J-10			
				21 x 16		N-7			
				20 x 20	20 x 20	W-6	20 x 20	20 x 20	W-6 [Z-1]
				1 x 10	12 x 12	T-1	12 x 9		Z-1 [Z-1]
	Second-Positive	$C\ ^3\Pi_u$	$B\ ^3\Pi_g$	4 x 17		B-3	4 x 17		B-3 [B-2]
				4 x 6		F-4, J-4	4 x 12		Z-1 [Z-1]
				4 x 12		J-5			
				4 x 21		N-7			
	Fourth-Positive	$D\ ^3\Sigma_u^+$	$B\ ^3\Pi_g$	Obsolete		W-6			
				0 x 10	(0 x10)	W-7			
	Gaydon Green	(?)	(?)	4 x 5		N-14			

TABLE 1 (continued)

Molecule	System Name	Transition: Upper State	Transition: Lower State	Morse Potential[a]: $q_{v'v''}$ (Note c,d)	Morse Potential[a]: $r_{v'v''}$ (Note c,d)	Morse Potential[a]: Reference	RKR Potential[b]: $q_{v'v''}$ (Note c,d)	RKR Potential[b]: $r_{v'v''}$ (Note c,d)	RKR Potential[b]: Reference (Note c)
N_2 (con'd)	Lyman-Birge-Hopfield	a $^1\Pi_g$	X $^1\Sigma_g^+$	7 x 7 16 x 27	6 x 6	J-7 N-5, N-7 N-22	15 x 20 (6 x 21) 6 x 20	(6 x 21)	B-1 [B-2] S-4 [B-2] Z-1 [Z-1]
	Birge-Hopfield #2	b $^1\Pi_u$	X $^1\Sigma_g^+$	5 x 27		N-5, (N-11)			
	Birge-Hopfield #1	b' $^1\Sigma_u^+$	X $^1\Sigma_g^+$	(15 x 22) 15 x 20	(15 x 22)	W-4, S-3 W-6			
	-----	w $^1\Delta_u$	X $^1\Sigma_g^+$				6 x 20		B-1 [B-2]
	Ogawa-Tanaka (or Wilkinson-Mulliken)	w $^1\Delta_u$	a $^1\Pi_g$				6 x 15		B-3 [B-2]
	------	a $^1\Pi_g$	a' $^1\Sigma_u^-$				5 x 19		B-3 [B-2]
	------	a' $^1\Sigma_u^-$	X $^1\Sigma_g^+$				19 x 20		B-1 [B-2]
N_2^+	Meinel	A $^2\Pi_u$	X $^2\Sigma_g^+$	6 x 6 5 x 21 5 x 5	5 x 5	F-1 N-7 N-20			
	First-Negative	B $^2\Sigma_u^+$	X $^2\Sigma_g^+$	6 x 17 6 x 6 29 x 21 20 x 20	20 x 20	C-1 J-4 N-7 W-6			
	Second-Negative	C $^2\Sigma_u^+$	X $^2\Sigma_g^+$	10 x 21		N-5			
	Janin-d' Incan	D $^2\Pi_g$	A $^2\Pi_u$	11 x 5 11 x 9	11 x 9	N-5 N-8			

TABLE 1 (continued)

Molecule	System Name	Transition: Upper State	Transition: Lower State	Morse Potential[a]: $q_{v'v''}$ (Note c,d)	Morse Potential[a]: $r_{v'v''}$ (Note c,d)	Morse Potential[a]: Reference	RKR Potential[b]: $q_{v'v''}$ (Note c,d)	RKR Potential[b]: $r_{v'v''}$ (Note c,d)	RKR Potential[b]: Reference (Note e)
$N_2^+ \rightarrow N_2$		$X\ ^2\Sigma_g^+$	$X\ ^1\Sigma_g^+$	21 x 27		N-5			
				21 x 0		N-7			
		$A\ ^2\Pi_u$	$X\ ^1\Sigma_g^+$	5 x 27		N-5			
				5 x 0		N-7			
		$B\ ^2\Sigma_u^+$	$X\ ^1\Sigma_g^+$	29 x 27		N-5			
				29 x 0		N-7			
		$C\ ^2\Sigma_u^+$	$X\ ^1\Sigma_g^+$	10 x 27		N-5			
		$D\ ^2\Pi_g$	$X\ ^1\Sigma_g^+$	11 x 27		N-5			
NO	Gamma	$A\ ^2\Sigma$	$X\ ^2\Pi$	2 x 2		F-5	12 x 36		F-5 [V-1]
				6 x 6		J-4	0 x 10		W-7 [V-1]
				8 x 10	8 x 10	K-1	2 x 10	(2 x 10)	W-7 [V-2]
				7 x 18		N-1			
				15 x 23		N-12			
				11 x 13		O-1			
				12 x 20		O-2			
	Beta	$B\ ^2\Pi$	$X\ ^2\Pi$	2 x 12		J-7	12 x 33		F-5 [V-1]
				10 x 9		K-1			
				6 x 18		N-1			
				2 x 13		N-3			
				19 x 23		N-12			
				15 x 15		O-1			
				31 x 23		O-2			
	(Beta prime)	$B'\ ^2\Delta$	$X\ ^2\Pi$	6 x 23		N-12			
	Delta	$C\ ^2\Pi$	$X\ ^2\Pi$	4 x 23		N-12			
				6 x 6		O-3			
	Epsilon	$D\ ^2\Sigma^+$	$X\ ^2\Pi$	11 x 23		N-12			
				6 x 6		O-3			

TABLE 1 (continued)

Molecule	System Name	Transition: Upper State	Transition: Lower State	Morse Potential[a]: $q_{v'v''}$ (Note c,d)	Morse Potential[a]: $r_{v'v''}$ (Note c,d)	Morse Potential[a]: Reference	RKR Potential[b]: $q_{v'v''}$ (Note c,d)	RKR Potential[b]: $r_{v'v''}$ (Note c,d)	RKR Potential[b]: Reference (Note e)
NO(cont'd)	Feast 1	D $^2\Sigma^+$	A $^2\Sigma^+$	11 x 15		N-12			
	Gamma (prime)	E $^2\Sigma^+$	X $^2\Pi$	5 x 23		N-12			
	Feast 2	E $^2\Sigma^+$	A $^2\Sigma^+$	5 x 15		N-12			
	Ogawa 1	B' $^2\Delta$	B $^2\Pi$	6 x 19		N-12			
	M	a $^4\Pi$	X $^2\Pi$	3 x 23		N-12			
	Ogawa 2	b $^4\Sigma^-$	a $^4\Pi$	6 x 7 3 x 3		C-1 N-12			
NO^+		A $^1\Pi$	X $^1\Sigma^+$	(?) 5 x 17 (20 x 20)	(20 x 20)	(N-11) N-10 W-7 (S-4)			
$NO^+ \rightarrow NO$		X $^1\Sigma^+$	X $^2\Pi$	10 x 0[h?]		W-2, (N-10)			
		A $^1\Pi$	X $^2\Pi$	10 x 0[h?]		W-2, (N-10)			
NaH		A $^1\Sigma^+$	X $^1\Sigma^+$	0 x 0		H-1			
O_2	IR Atmospheric	a $^1\Delta_g$	X $^3\Sigma_g^-$	2 x 2 5 x 6		N-3 N-15			
	Atmospheric	b $^1\Sigma_g^+$	X $^3\Sigma_g^-$	6 x 6 3 x 6		F-1 N-15			
	Noxon	b $^1\Sigma_g^+$	a $^1\Delta_g$	3 x 5		N-15			
	Herzberg I	A $^3\Sigma_u^+$	X $^3\Sigma_g^-$	10 x 9 12 x 12		J-7 N-15	11 x 2		J-9 [J-9]
	Herzberg II	c $^1\Sigma_u^-$	X $^3\Sigma_g^-$	6 x 6		N-15			
	Herzberg III	D $^3\Delta_u$	X $^3\Sigma_g^-$	6 x 6		N-15			

Molecule	System Name	Transition: Upper State	Transition: Lower State	Morse Potential [a]: $q_{v'v''}$ (Note c,d)	Morse Potential [a]: $r_{v'v''}$ (Note c,d)	Morse Potential [a]: Reference	RKR Potential [b]: $q_{v'v''}$ (Note c,d)	RKR Potential [b]: $r_{v'v''}$ (Note c,d)	RKR Potential [b]: Reference (Note e)
O_2 (Con'd)	Schumann-Runge	B $^3\Sigma_u^-$	X $^3\Sigma_g^-$	25 x 15		F-1			
				14 x 14		H-2			
				fragments		J-6	fragments		J-6, J-11, 12, R-2
				15 x 2		J-7			
				15 x 21		N-2			
				21 x 21		N-5			
				21 x 21		N-9			
				15 x 0	15 x 0	N-21			
				21 x 25		O-4			
	Chamberlain (Airglow)	D $^3\Delta_u$	a $^1\Delta_g$	6 x 5		N-15			
	Broida-Gaydon	A $^3\Sigma_u^+$	b $^1\Sigma_g^+$	12 x 3		N-15			
O_2^+	Second Negative	A $^2\Pi_u$	X $^2\Pi_g$	9 x 9		J-4			
				8 x 8		N-3			
				15 x 15		N-19			
					12 x 12	N-22			
				20 x 20	20 x 20	W-6			
	First Negative	b $^4\Sigma_g^-$	a $^4\Pi_u$	7 x 7		J-7			
				10 x 10		N-19			
				20 x 20	20 x 20	W-6			
$O_2^+ \rightarrow O_2$		X $^2\Pi_g$	X $^3\Sigma_g^-$	10 x 0		W-2			
				(?)		N-11			
		A $^2\Pi_u$	X $^3\Sigma_g^-$	20 x 0		W-2			
				(?)		N-11			
		b $^4\Sigma_g^-$	X $^3\Sigma_g^-$	10 x 0		W-2			
				(?)		N-11			
		a $^4\Pi_u$	X $^3\Sigma_g^-$	15 x 0		W-2			
				(?)		N-11			

TABLE 1 (continued)

Molecule	System Name	Transition: Upper State	Transition: Lower State	Morse Potential[a]: $q_{v'v''}$ (Note c,d)	Morse Potential[a]: $r_{v'v''}$ (Note c,d)	Morse Potential[a]: Reference	RKR Potential[b]: $q_{v'v''}$ (Note c,d)	RKR Potential[b]: $r_{v'v''}$ (Note c,d)	RKR Potential[b]: Reference (Note e)
OH	Violet	$A\ ^2\Sigma^+$	$X\ ^2\Pi_i$	10 x 12	10 x 12	F-8			
				4 x 3		H-1			
				7 x 7		J-7			
				4 x 4		L-1			
				4 x 4		N-2			
				4 x 4		N-16			
				3 x 3	3 x 3	N-21			
		$B\ ^2\Sigma^+$	$X\ ^2\Pi_i$	1 x 12	1 x 12	F-8			
		$B\ ^2\Sigma^+$	$A\ ^2\Sigma^+$	1 x 10	1 x 10	F-8			
		$C\ ^2\Sigma^+$	$X\ ^2\Pi_i$	3 x 12	3 x 12	F-8			
		$C\ ^2\Sigma^+$	$A\ ^2\Sigma^+$	3 x 10	3 x 10	F-8			
PH									
PbO		A	$X\ ^1\Sigma^+$	0 x 0		H-1			
				5 x 8		N-2			
		D	$X\ ^1\Sigma^+$	0 x 0		H-1			
				4 x 6		N-2			
RbH		$A\ ^1\Sigma^+$	$X\ ^1\Sigma^+$	0 x 0		H-1	11 x 5	(11 x 5)	J-14[J-14]
				(5 x 10)-h		G-1			
S_2		$B\ ^3\Sigma_u^-$	$X\ ^3\Sigma_g^-$	12 x 12	12 x 5	H-3			
SH		$A\ ^2\Sigma^+$	$X\ ^2\Pi_i$	3 x 3		N-3			
ScF		$C\ ^1\Sigma$	$X\ ^1\Sigma^+$	(?)		M-3			

TABLE I (continued)

Molecule	System Name	Transition: Upper State	Transition: Lower State	Morse Potential[a]: $q_{v'v''}$ (Note c,d)	Morse Potential[a]: $r_{v'v''}$ (Note c,d)	Morse Potential[a]: Reference	RKR Potential[b]: $q_{v'v''}$ (Note c,d)	RKR Potential[b]: $r_{v'v''}$ (Note c,d)	RKR Potential[b]: Reference (Note e)
SiF	Alpha	$A\ ^2\Sigma$	$X\ ^2$	3 x 8	(3 x 8)	W-5			
	Beta	$B\ ^2\Sigma$	$X\ ^2$	3 x 10	(3 x 10)	W-5			
SiN		$B\ ^2\Sigma^+$	$X\ ^2\Sigma^+$	5 x 10	(5 x 10)	W-5			
SiO		$A\ ^1$	$X\ ^1\Sigma^+$	10 x 10 ( )		N-1 S-4			
ScO	Orange	$A\ ^2$	$X\ ^4\Sigma$	8 x 8		O-5			
	Blue-Green	$B\ ^2\Sigma$	$X\ ^4\Sigma$	10 x 9		O-5			
SrO		$A\ ^1\Sigma$	$X\ ^1\Sigma$	6 x 6		N-1			
TiO	Gamma (IR)	$A\ ^3$	$X\ ^3$	6 x 6 5 x 5	 5 x 5	F-1, O-6 P-2			
	Alpha (Blue-Green)	B or C ^{3}	$X\ ^3$	5 x 6		O-6			
VO	Gamma (Yellow-Blue)	$A\ ^2\Delta$	$X\ ^2$	10 x 10 6 x 6 5 x 5		N-1 O-6 P-2			
YO	Orange	$A\ ^2$	$X\ ^2\Sigma$	4 x 4		O-6			
		$B\ ^2\Sigma$	$X\ ^2\Sigma$	8 x 10 4 x 4		O-5 O-6			
ZrO	Gamma	$A\ ^3$	$X\ ^3$	4 x 4 6 x 6 2 x 4	 6 x 6 4 x 4	O-6 N-24 S-9			
	Beta	$B\ ^3$	$X\ ^3\Delta$	6 x 6	6 x 6	N-24			

TABLE 1 (continued)

Molecule	System Name	Transition		Morse Potential[a]			RKR Potential[b]		
		Upper State	Lower State	$q_{v'v''}$ (Note c,d)	$r_{v'v''}$ (Note c,d)	Reference	$q_{v'v''}$ (Note c,d)	$r_{v'v''}$ (Note c,d)	Reference (Note c)
ZrO (con'd)	Alpha	$C\ ^3\Delta$	$X\ ^3\Sigma$	5 x 6		N-24			
				6 x 6		O-6			
				3 x 4	3 x 4	S-5			
	A (b-a)	$b\ ^1\Sigma$ or $^1\Pi$	$a\ ^1\Sigma$ or $^1\Delta$	6 x 6	6 x 6	N-24			
	B (d-c)	$d\ ^1\Sigma$ or $^1\Delta$	$c\ ^1\Sigma$ or $^1\Delta$	3 x 2	3 x 2	N-24			

REFERENCES FOR APPENDIX A, TABLE 1.

B1 BENESCH,W.,VANDERSLICE,J.T.,TILFORD,S.G.,AND WILKINSON,P.G.
ASTROPHYS. J., V.143,P.236 (1966).

B2 BENESCH,W.,VANDERSLICE,J.T.,TILFORD,S.G.,AND WILKINSON,P.G.
ASTROPHYS. J., V.142,P.1227 (1965).

B3 BENESCH,W.,VANDERSLICE,J.T.,TILFORD,S.G.,AND WILKINSON,P.G.
ASTROPHYS. J., V.144,P.408 (1966).

B4 BATES,D.
MON. NOT. ROY. ASTRON. SOC., V.112,P.614 (1952).

C1 CHILDS,C.R.
J. QUANT. SPECTROSC. RADIAT. TRANSFER, V.4,P.283 (1964).

D1 DRAKE,G.W.F.,TYTE,D.C.,AND NICHOLLS,R.W.
J. QUANT. SPECTROSC. RADIAT. TRANSFER, V.7,P.639 (1967).

F1 FRASER,P.A.,JARMAIN,W.R.,AND NICHOLLS,R.W.
ASTROPHYS. J., V.119,P.286 (1954).

F2 FRASER,P.A.
PROC. PHYS. SOC. (LONDON), V.67,P.939 (1954).

F3 FRASER,P.A.
PROC. PHYS. SOC. (LONDON), V.66,P.1153 (1953).

F4 FRASER,P.A. AND JARMAIN,W.R.
PROC. PHYS. SOC. (LONDON), V.66 P.1145 (1953).

F5 FLINN,D.J.,SPINDLER,R.J.,FIFER,S.,AND KELLY,M.
J. QUANT. SPECTROSC. RADIAT. TRANSFER, V.4,PP.271 (1964).

F6 FALLON,R.J.,VANDERSLICE,J.T.,AND CLONEY,R.D.
J. CHEM. PHYS., V.37,P.1097 (1962).

F7 FELENBOK,P.
PROC. PHYS. SOC. (LONDON), V.86,P.676 (1965).

F8 FELENBOK,P.
ANN. DE ASTROPHYS., V.26,P.393 (1963).

G1 GAYDON,A.G. AND PEARSE,R.W.B.
PROC. ROY. SOC. (LONDON), V.173,P.37 (1939).

G2 GIEGER,J. AND TOPSCHOWSKY,M.
Z. NATURFORSCH., V.21A,P.626 (1966).

H1 HALMANN,M. AND LAULICHT,I.
ASTROPHYS. J., SUPPL. SER., V.12,P.307 (1966).

H2 HALMANN,M. AND LAULICHT,I.
J. CHEM. PHYS., V.44,P.2398 (1966).

H3 HERMAN,C. AND PELENBOK,P.
J. QUANT. SPECTROSC. RADIAT. TRANSFER, V.3,P.247 (1963).

J1 JAIN,D.C.
J. QUANT. SPECTROSC. RADIAT. TRANSFER, V.4,P.427 (1964).

J2 JARMAIN,W.R. AND FRASER, P.A.
PROC. PHYS. SOC. (LONDON), V.66,P.1153 (1953).

J3 JARMAIN,W.R.,EBISUZAKI,R.,AND NICHOLLS,R.W.
CAN. J. PHYS., V.38,P.510 (1960).

J4 JARMAIN,W.R.,FRASER,P.A.,AND NICHOLLS,R.W.
ASTROPHYS. J., V.118,P.228 (1953).

J5 JARMAIN,W.R. AND NICHOLLS,R.W.
CAN. J. PHYS., V.32,P.201 (1954).

J6 JARMAIN,W.R.
CAN. J. PHYS., V.41,P.414,P.1926 (1963).

J7 JARMAIN,W.R.,FRASER,P.A.,AND NICHOLLS,R.W.
ASTROPHYS. J., V.122,P.55 (1955).

J8 JAMES,T.C.
J. MOL. SPECTRY., V.20,P.77 (1966).

J9 JARMAIN,W.R. AND NICHOLLS,R.W.
PROC. PHYS. SOC. (LONDON), V.90,P.545 (1967).

J10 JARMAIN,W.R. AND NICHOLLS,R.W.
REP. NO. 20, UNIV. W. ONTARIO (1955).

J11 JARMAIN,W.R.
CAN. J. PHYS., V.38,P.217 (1960).

J12 JARMAIN,W.R.
SCI. REP. NO. 1, DEPT. PHYS., UNIV. W. ONTARIO (1961).

J13 JAIN,D.C. AND SAH,P.
CAN. J. PHYS., V.40,P.1269 (1962).

J14 JAIN,D.C. AND SAHNI,R.C.
PROC. PHYS. SOC. (LONDON), V.88,P.495 (1966).

K1 KIVEL,B.,MAYER,M.,AND BETHE,H.
ANN. PHYS., V.2,P.57 (1957).

L1 LEARNER,R.C.M.
PROC. ROY. SOC. (LONDON), V.269A,P.311 (1962).

M1 MURTHY,N.S. AND NAGARAJ,S.
PROC. PHYS. SOC. (LONDON), V.84,P.827 (1964).

M2 MURTHY,N.S.,SETTY, AND SUMATHI,
INDIAN J. PHYS., V.38,P.428 (1964).

M3 MCLEOD,JR.,D. AND WELTNER,JR.,W.
J. PHYS. CHEM., V.70,P.3293 (1966).

N1 NICHOLLS,R.W.
J. RES. NATL. BUR. STD., (U.S.), V.66A,P.227 (1962).

N2 NICHOLLS,R.W.,FRASER,P.A.,AND JARMAIN,W.R.
COMBUST. FLAME, V.3,P.13 (1959).

N3 NICHOLLS,R.W.,FRASER,P.A.,JARMAIN,W.R.,AND MCEACHRAN,R.P.
ASTROPHYS. J., V.131,P.399 (1960).

N4 NICHOLLS,R.W.
J. RES. NATL. BUR. STD., (U.S.), V.68A,P.75 (1964).

N5 NICHOLLS,R.W.
J. QUANT. SPECTROSC. RADIAT. TRANSFER, V.2,P.433 (1962).

N6 NICHOLLS,R.W.
CAN. J. PHYS., V.40,P.1772 (1962).

N7 NICHOLLS,R.W.
J. RES. NATL. BUR. STD., (U.S.), V.65A,P.451 (1961).

N8 NICHOLLS,R.W.
CAN. J. PHYS., V.40,P.523 (1962).

N9 NICHOLLS,R.W.
CAN. J. PHYS., V.38,P.1705 (1960).

N10 NICHOLLS,R.W.
J. QUANT. SPECTROSC. RADIAT. TRANSFER, V.5,P.647 (1965).

N11 NICHOLLS,R.W.
UNPUBLISHED WORK, QUOTED BY NICHOLLS (N10).

N12 NICHOLLS,R.W.
J. RES. NATL. BUR. STD., (U.S.), V.68A,P.535 (1964).

N13 NICHOLLS,R.W.
J. RES. NATL. BUR. STD., (U.S.), V.69A,P.397 (1965).

N14 NICHOLLS,R.W.
J. CHEM. PHYS., V.42,P.804 (1965).

N15 NICHOLLS,R.W.
J. RES. NATL. BUR. STD., (U.S.), V.69A,P.369 (1965).

N16 NICHOLLS,R.W.
IN SUPERSONIC FLOW, CHEMICAL PROCESSES, AND RADIATIVE TRANSFER,
P.413, (ED. OLFE,D.B. AND ZACKKAY,V.), PERGAMON PRESS, N.Y. (1964

N17 NICHOLLS,R.W.
ASTROPHYS. J., V.141,P.819 (1965).

N18 NICHOLLS,R.W.
J. CHEM. PHYS., V.38,P.1029 (1963).

N19 NICHOLLS, R.W.
CAN. J. PHYS., V.43,P.1390 (1965).

N20 NICHOLLS,R.W.
J. ATMOS. TERRES. PHYS., V.12,P.211 (1958).

N21 NICHOLLS,R.W.
PROC. PHYS. SOC. (LONDON), V.A69,P.741 (1956).

N22 NICHOLLS,R.W.
PROC. PHYS. SOC. (LONDON), V.A69,P.713 (1956).

N23 NAMIOKA,T.
J. CHEM. PHYS., V.43,P.1636 (1965).

N24 NICHOLLS,R.W. AND TYTE,D.C.
PROC. PHYS. SOC. (LONDON), V.91,P.489 (1967).

O1 ORTENBERG,F.S.
OPT. SPECTRY.(USSR), V.16,P.398 (1964).

O2 ORY,H.A.,GITTLEMAN,A.P.,AND MADOX,J.P.
ASTROPHYS. J., V.139,P.346 (1964).

O3 ORY,H.A.
J. CHEM. PHYS., V.40,P.562 (1964).

O4 ORY,H.A. AND GITTLEMAN,A.P.
ASTROPHYS. J., V.139,P.357 (1964).

O5 ORTENBERG,F.S.,GLASKO,V.B.,AND DMITRIEV,A.I.
SOVIET ASTRON.-AJ, V.8,P.258 (1964).

O6 ORTENBERG,F.S. AND GLASKO,V.B.
SOVIET ASTRON.-AJ, V.6,P.714 (1963).

O7 ORTENBERG,F.S.
OPT. SPECTRY.(USSR), V.9,P.82 (1960).

P1 PATHAK,A.N. AND MAHESHWARI,R.C.
INDIAN J. PURE APPL. PHYS, V.5,P.138 (1967).

P2 PRASAD,S.S.
PROC. PHYS. SOC. (LONDON), V.82,P.419 (1963).

P3 PRASAD,S.S.
INDIAN J. PHYS., V.37,P.457 (1963).

P4 PATCH,R.W.
J. CHEM. PHYS., V.41,P.1881 (1964).

P5 PATHAK,A.N. AND SINGH,P.D.
PROC. PHYS. SOC. (LONDON), V.87,P.1008 (1966).

R1 READ,S.M. AND VANDERSLICE,J.T.
J. CHEM. PHYS., V.36,P.2366 (1962).

R2 REES,A.L.G.
PROC. PHYS. SOC. (LONDON), V.59,P.998 (1947).

S1 SPINDLER,R.J.
J. QUANT. SPECTROSC. RADIAT. TRANSFER, V.5,P.165 (1965).

S2 SINGH,N.L. AND JAIN,D.C.
CAN. J. PHYS., V.40,P.520 (1962).

S3 SPINDLER,R.J.
UNPUBLISHED (1966).

S4 SPINDLER,R.J. AND WENTINK,T.,JR.
UNPUBLISHED (1967).

S5 SINGH,P.D. AND PATHAK,A.N.
PROC. PHYS. SOC. (LONDON), V.90,P.543 (1967).

S6 SHARMA,A.
J. QUANT. SPECTROSC. RADIAT. TRANSFER, V.7,P.289 (1967).

S7 SPINDLER,R.J.
NASA REP. CR-72107, AVCO, LOWELL MASS. REP. AVSSD-0287-66-RR (1966).

S6 SRIVASTARA,Y.P. AND MAHESHWARI,R.C.
PROC. PHYS. SOC. (LONDON), V.90,P.1177 (1967).

S9 SINGH,P.D. AND PATHAK,A.N.
PROC. PHYS. SOC. (LONDON), V.91,P.497 (1967).

T1 TURNER,R.G. AND NICHOLLS,R.W.
CAN. J. PHYS., V.32,P.475 (1954).

V1 VANDERSLICE,J.T.,MASON,E.,MAISCH,W.,AND LIPPINCOTT,E.
J. CHEM. PHYS., V.31,P.738 (1959).

V2 VANDERSLICE,J.T.
J. CHEM. PHYS., V.37,P.384 (1962).

W1 WHYLER,A.A.
ASTROPHYS. J., V.127,P.763 (1958).

W2 WACKS,M.E.
J. CHEM. PHYS., V.41,P.930 (1964).

W3 WENTINK,T.,JR. AND ISAACSON,L.
J. CHEM. PHYS., V.46,P.603 (1967).

W4 WENTINK,T.,JR.
UNPUBLISHED (1967).

W5 WENTINK,T.,JR.,ISAACSON,L.,MARRAM,E.P.,AND SPINDLER,R.J.
AVCO AVSSD-0105-67-RR,AFWL TR-67-30 (1967).

W6 WENTINK,T.,JR.,ISAACSON,L.,AND SPINDLER,R.J.
AWFL TR-65-139 (1965).

W7 WENTINK,T.,JR.,MARRAM,E.P.,AND ISAACSON,L.
AWFL TR-67-6 (1967).

Z1 ZARE,R.N.,LARSON,F.O.,AND BERG,R.A.
J. MOL. SPECTRY., V.15,P.117 (1965).